R-matrix calculations of electron-molecule collisions with C_2 and C_2^-

Gabriela Halmová

A thesis submitted to the University of London
for the degree of Doctor of Philosophy

Department of Physics and Astronomy
University College London

January 2008

ProQuest LLC
789 East Eisenhower Parkway
P.O. Box 1346
Ann Arbor, MI 48106-1346

Abstract

The C_2 molecule is very important astrophysically as well as terrestrially. Its spectrum is known from the comets, the interstellar mediums and the atmospheres of cool carbon stars. C_2 is present in flames and electric discharges through carbon-containing materials, and could be important at the edge of fusion plasmas. Nevertheless, there seem to be no preceding published studies of electron collisions with neutral C_2. On the other hand, there are a number of studies available for C_2^- ion.

The challenge of studying electron collisions with C_2 is the unusually large number of low-lying electronic states, which are themselves difficult to represent using standard *ab initio* methods. Furthermore, the C_2^- system supports several bound states even though the exact number is not firmly established.

This thesis describe the electron collision processes with the dicarbon molecule and its anion at the energies up to 10 eV. Specific attention is given to determine the formation of the bound states of C_2^- and a low-lying resonance of C_2^{2-} as a function of internuclear separation. While the calculations on the C_2^- system used the standard implementation of the UK R-matrix method, those on C_2^{2-} required both the molecular R-matrix method with pseudo-states and the partitioned R-matrix method to be employed. The effectiveness of these procedures for this problem is discussed.

Contents

List of Figures

List of Tables

Acknowledgements

There are many people, without whose help, this thesis would have proved to be too great a goal. Their time, support, motivation and sense of the ridiculous have all played a part in keeping me on the road to success.

First and foremost, I would like to thank Jonathan Tennyson, my enduring supervisor, for his support, guidance and teaching thoughout.

I would like to thank Jimena and all my fellow members of the TAMPA group for their useful suggestions and advice.

My gatitude goes to my family and friends for their understanding and patience and especially to my parents for supporting me through my journey, and for always letting me know they believed in me. Ďakujem !

David, Beverley, Joshua, Elliot, Sarah and Chip, my neighbours, friends and local heros. Endless supplies of jokes and food, holidaying and laughter. I have been part of your family and you have been mine. Thank you.
David, thank you for the constant up all night sessions, your fingers truly work wonders, on a keyboard !!

Finally, to my biggest fan (F.G.), I promise that I will never underestimate the value of a second chance in life nor waste it.

Chapter 1

Introduction

1.1 Overview

Electrons are present in all phases of matter and in all areas of the Universe. The electron-molecule scattering processes can be found in a number of natural procedures in different fields of physics and plays an important role in the development of many new technologies.

Electron collisions with molecules and molecular ions are important in cold plasmas such as planetary atmospheres and interstellar medium. For example, rotational electron excitation of interstellar molecules is an important technique in the cooling down of electrons. This technique determines the populations of rotational states and so establishes the intensities in the emission lines of the molecules (Dalgarno and McCray, 1972). The equally important cooling mechanism is the electron impact resonant vibrational excitation of N_2 in the earth's ionosphere (Hines et al., 1965).

Electron scattering is used in industry, the molecular lasers such as the CO_2 lasers require electron impact excitation of vibrational and rotational states of CO_2 and N_2 to provide the energy necessary for population inversion (Demaria, 1973). An accurate knowledge of the electron vibronic cross sections is essential in order to model and optimise the laser performance. The next area where the electron scattering plays significant role is material science. It is used to probe the structure of materials such as molecular crystals (Dorset, 1996). Electron collision cross sections are necessary for designing and optimisation of procedures involving plasmas, for example plasma etching (Pearton and Ren, 1994), producing of magnetohydrodynamic power (Spence and Phelps, 1976) and

thin film chemical vapour deposition mechanisms (Springer et al., 1997).

Electron-molecule collision processes are essential in fusion plasmas. The electron impact dissociation of molecules has been cited as the most important electron impact cross section because it determines the radical densities in the plasma (Kushner, 1998). The vibrationally excited molecules in detached divertor plasmas enhance plasma recombination due to dissociative attachment which takes place by mutual neutralisation and ion conversion. The molecular ions existent in these cold plasmas are destroyed by dissociative recombination, which is a dominant process (Fantz et al., 1999; Behringer and Fantz, 2000; Fantz et al., 2001; Heger et al., 2001; Hey et al., 2000).

The experimental data for developments in many of the above mentioned areas are not available. Consequently theoretical calculations of electron-molecule scattering processes are essential in providing the necessary data. The electron-molecule system, with its many degrees of freedom, presents a challenging test of current quantum mechanical techniques and contributes to the development of new methods.

1.2 Carbon dimer

C_2 molecule as well as C and C_3 are the primary components of equilibrium carbon vapour at temperatures in the range of 2000 - 5000 K. These species are reaction intermediates in a wide variety of chemical system involving hydrocarbons, including photolysis, electric discharges, and combustion systems. The largest fraction of the carbon present in the universe is in the form of C or one of its ions, while the molecular form of CO accounts for the second largest fraction. C_2 and C_3 are also present in astrophysical sources and are thought to be important reactants in the chemistry of the interstellar medium. The spectroscopy of these species has been studied for decades, making C_2 and C_3 the most well characterised of all the carbon clusters.

The C_2 molecule is extensively studied and its spectrum is well known from comets, the interstellar medium and atmospheres of cool carbon stars (see chapter 4). C_2 is abundant in flames and electric discharges through carbon-containing materials. It is also used in production of synthetic diamonds (for example http://www.chm.bris.ac.uk/pt/diamond/end.htm).

The C_2 molecule has $X\ ^1\Sigma_g^+$ ground electronic state. There are three low lying electronic states that have also been characterised, the $a\ ^3\Pi_u$ state, lying 0.089 eV above the ground state, the $b\ ^3\Sigma_g^-$ state at 0.798 eV, and the $A\ ^1\Pi_u$ state at 1.040 eV. In

addition to these low-lying states, about 14 other electronic states have been identified. Since C_2 is most often produced in an emissive state, many well-known band systems have been characterised. The most prominent of these is the Swan system ($d\ ^3\Pi_g \leftarrow a\ ^3\Pi_u$) at 2.41 eV. Others includes the Phillips bands ($A\ ^1\Pi_u \leftarrow X\ ^1\Sigma_g^+$) and Mulliken band ($D\ ^1\Sigma_u^+ \leftarrow X\ ^1\Sigma_g^+$) at 5.36 eV. The structural and spectroscopic properties of C_2 known up to 1979 were tabulated by Huber and Herzberg (1979). Recently, a new band system of C_2 ($d\ ^3\Pi_g \leftarrow c\ ^3\Sigma_u^+$) was observed by laser induced fluorescence spectroscopy (Kokkin et al., 2006). This was the first direct detection of the $c\ ^3\Sigma_u^+$ state of C_2. The spectroscopy and kinetics of all the C_2 electronic states studied up to 1992 were reviewed by Martin (1992). Calculated and experimental constants, vibronic frequencies, excited states lifetimes, oscillator strengths and electronic transition moments for most of the observed electronic states are reported in these references.

In the recent years there have been an increase in interest in the study of C_2 caused by employment of the carbon-based materials such as graphite in fusion experiments (Stark et al., 2005; Fantz et al., 2005). The chemical erosion of carbon-contained materials are often used as a wall material in fusion experiments. The advantages of the carbon composites are the excellent thermal and mechanical properties such as the capability to endure high heat loads. On the other hand sputtering and chemical erosion of the carbon material in hydrogen edge plasmas lead to consumption of the material and in carbon and hydrocarbon impurities. The chemical erosion of carbon is commonly quantified by the erosion yield which is the ratio of the carbon flux to the incident hydrogen flux. Fantz et al. (2005) suggested a technique using the intensity ratios (C_2/CH molecular bands) to be used as a monitor for particle ratios (C_2H_y/CH_4). The correlation factors from the photon fluxes to the particle fluxes were established from experiments in the divertor of ASDEX Upgrade (Gruber et al., 2001).

The ASDEX Upgrade shown in a figure 1.1 (http://www.ipp.mpg.de/eng/for/projekte /asdex/for_proj_asdex.html) is, compared to other international tokamaks, a mid-size tokamak experiment. A tokamak is a machine producing a toroidal (doughnut-shaped) magnetic field for confining a plasma. It is one of several types of magnetic confinement devices and the leading candidate for producing fusion energy. ASDEX Upgrade started in 1990 as a sequel of its successful predecessor ASDEX, which was in operation from 1980 until 1990. Its name is derived from Axial Symmetric Divertor EXperiment. Like ASDEX, ASDEX Upgrade has a poloidal divertor, which was optimised to meet the

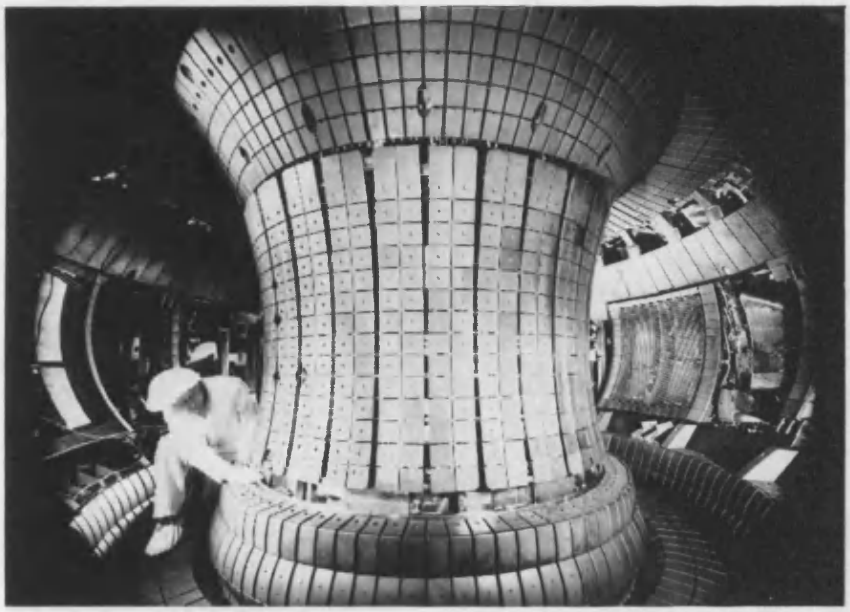

Figure 1.1: The ASDEX Upgrade divertor tokamak: inside view of the vacuum vessel with divertor II.

requirements of a future fusion reactor.

The plasma is controlled through a system of 12 vertical field coils and kept in its elliptical shape with an X-point above the bottom divertor. The purely toroidal field is usually held constant during the entire discharge (figure 1.2). Nevertheless it can also be varied during the discharge to some degree, if the physical requirements need such a field variation. Additionally there are two vertical field coils close to the plasma for fast control of the plasma.

1.3 C_2^- ion

Production of neutral carbon clusters is often accompanied by the formation of carbon cluster ions. Although the relative abundances of these ions is usually much lower than those of the neutrals. Their high chemical reactivity makes them important components in the growth and annealing of carbon clusters. C_2^- is the most characterised of all the carbon cluster ions. This molecule is particularly interesting because it possesses excited valence electronic states which are bound with respect to electron autodetachment.

C_2^- is the best studied diatomic negative ion. Herzberg and Lagerqvist (1968) observed very simple $\Sigma - \Sigma$ bands which after extensive studies were assigned to the $^2\Sigma_u^+$

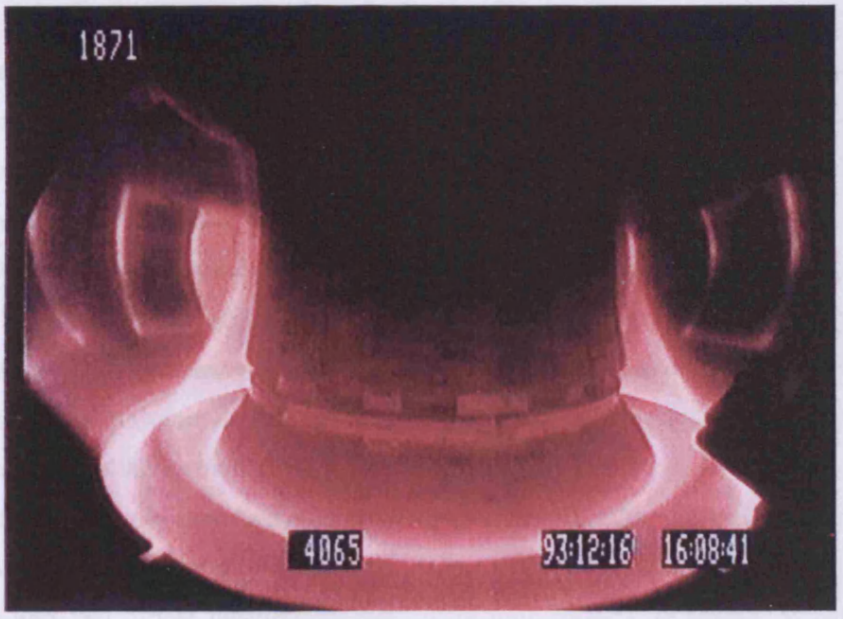

Figure 1.2: The ASDEX Upgrade divertor tokamak: picture of a typical plasma discharge.

- $^2\Sigma_g^+$ transition of C_2^-. These bands were previously assigned to C_2 by McCarty and Robinson (1959). Further studies of this band system using carbon vapour trapped in inert gas matrices confirmed the new explanation of these bands (Milligan and Jacox, 1969; Frosch, 1971; Bondybey and Nibler, 1972). Photodetachment spectroscopy experiments on C_2^- were conducted by Lineberger and Patterson (1972), Jones et al. (1980) and Hefter et al. (1983). Jones et al. (1980) and Hefter et al. (1983) observed autodetaching resonance states of C_2^-. However these resonances are associated with vibrational excited states of the bound C_2^- electronic states, which have sufficient energy to autodetach.

There have been few theoretical studies performed on C_2^-. *Ab initio* electronic structure calculations include: multireference configuration-interaction (MRD-CI) calculations by Zeitz et al. (1979), multiconfiguration-self-consistent field (MCSCF) calculations by Rosmus and Werner (1984), quadratic configuration interaction with single and double excitations (QCISD) calculations by Wang et al. (2001) and coupled-cluster with single and double excitations (CCSD) calculations by Watts and Bartlett (1992). In these references the following values were calculated: the equilibrium bond length, the vibrational frequency, the dissociation energy and molecular constants for the $X\ ^2\Sigma_g^+$ ground state and the $A\ ^2\Pi_u$ and $B\ ^2\Sigma_u^+$ excited state. They will be discussed further in

chapter 5.

Experimental studies of electron collisions with C_2^- were published by Andersen et al. (1996) and Pedersen et al. (1998, 1999). These measured the electron impact detachment cross section of C_2^-. They observed a resonance structure in the $e^- + C_2^- \longrightarrow C_2 + 2e^-$ detachment channel at the energy about 10 eV. In addition to the pure detachment cross section, they measured the cross section for electron impact dissociation of C_2^- $e^- + C_2^- \longrightarrow C + C^- + e^-$ and observed a resonance structure at approximately the same energy as in the detachment channels, but broader. Similar resonances were observed in several other diatomic anions such as B_2^- (Pedersen et al., 1998), O_2^-, BN^-, OH^- (Pedersen et al., 1999) and Cl_2^- (Collins et al., 2005)

These experiments were carried on the Aarhus STorage RIng in Denmark (ASTRID) which can store negative ions (Andersen et al., 1996). The ring has a circumference of 40 m and two dipole magnets in each of its four corners illustrated in figure 1.3. The negative ions are directed into ASTRID from an injector at 150 kV. Several μA of C_2^- beam current are generated by a sputter ion source. The ions are accelerated by an RF cavity up to the energy of 4.4 MeV. This acceleration is achieved after few seconds. After being accelerated, the storage lifetime of the beam is about 1 s. The electrons are distributed by an electron cooler which can produce an electron beam of several mA at the energy range 50 and 2000 eV. The electrons and negative ions are merged in the straight section of the electron cooler. In order to identify the detachment and dissociation reactions by detection of the neutral particles after interaction with the electrons, an energy-sensitive solid state detector was placed behind the dipole magnets.

1.4 Objectives

In order to achieve the best representation of low energy electron collisions with dicarbon molecule and its negative ion, the objectives of this work are as follow:

- To design target models for C_2 and C_2^- to ensure that the vertical excitation energies and ground state energy are sufficient.
- To run R-matrix electron collision calculations for the C_2 molecule on a desktop PC and obtain excitation cross sections.
- To look for low lying resonances and determine bound states.

Figure 1.3: ASTRID (Aarhus STorage RIng in Denmark): a dual-mode ring which can store electrons or ions of either polarity (http://www.isa.au.dk/animations/pictures/pic-index.html).

- To run R-matrix electron collision calculations for C_2^- anion on a Sun Cluster (supercomputer) and obtain ionisation cross sections.
- To search for bound states and low lying resonances.

1.5 Layout of the thesis

Chapter 2 describes some approximations used in order to solve the electron-molecule scattering problem. The Born-Oppenheimer approximation, Hartree-Fock self consistent field method, configuration interaction and fixed-nuclei formulation are introduced.

The molecular R-matrix method for polyatomic molecules and various implementations are explained in chapter 3. The programs used for these calculations are also introduced.

Chapter 4 describes the electron collisions with C_2 molecule as a function of internuclear distance, R. These calculations focus on determing the low-lying resonances (below 10 eV) and electron impact electronic excitation cross sections for the two lowest states. The lowest 26 singlet and triplet target states were coupled, all of which lie less

than 10 eV above the ground state at the C_2 equilibrium geometry. This is significantly more physical states than were required to obtain stable results for electron-molecule collisions studied previously using standard close-coupled expansion.

In chapter 5 results are presented for bound states of the C_2^- system. These calculations were performed for 20 C_2 internuclear distances and 16 symmetries.

Chapter 6 describes the employment of the R-matrix method to the electron collisions with C_2 anion at its equilibrium geometry. The various scattering models are described. These calculations concentrate on obtaining low-lying resonances (below 15 eV) and electron impact detachment cross sections.

Chapter 7 summarises the results and gives suggestions for improvements to the calculations. Possible future directions of the work are discussed.

Chapter 2

Theoretical background

2.1 Introduction

This chapter describes the use of some approximations used in order to solve the electron-molecule scattering problem. The first approximate method for solving the multiple-electron Schrödinger equation, the Born-Oppenheimer approximation is introduced in section 2.2. Born and Oppenheimer (1927) presented a solution of the molecular Hamiltonian as separate solutions of the nuclear and the electronic motions for a system of N_n nuclei and N_e electrons. In chapter 2.3, the Hartree-Fock method is described. This method was developed by Hartree (1928) and later refined to include electron exchange effects by Fock (1930). In order to include the correlation between electrons in the multiple-electron Schrödinger equation, the configuration interaction is introduced after the Hartree-Fock approximation. This method is described in section 2.4. Detailed explanations for these methods can be found, for example, in Szabo and Ostlund (1996) from which much of the material below is taken. Finally, the fixed-nuclei formulation is presented (in section 2.5), and used to further simplify the scattering problem.

2.2 Born-Oppenheimer approximation

The molecular Hamiltonian for N_e electrons and N_n nuclei in the non-relativistic time-independent Schrödinger equation can be written in atomic units as

$$H = -\frac{1}{2}\sum_{j=1}^{N_e}\nabla_j^2 - \sum_{\alpha=1}^{N_n}\frac{1}{2M_\alpha}\nabla_\alpha^2 - \sum_{\alpha=1}^{N_n}\sum_{j=1}^{N_e}\frac{Z_\alpha}{|\mathbf{r}_j - \mathbf{R}_\alpha|} + \sum_{i=1}^{N_e}\sum_{j>i}^{N_e}\frac{1}{|\mathbf{r}_i - \mathbf{r}_j|} + \sum_{\alpha=1}^{N_n}\sum_{\beta>\alpha}^{N_n}\frac{Z_\alpha Z_\beta}{\mathbf{R}_{\alpha\beta}} \tag{2.1}$$

where M_α represents the ratio of the mass of nucleus α to the mass of an electron, Z_α is the atomic number of the nucleus α, $\mid \mathbf{r}_j - \mathbf{R}_\alpha \mid$ is the distance between the j-th electron and the α nucleus, $\mid \mathbf{r}_i - \mathbf{r}_j \mid$ is the distance between the i-th and j-th electrons and $\mathbf{R}_{\alpha\beta}$ is the distance between the α and the β nuclei (see figure 2.1). The first term is the operator for the kinetic energy of the electrons and the second one is the operator for the kinetic energy of the nuclei. The third term represents the coulomb attraction between the electrons and the nuclei. The remaining two terms stand for the repulsion between the electrons and between the nuclei, respectively.

In order to solve the equation 2.1, to a good approximation, one has to separate the nuclear and the electronic motions. The Born-Oppenheimer approximation allows this separation to be made meaning one can consider the electrons in a molecule to be moving in the field of fixed nuclei. In order to solve the electronic problem, the second term in equation 2.1, the kinetic energy of the nuclei can be neglected and the last term, the repulsion between the nuclei, can be regarded as constant. The remaining Hamiltonian describes the motion of N electrons in the field of N_n point charges. This electronic Hamiltonian can be written

$$H_{elec} = -\frac{1}{2}\sum_{j=1}^{N_e}\nabla_j^2 - \sum_{\alpha=1}^{N_n}\sum_{j=1}^{N_e}\frac{Z_\alpha}{|\mathbf{r}_j - \mathbf{R}_\alpha|} + \sum_{i=1}^{N_e}\sum_{j>i}^{N_e}\frac{1}{|\mathbf{r}_i - \mathbf{r}_j|} \tag{2.2}$$

The Schrödinger equation including the electronic Hamiltonian, $H_{elec}\psi_{elec}(\mathbf{r}_j;\mathbf{R}_\alpha) = \varepsilon_{elec}\psi_{elec}(\mathbf{r}_j;\mathbf{R}_\alpha)$, and its solutions depend explicitly on the electronic coordinates, $\mathbf{r}_j$ and parametrically on the nuclear coordinates, $\mathbf{R}_\alpha$. This means that for a different arrangement of the nuclei, the electronic wave function ψ_{elec} is a different function of the electronic coordinates. The total energy for fixed nuclei includes the constant repulsion between the nuclei, $V = \varepsilon_{elec} + \sum_{\alpha=1}^{N_n}\sum_{\beta>\alpha}^{N_n}\frac{Z_\alpha Z_\beta}{\mathbf{R}_{\alpha\beta}}$ which can be calculated independently after solving the electronic problem. This energy, in bound state problems, is known as the electronic potential. The nuclear motion can be solved under the same assumptions as in the electronic problem. Due to the much faster motion of the electrons, the electronic coordinates in the equation 2.1 can be replaced by their average values averaged

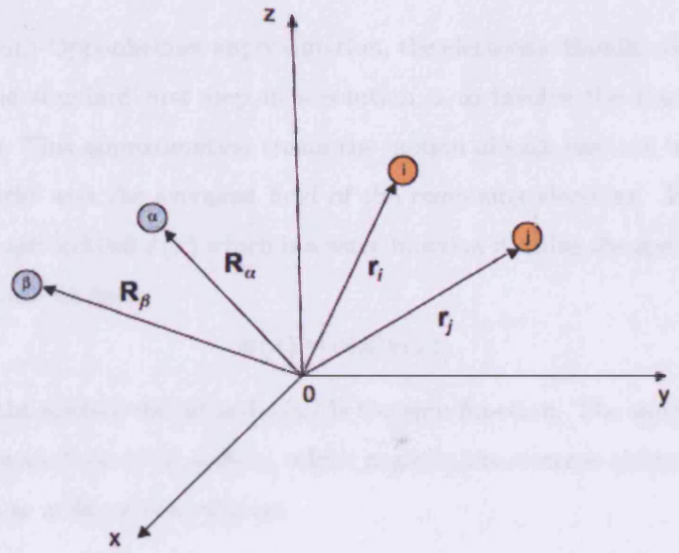

Figure 2.1: A molecular coordinate system: i, j = electrons; α, β = nuclei (Szabo and Ostlund, 1996).

over the electronic wave function. The nuclear Hamiltonian for the motion of the nuclei in the average field of the electrons can be written as

$$\begin{aligned} H_{nucl} &= -\frac{1}{2}\sum_{\alpha=1}^{N_n}\nabla_\alpha^2 + \left\langle -\sum_{j=1}^{N_e}\frac{1}{2}\nabla_j^2 - \sum_{\alpha=1}^{N_n}\sum_{j=1}^{N_e}\frac{Z_\alpha}{|\mathbf{r}_j-\mathbf{R}_\alpha|} + \sum_{i=1}^{N_e}\sum_{j>i}^{N_e}\frac{1}{|\mathbf{r}_i-\mathbf{r}_j|}\right\rangle \\ &\quad + \sum_{\alpha=1}^{N_n}\sum_{\beta>\alpha}^{N_n}\frac{Z_\alpha Z_\beta}{\mathbf{R}_{\alpha\beta}} \\ &= -\frac{1}{2}\sum_{\alpha=1}^{N_n}\nabla_\alpha^2 + \varepsilon_{elec}(\mathbf{R}_\alpha) + \sum_{\alpha=1}^{N_n}\sum_{\beta>\alpha}^{N_n}\frac{Z_\alpha Z_\beta}{\mathbf{R}_{\alpha\beta}} \\ &= -\frac{1}{2}\sum_{\alpha=1}^{N_n}\nabla_\alpha^2 + V(\mathbf{R}_\alpha) \end{aligned} \tag{2.3}$$

The total energy $V(\mathbf{R}_\alpha)$ provides a potential for nuclear motion. This function gives a potential energy surface as a function of nuclear geometries, $\mathbf{R}_\alpha$. In the Born-Oppenheimer approximation the nuclei move on a potential energy surface obtained by solving the electronic problem.

2.3 Hartree-Fock self consistent field method

Even within Born-Oppenheimer approximation, the electronic Hamiltonian (2.2) cannot be solved. The standard first step in a solution is to involve the Hartree-Fock (HF) approximation. This approximation treats the motion of each electron in the attractive field of the nuclei and the averaged field of the remaining electrons. Each electron is described by a spin orbital $\psi(\mathbf{x})$ which is a wave function defining the spatial distribution of an electron and its spin

$$\psi(\mathbf{x}) = \phi(\mathbf{x})\chi(\omega), \tag{2.4}$$

where $\phi(\mathbf{x})$ is the spatial orbital and $\chi(\omega)$ is the spin function. The simplest wave function to describe an N-electron system, which neglects the electron-electron interactions, can be written as a Slater determinant

$$\Psi_0(N) = (N!)^{-\frac{1}{2}} det|\phi_1(\mathbf{x}_1)\phi_2(\mathbf{x}_2)\cdots\phi_N(\mathbf{x}_N)| \tag{2.5}$$

where N electrons occupy N spin orbitals without specifying which electrons lie in which orbital. From the variational principle the best wave function is the one which gives the lowest electronic energy E_0 with the condition that the spin orbitals remain orthonormal. The HF equation can be derived by minimising E_0, this gives

$$f(i)|\phi_a(i)\rangle = \varepsilon_a|\phi_a(i)\rangle \tag{2.6}$$

where $f(i)$ is an effective one-electron operator, called the Fock operator, $\phi_a(i)$ is the spin orbital of the i-th electron and ε_a is the orbital energy of the spin orbital ϕ_a. The Fock operator is determined as the sum of a core-Hamiltonian operator $h(i)$ and an effective one-electron potential operator $G(i)$, called the HF potential

$$f(i) = h(i) + G(i) \tag{2.7}$$

where $h(i)$ is the kinetic energy and potential energy for attraction to the nuclei of a single electron

$$h(i) = -\frac{1}{2}\nabla_i^2 - \sum_{\alpha=1}^{N_n}\frac{Z_\alpha}{|\mathbf{r}_i - \mathbf{R}_\alpha|} \tag{2.8}$$

and the HF potential can be written as

$$G(i) = \sum_{b\neq a}[J_b(i) - K_b(i)] \tag{2.9}$$

where $J_b(i)$ and $K_b(i)$ represent the Coulomb and exchange operators respectively. They can be defined as

$$J_b(i)\phi_a(i) = \left[\int \phi_b^*(j)\phi_b(j)\frac{1}{r_{ij}}d\mathbf{x}_j\right]\phi_a(i) \tag{2.10}$$

$$K_b(i)\phi_a(i) = \left[\int \phi_b^*(j)\phi_a(j)\frac{1}{r_{ij}}d\mathbf{x}_j\right]\phi_b(i) \tag{2.11}$$

The Coulomb term is described as an average of the interactions between the i-th and j-th electrons over all the coordinates of the j-th electron. The exchange operator takes into account the interactions between the orbital and the $(N-1)$ other orbitals. The HF potential $G(i)$ depends on the spin orbitals so the nonlinear HF equation can be solved iteratively using the self-consistent field (SCF) approach. The main idea is to guess the initial set of spin orbitals, obtain the one-electron HF potential and solve the HF equation to get a new improved set of spin orbitals. The procedure has to be repeated until the self-consistency is reached. Two types of spin orbitals are obtained this way: occupied, the N spin orbitals with the lowest energies, and virtual,which lie at higher energies and are not occupied. The variational HF ground state Ψ_0 is described by a single Slater determinant, which arises from a set of occupied spin orbitals. The spatial molecular orbitals imposed in the HF method correspond to a linear combination of atomic orbitals

$$\phi(\mathbf{r}) = \sum_{\mu=1}^{K} C_\mu \varphi_\mu(\mathbf{r}) \tag{2.12}$$

where $\varphi_\mu(\mathbf{r})$ is a basis set of K spatial functions.

Two types of functions can be used for an atomic orbitals: Slater-type orbitals (STOs) introduced by Slater (1960) and Gaussian-type orbitals (GTOs) suggested by Boys (1950). These can be written as

$$\phi^S_{n,l,m}(r) = \sqrt{\frac{(2\zeta)^{2n+1}}{(2n)!}}r^{n-1}e^{-\zeta r}Y_{lm}(\theta,\phi) \tag{2.13}$$

$$\phi^G_{n,l,m}(r,\theta,\phi) = Nr^{n-1}e^{-\alpha r^2}Y_{lm}(\theta,\phi) \tag{2.14}$$

Both functions are the product of radial (r describe the distance between the electron and the nucleus) and angular functions (the $Y_{lm}(\theta,\phi)$ are spherical harmonics). ζ and α are the orbital exponents which determine the size of the basis function and N is the normalisation constant. STOs are based on solutions of the hydrogenic atom problem. GTOs have the computational advantage that the product of two GTOs centred on two different atoms is a single GTO centred on a point between the two atomic centres along

the axis connecting them. Thus the two-electron integrals on three or four atomic centres can be reduced to the sums of the two centre integrals.

Most of the properties of molecule which can be evaluated from a molecular wave function, such as dipole moment, are described by sum of one-electron operators. These can be written in the general form

$$\mathcal{O}_1 = \sum_{i=1}^{N} h(i) \tag{2.15}$$

where $h(i)$ is not necessarily the core-Hamiltonian, but any operator depending only on the coordinates of a single electron. The value for such operators will have a form

$$\langle \mathcal{O}_1 \rangle = \langle \Psi_0 | O_1 | \Psi_0 \rangle = \sum_{a}^{N/2} (\psi_a | h | \psi_a) = \sum_{\mu\nu} P_{\mu\nu} (\nu | h | \mu) \tag{2.16}$$

so that, in addition to the density matrix $\mathrm{P}_{\mu\nu}$, only the set of one-electron integrals $(\nu|h|\mu)$ has to be evaluated to calculate one-electron expectation value.

The classical definition of the dipole moment for a collection of charges q_i with position vectors $\mathbf{r}_i$ is

$$\vec{\mu} = \sum_{i} q_i \mathbf{r}_i \tag{2.17}$$

The quantum mechanical definition of the dipole moment can be written as

$$\vec{\mu} = \langle \Psi_0 | - \sum_{i=1}^{N} \mathbf{r}_i | \Psi_0 \rangle + \sum_{A} Z_A \mathbf{R}_A \tag{2.18}$$

where the first term is the quantum mechanical contribution of the electrons and the second term is classical contribution of the nuclei of charge Z_A to the dipole moment. The electronic dipole operator is $-\sum_{i=1}^{N} \mathbf{r}_i$, a sum of one-electron operators. The dipole moment can be rewritten by using equation 2.16 as

$$\vec{\mu} = -\sum_{\mu} \sum_{\nu} P_{\mu\nu} (\nu | \mathbf{r} | \mu) + \sum_{A} Z_A \mathbf{R}_A \tag{2.19}$$

2.4 Configuration interaction

The solution obtained with HF approximation is not the exact solution of the non-relativistic time-independent electronic Schrödinger equation. The HF approximation is useful in many cases but it has its limitations since the motion of electrons with opposite spin is not correlated. The difference between the exact non-relativistic energy of the system, E_0, and the HF energy, E_{HF}, is known as the correlation energy, E_{corr}

$$E_{corr} = E_0 - E_{HF} \tag{2.20}$$

This energy can be obtained by the configuration interaction (CI) method. The basic idea is to diagonalise the N-electron Hamiltonian in a basis of N-electron functions. In other words, the correlation effects can be calculated by the variational method with the exact wave function written as a linear combination of either Slater determinants or configuration state functions (CSFs). CSFs are spin-adapted antisymmetrised linear combinations of Slater determinants. The variational function can be written as

$$\Phi = c_0\Psi_0 + \sum_{ar} c_a^r \Psi_a^r + \frac{1}{2!}\sum_{abrs} c_{ab}^{rs}\Psi_{ab}^{rs} + \cdots \tag{2.21}$$

where Ψ_a^r is a singly excited configuration with an electron excited from the occupied orbital a in Ψ_0 to a virtual orbital r, Ψ_{ab}^{rs} is a doubly occupied configuration with two electrons excited from the occupied orbitals a and b to the virtual ones r and s. The factorial before the summation assure that a given excitation is included only once. The complete solution for a given basis of the non-relativistic Schrödinger equation can be obtained if the expansion includes n-tuply excited configuration. In this case the CI is called full CI (FCI) and produces a complete solution of the non-relativistic Schrödinger equation. The size of Hamiltonian matrix expands with the size of the basis set so the FCI calculations are achievable for a few small molecules using a proper basis set. A couple of the modifications can be introduced to shorten the CI function for example by using only singly and doubly excited configurations.

Another possibility is to use the complete active space CI (CASCI), which was used in the calculations described in chapter 4. In CASCI the orbitals can be divided into core, virtual and active orbitals. The lowest energy core orbitals are doubly occupied in all CSFs, the higher energy virtual orbitals are unoccupied and the medium energy active orbitals vary in occupancy (Shimamura, 1998). The CASCI is an FCI expansion within the active orbitals.

Another set of orbitals for use in a CI calculation were introduced by Löwdin (1955). They are called natural orbitals (NOs). The CI expansion with NOs is faster converging than with the HF orbitals. The NOs are the elements of an orthonormal basis which is related to the HF orbitals by a unitary transformation where the one electron reduced density matrix is diagonal and can be written as (Szabo and Ostlund, 1996)

$$\gamma(\mathbf{x}_1, \mathbf{x}_1') = N \int d\mathbf{x}_2 \cdots d\mathbf{x}_N \Phi(\mathbf{x}_1, \mathbf{x}_2, \cdots, \mathbf{x}_N)\Phi^*(\mathbf{x}_1', \mathbf{x}_2, \cdots, \mathbf{x}_N) \tag{2.22}$$

The one electron reduced density matrix can be expanded in the orthonormal basis of

HF spin orbitals ψ_i as

$$\gamma(\mathbf{x}_1, \mathbf{x}_1') = \sum_{ij} \psi_i(\mathbf{x}_1)\gamma_{ij}\psi_j^*(\mathbf{x}_1') \tag{2.23}$$

where

$$\gamma_{ij} = \int d\mathbf{x}_1 d\mathbf{x}_1' \psi_i^*(\mathbf{x}_1)\gamma(\mathbf{x}_1, \mathbf{x}_1')\psi_j(\mathbf{x}_1') \tag{2.24}$$

When Φ is the HF ground state wave function Ψ_0, the one electron reduced density matrix can be written as

$$\gamma^{HF}(\mathbf{x}_1, \mathbf{x}_1') = \sum_{a} \psi_a(\mathbf{x}_1)\psi_a^*(\mathbf{x}_1') \tag{2.25}$$

In general, when Φ is not Ψ_0, the one electron reduced density matrix in the basis of HF spin orbitals is not diagonal. Since γ is Hermitian, an orthonormal basis η_i in which the one electron reduced density matrix is diagonal can be defined and can be written as

$$\gamma(\mathbf{x}_1, \mathbf{x}_1') = \sum_{i} \lambda_i \eta_i(\mathbf{x}_1)\eta_i^*(\mathbf{x}_1') \tag{2.26}$$

where λ_i is the occupation number of the NOs in the wave function Φ and describes the average number of electrons in each NO. The NOs used in this work were obtained using approximate wave functions. They are therefore known as pseudo natural orbitals and are generated using single and double excitations into the orbital space of the target basis functions. The starting molecular orbitals used in the target calculations are the NOs with the largest occupation numbers, which are usually the ones with the lowest energy. The pseudo natural orbitals are averaged by giving different weights to target states. These orbitals are state-averaged NOs (see chapter 4).

2.5 Fixed-nuclei formulation

To describe electron-molecule collisions it is important to distinguish between electronic and nuclear coordinates within the molecule. A convenient reference frame can simplify the equations describing the collision process. Two reference frames can be determined (Lane, 1980): the laboratory (LAB) frame for the description of the collisions and the BODY frame which are shown in figures 2.2 and 2.3 respectively. The BODY frame has a system of coordinates fixed with respect to the molecule and by convention the body-fixed z axis is chosen along the maximum symmetry axis of the molecule. The BODY frame was used in the calculations in this thesis. In the LAB frame the z axis is usually fixed along the initial momentum k_0 of the incident electron. Both coordinate systems

have the common origin at the centre of mass of the molecule. $\mathbf{r}$ and $\mathbf{R}$ correspond to the electronic and nuclear coordinates of the molecule and γ represents the scattering electron coordinate in the BODY frame and the primed coordinates refer to the LAB frame. The electronic contribution to Hamiltonian for the electron-molecule system can be written as

$$H_{N+1}^{(elec)} = -\frac{1}{2}\nabla_\gamma^2 + H_N^{(elec)} + V_{em} \tag{2.27}$$

where $\frac{1}{2}\nabla_\gamma^2$ is the Laplacian in the BODY frame. H_N^{elec} is the target Hamiltonian and V_{em} is the electron-target molecule interaction potential energy. For a molecule with N_e electrons and N_n nuclei they can be written as

$$H_N^{(elec)} = -\frac{1}{2}\sum_{j=i}^{N_e}\nabla_j^2 - \sum_{\alpha=1}^{N_n}\sum_{j=1}^{N_e}\frac{Z_\alpha}{|\mathbf{r}'_j - \mathbf{R}_\alpha|} + \sum_{i=1}^{N_e}\sum_{j>i}^{N_e}\frac{1}{|\mathbf{r}'_i - \mathbf{r}'_j|} \tag{2.28}$$

$$V_{em}(\gamma', \mathbf{r}', \mathbf{R}) = -\sum_{\alpha=1}^{N_n}\frac{Z_\alpha}{|\gamma' - \mathbf{R}_\alpha|} + \sum_{j=1}^{N_e}\frac{1}{|\gamma' - \mathbf{r}'_j|} \tag{2.29}$$

For a diatomic target molecule the electronic states are described by $\psi_\alpha^{elec}(\mathbf{r},\mathbf{R})$, where α represents the electronic quantum numbers and r all the electron coordinates of the target. These wave functions must satisfy the electronic Schrödinger equation

$$[H_N^{(elec)} - E_\alpha^{elec}(\mathbf{R})]\psi_\alpha^{elec}(\mathbf{r};\mathbf{R}) = 0 \tag{2.30}$$

where $E_\alpha^{elec}(\mathbf{R})$ are the electronic states of the molecule. In the Schrödinger equation for $N_e + 1$ system the nuclear Hamiltonian is neglected

$$(H_{N+1}^{(elec)} - \varepsilon)\Psi_\varepsilon^{FN}(\gamma, \mathbf{r}; \mathbf{R}) = 0 \tag{2.31}$$

The fixed-nuclei approximation is accurate in the region where the electrons are close to the nuclei and their motion can be regarded as dominant in the interaction potential energy V_{em}. In the frame transformation procedure (Chang and Fano, 1972) the configuration space is divided into several regions. These depend on the distance between the scattered electron and the target molecule. Within the BODY frame the fixed-nuclei method is used only in the region where the short range interactions are strong but the electron spend, in this region, a small part of the collision time. At some boundary, the solutions can be transformed to the LAB frame and continued into the asymptotic region by introducing the nuclear Hamiltonian, H^n. A suitable radius can be found in order to ignore H^n in the inner region and difficult short range interactions in the outer region. The nuclear contribution to the molecular Hamiltonian can be written as

$$H_N(\mathbf{r}', \mathbf{R}) = H_N^{(elec)}(\mathbf{r}', \mathbf{R})H_N^n(\mathbf{R}) \tag{2.32}$$

2.5 Fixed-nuclei formulation

In the adiabatic approximation for the motion of the nuclei, the inner region can be extended to infinity and the problem can be solved in the BODY frame ignoring H^n.

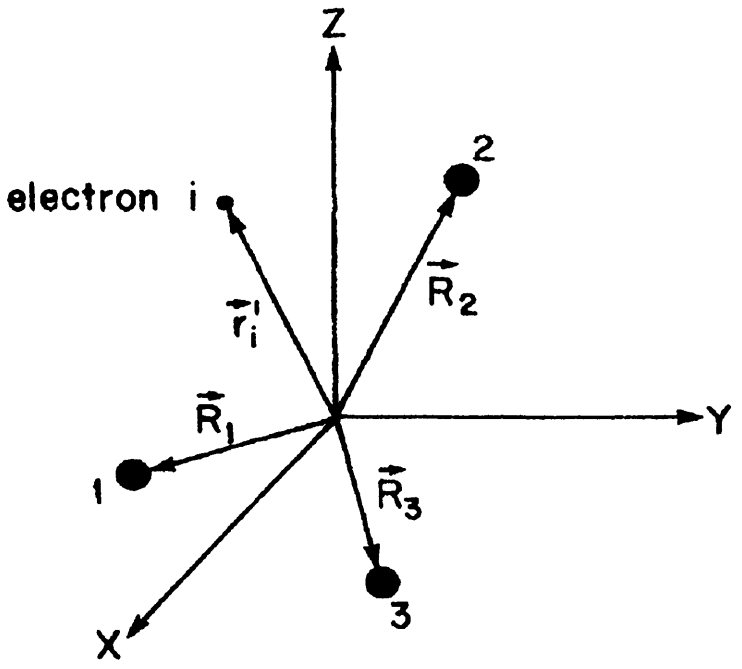

Figure 2.2: A molecular coordinate system in the LAB frame: i = electron; 1, 2, 3 = nuclei (Lane, 1980).

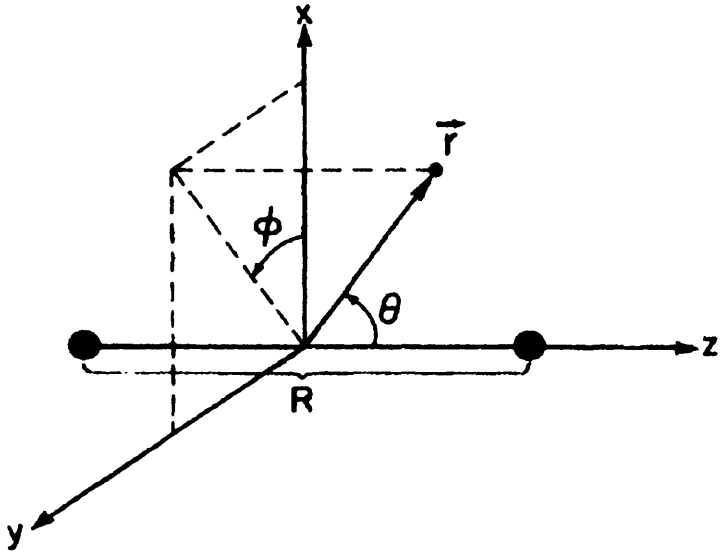

Figure 2.3: A molecular coordinate system in the BODY frame (Lane, 1980).

Chapter 3

R-matrix theory

3.1 General overview

The R-matrix approach was originally used for the study of nuclear collisions by Wigner (1946) and Wigner and Eisenbud (1947). Burke et al. (1971), Burke and Robb (1975) and Burke (1976) later developed this method for electron-atom collisions. Electron-molecule collisions were first implemented to the method by Schneider (1975); Schneider and Hay (1976) and further developed for diatomic molecules by Burke et al. (1977). Nestmann et al. (1994) and later Morgan et al. (1997) extended the method to polyatomic molecules.

The R-matrix theory is based on dividing configuration space into two regions: the inner region and the outer region (figures 3.1). The boundary between these regions is defined by a sphere of radius a centred at the centre of mass of the molecule. The sphere is chosen to just enclose the target charge distribution. In the inner region the potential is strong and multicentred, therefore exchange and correlation between the scattered electron and the electrons of the target molecule are important. The wave functions can be found by using adapted quantum chemistry methods. In the outer region exchange and correlation effects are neglected. Only the long range multipole potential is important and the single centre expansion of the wave function can be used.

In the internal region, a series of energy independent eigenfunctions and eigenvalues are calculated for the $(N + 1)$ electron system using a close coupling expansion, equation 3.5. The final inner region wave function is a linear combination of these

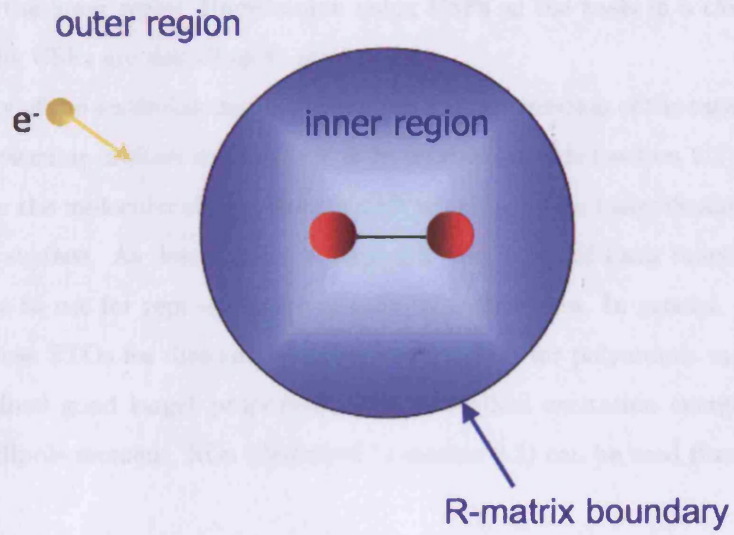

Figure 3.1: Division of configuration space in the fixed nuclei R-matrix theory.

with coefficients obtained by matching with the computed outer region functions at the boundary using the R-matrix. This is a sum over quantities, connected to the overlap integrals of the internal and external wave functions, assessed at the surface of the sphere and the eigenenergies of the internal states (Burke et al., 1977).

In the external region, the R-matrix constructed on the boundary is propagated outwards (Baluja et al., 1982; Morgan, 1984) until the internal solutions can be matched with asymptotic solutions. Asymptotic expansion methods (Noble and Nesbet, 1984) are applied to obtain the K-matrix from which eigenphase sums and T-matrix can be computed. The scattering informations, such as cross sections, can be derived from the T-matrix.

The R-matrix method for electron-atom and electron-molecule scattering is well summarised by Burke and Berrington (1993). The following sections discuss the R-matrix method as applied to polyatomic molecules based upon employing the UK R-matrix code which is in turn documented by Morgan et al. (1998) and Tennyson and Morgan (1999).

3.2 The inner region

The energy-independent $(N + 1)$-electrons scattering eigenfunctions are obtained by diagonalising the inner region Hamiltonian using CSFs as the basis in a close coupling expansion. The CSFs are described in section 2.3.

The quality of the scattering model depends on a representation of the target molecule. The target molecular orbitals are built up from atomic orbitals (section 2.3). These orbitals describe the molecular charge distribution which must be insignificantly small on the R-matrix surface. As described in section 2.3, two types of basis functions: STOs and GTOs are in use for representation of molecular structure. In general, the UK R-matrix codes use STOs for diatomic molecules and GTOs for polyatomic molecules. In order to obtained good target properties, such as vertical excitation energies and the ground state dipole moment, NOs (described in section 2.3) can be used throughout the calculations.

The target molecular orbitals are enhanced with a set of continuum orbitals, centred on the centre of gravity of the molecule. These orbitals have a longer range then the orbitals centred on the nuclei. They describe the scattered electron and do not vanish on the R-matrix boundary. The continuum functions can be written as

$$\eta_{il_i}(\mathbf{r_G}) = \frac{1}{r_G} u_{il}(r_G) Y_{l_i m_i}(\hat{\mathbf{r}}_\mathbf{G}) \tag{3.1}$$

where the Y_{lm} are complex spherical harmonics for the diatomic code. The polyatomic code uses real or "tesseral" spherical harmonics. $\hat{\mathbf{r}}_\mathbf{G}$ are the electron coordinates relative to the centre of gravity of the target molecule and the u_{il} are effective atomic orbitals. In the diatomic code, these are obtained by solving the model single channel scattering problem (Gillan et al., 1995)

$$\left[\frac{\partial^2}{\partial r^2} - \frac{l(l+1)}{r^2} + 2V_0(r) + k_i^2\right] u_{il}(r) = 0 \tag{3.2}$$

subject to the boundary condition

$$u_{il}(0) = 0 \tag{3.3}$$

and

$$\frac{1}{u_{il}} \frac{du_{il}}{dr}\bigg|_{r=a} = b \tag{3.4}$$

where in equation (3.2) k_i^2 are the eigenenergies in Rydbergs, V_0 is an arbitrary spherical potential and b in equation (3.4) is an arbitrary constant.

3.2 The inner region

The continuum basis functions used in polyatomic R-matrix calculations are the Gaussian functions and do not depend upon fixed boundary condition. Originally, the Gaussian continuum basis functions were found by fitting a GTO basis set to Bessel functions within the R-matrix sphere (Nestmann and Peyerimfoff, 1990). Subsequently using this method Faure et al. (2002) produced a program which constructs GTO continuum basis sets for representing both Bessel and Coulomb functions. The integrals including continuum basis functions are performed over the whole configuration space and the contribution from the region outside the R-matrix sphere is subtracted from the integrals over infinite range (Morgan et al., 1997). The continuum molecular orbitals are orthogonalised to the target orbitals using Schmidt orthogonalisation. Afterwards, symmetric or Löwdin orthogonalisation is used to orthogonalised continuum molecular orbitals among themselves and eliminate linearly dependent functions (Nestmann et al., 1994; Morgan et al., 1997).

The inner region scattering energy independent eigenfunctions of the $(N+1)$-electron system can be represented by

$$\psi_k^{N+1} = \mathcal{A} \sum_I \psi_I^N(\mathbf{X}_1, \cdots, \mathbf{X}_N) \sum_j \bar{\xi}_j(\mathbf{X}_{N+1}) a_{Ijk} + \sum_m \chi_m(\mathbf{X}_1, \cdots, \mathbf{X}_N, \mathbf{X}_{N+1}) b_{mk} \tag{3.5}$$

where $\mathcal{A}$ is the anti-symmetrisation operator, $\mathbf{X}_n = (\mathbf{r}_n, \sigma_n)$ with $\mathbf{r}_n$ the spatial coordinate and σ_n the spin state of the n^{th} electron, $\bar{\xi}_j$ is a continuum molecular orbital spin coupled with the scattered electron and a_{Ijk} and b_{mk} are variational coefficients.

The first summation runs over CI target states. It represents one electron in a continuum state with the remaining electrons in a target state, known as a 'target+continuum' configuration.

The summation in the second term runs over configurations χ_m in which all the electrons occupy target molecular orbitals and are known as L^2 functions. Considering the fact that the molecular orbitals are orthogonal, the L^2 functions are required to guarantee that important regions of configuration space are included. These configurations also account for correlation effects, including virtual excitation to higher electronic states, excluded in the first expansion.

As stated above, in the polyatomic R-matrix computations the continuum orbitals are not limited by the spherical boundary conditions at $r = a$. In order to make the Hamiltonian matrix Hermitian inside the R-matrix sphere, the surface or Bloch (Bloch,

1957) operator is included. This operator can be written as

$$L_{N+1} = \frac{1}{2}\sum_{i=1}^{N+1}\sum_{j}|\psi_j^N Y_{l_j m_{l_j}}(\hat{r}_i)\rangle\delta(r_i - a)\left(\frac{d}{dr_i} - \frac{b-1}{r_i}\right)\langle\psi_j^N Y_{l_j m_{l_j}}(\hat{r}_i)| \tag{3.6}$$

where a is the radius of the R-matrix sphere and b is an arbitrary constant defined by equation 3.4. The variational coefficients from equation 3.5 are determined by diagonalising the modified internal region Hamiltonian

$$\langle\Omega_p^{N+1}|H_{N+1} + L_{N+1}|\Omega_{p'}^{N+1}\rangle \tag{3.7}$$

where the Ω_p^{N+1} are the basis configurations, in order to derive the internal region $(N+1)$ eigenfunctions ψ_k^{N+1}.

The variational coefficients a_{Ijk} and b_{mk} are obtained by diagonalisation of the Born-Oppenheimer Hamiltonian matrix. The matrix elements are determined as the individual target configurations and are reconstructed to ones written as the CI target wave functions given by equation 3.5. The size of the transformed Hamiltonian matrix is significantly reduced as the number of the target states is usually smaller than the number of terms in the CI expansion. This process is called CI contraction (Tennyson, 1996).

The R-matrix on the boundary can be defined from the solutions of the Hamiltonian matrix. The R-matrix contains a complete description of the scattering problem in the internal region and provides the boundary conditions necessary to match the inner and outer regions wave functions, and solve the problem in the outer region.

The Schrödinger equation of the $(N + 1)$-electron system can be written as

$$H_{N+1}|\Psi\rangle = E|\Psi\rangle \tag{3.8}$$

where Ψ is the total $(N + 1)$-electron wave function and E is the total energy of the system. The R-matrix on the boundary can be obtained by the method developed by Shimamura (1977) using the Bloch operator. The equation 3.8 can be rewritten as

$$(H_{N+1} + L_{N+1} - E)|\Psi\rangle = L_{N+1}|\Psi\rangle \tag{3.9}$$

simply by adding and subtracting the Bloch operator. This operator projects the total wave function onto all the available products of the R-matrix surface. This projection is a wave function in the relative coordinate system of the scattered fragments. The equation 3.9 can be written in form of

$$|\Psi\rangle = (H_{N+1} + L_{N+1} - E)^{-1}L_{N+1}|\Psi\rangle. \tag{3.10}$$

Considering the fact that the internal region ψ_k^{N+1} are the eigenfunctions of the $(H_{N+1}+L_{N+1})$ Hamiltonian matrix with eigenvalues e_k, the inverse operator can take the form of an expansion over these functions to get

$$|\Psi\rangle = \sum_k \frac{|\psi_k^{N+1}\rangle\langle\psi_k^{N+1}|L_{N+1}|\Psi\rangle}{(e_k - E)} \tag{3.11}$$

with

$$\langle\psi_k^{N+1}|L_{N+1}|\Psi\rangle = \frac{1}{2}\sum_j F_j(r)\left(\frac{dF_j}{dr} - bF_j(r)\right)_{r=a} \tag{3.12}$$

where $F_j(r)$ are the truncated radial functions evaluated on the R-matrix sphere and calculated as

$$F_i(r) = \langle\psi_{I_i}^N Y_{l_i m_{l_i}}|\Psi\rangle. \tag{3.13}$$

In order to define the scattering wave function entirely it is essential to construct $F_j(r)$ and their derivatives at the R-matrix sphere. This can be done by substituting in the Bloch operator from equation 3.6 (Gillan et al., 1995)

$$F_i(r) = \sum_j R_{ij}(E)\left(a\frac{dF_j}{dr} - bF_j\right)_{r=a} \tag{3.14}$$

where $R_{ij}(E)$ is the R-matrix determined as

$$R_{ij}(E) = \frac{1}{2a}\sum_k \frac{f_{ik}(a)f_{jk}(a)}{e_k - E}. \tag{3.15}$$

The sum 3.15 is over the surface amplitudes f_{ik} and subsequently over the eigenfunctions ψ_k^{N+1}. The surface amplitudes f_{ik} can be written as

$$f_{ik} = \langle\psi_{I_i}^N Y_{l_i m_{l_i}}|\psi_k^{N+1}\rangle \tag{3.16}$$

where $\langle\psi_{I_i}^N Y_{l_i m_{l_i}}|$ are channel functions.

3.3 The outer region

The R-matrix from equation 3.15 is propagated to an appropriate radius (Morgan, 1984), where the interaction between the target molecule and scattered electron is considered to be small. Eventually the solutions to the scattering problem are produced by using a Gailitis expansion (Gailitis, 1976). In the external region the exchange and detailed electron-electron correlation between the scattering electron and the target electrons are negligible. The physical interactions dictate the scattering. The scattering electron

moves in the long-range multipole potential of the target molecule and a single centre close coupling expansion of the scattering wave function can be used (Gillan et al., 1995)

$$\Psi = \sum_i \overline{\phi}_i(\mathbf{x}_1 \cdots \mathbf{x}_N, \sigma_{N+1})\mathbf{r}_{N+1}^{-1} F_i(\mathbf{r}_{N+1}) Y_{l_i m l_i}(\hat{\mathbf{r}}_{N+1}) \tag{3.17}$$

where $\mathbf{x}_j = (\hat{\mathbf{r}}_j, \sigma_j)$, is the position and spin of the j^{th} target electron. The functions $\overline{\phi}_i$ are produced by coupling the scattering electron spin σ_{N+1} with the target state ϕ_i, and the F_i are reduced radial wave functions. The equation 3.17 can be introduced into the Schrödinger equation and projected onto the channel functions $[\overline{\psi}_i Y_{l_i m_{l_i}}]$. A set of coupled homogeneous differential equations for the radial wave functions F_i can be written as

$$\left(\frac{\partial^2}{\partial r^2} - \frac{l_i(l_i+1)}{r^2} + k_i^2\right) F_i(r) = 2\sum_j V_{ij}(r) F_j(r) \tag{3.18}$$

where V_{ij} is the potential matrix in the outer region which determines the coupling between the channels i and j. The quantity k_i^2 is defined as

$$k_i^2 = 2(E - \epsilon_i). \tag{3.19}$$

where ϵ_i is the eigenenergy of the target state ψ_I and E is the total energy of the system. Equation 3.18 can be solved by propagating the R-matrix from the boundary to the adequately large distances where the interaction between the scattering electron and target molecule can be treated as negligible (Baluja et al., 1982; Morgan, 1984). Gailitis (1976) asymptotic expansion methods are then used to solved the outer region problem (Noble and Nesbet, 1984). In the limit case $r \to \infty$ the reduced radial functions F_i in the equation 3.18 have asymptotic solutions j for each open channel i

$$F_{ij} \sim \frac{1}{\sqrt{k_i}}\left(\sin(k_i r - \frac{1}{2}l_i\pi)\delta_{ij} + \cos(k_i r - \frac{1}{2}l_i\pi)K_{ij}\right) \tag{3.20}$$

and $F_{ij} \sim 0$ for closed channels. The coefficients K_{ij} describe the real symmetric K-matrix, which contains all the scattering information. The radial function decays exponentially in the closed channels

$$F_{ij} \sim e^{-|k_i|r} \tag{3.21}$$

which suggest that there is no flux lost at infinity. Equation (3.21) is only valid if there are no long-range potentials coupling open and closed channels. If all n scattering channels are open, the asymptotic form of the radial functions $F_i(r)$ may be written in the form

$$F(r) \sim k^{-1/2}(F + GK) \tag{3.22}$$

where the channel momenta, k, are written as a diagonal matrix. The diagonal matrices F and G correspond to regular and irregular Coulomb (or Riccatti-Bessel) functions in each scattering channel. The asymptotic expression (3.22) defines the reaction K-matrix, K, appropriate for standing wave boundary conditions. The eigenphase sums, δ, can be obtained straight from the diagonalised K-matrix K^D_{ii}

$$\delta = \sum_i \arctan(K^D_{ii}) \tag{3.23}$$

where the sum is over the channels. The eigenphase sums can be used to search for resonances and will be discussed later. The K-matrix can be transformed into the scattering matrix $\mathbf{S}$

$$\mathbf{S} = (\mathbf{1} + i\mathbf{K})(\mathbf{1} - i\mathbf{K})^{-1}. \tag{3.24}$$

The T-matrix is obtained from the $\mathbf{S}$ matrix, $\mathbf{T} = \mathbf{S} - 1$, and can be employed to get the integral and differential cross sections. The integral cross section for excitation from the state i to i' can be written as (Burke, 1982)

$$\sigma(i \rightarrow i') = \frac{\pi}{k_i^2} \sum_S \frac{(2S+1)}{2(2S_i+1)} \sum_{\Gamma l l'} |T^{\Gamma S}_{i l i' l'}|^2 \tag{3.25}$$

where S_i is the spin angular momentum of the i^{th} target state, S is the total spin angular momentum, Γ runs over symmetry, l and l' are orbital angular momentum quantum numbers related to i and i' states. The number of partial waves required to converge the cross section can be very large as the interaction potential includes long range multipole potentials. The partial waves, which lie above a certain minimum angular momentum L_m, are only weakly scattered. The partial wave expansion of the scattering amplitude is cut off at some value L_m. So the integral cross section (equation 3.25) includes contributions from a finite number of angular momenta L. The remaining terms can be gained by the first Born approximation (FBA) (Chu and Dalgarno, 1974; Gibson et al., 1987). The FBA cross section can be obtained in closed form (Watson and McKoy, 1979; Fliflet and McKoy, 1980) without turning to a partial wave expansion and includes contributions from all angular momenta. The final integral cross section is

$$\sigma^B(i \rightarrow i') = \sigma^R(i \rightarrow i') + \Delta\sigma \tag{3.26}$$

where $\sigma^R(i \rightarrow i')$ is the approximate cross section gained by the R-matrix approach and $\Delta\sigma$ is the Born correction defined by

$$\Delta\sigma = \sigma^{FBA} - \sigma^{FBA}_{Lm} \tag{3.27}$$

where σ^{FBA} is the plane wave Born approximation cross section and $\sigma^{FBA}_{L_m}$ is the cross section derived from a finite expansion of the first Born cross section containing the same number of partial waves as $\sigma^R(i \rightarrow i')$.

3.3.1 Resonances

The eigenphase sum as well as the cross section mostly varies slowly as a function of the energy. Nonetheless in some cases the eigenphase sum increases quickly in some energy intervals of width Γ about a given energy E^r. This causes a change in the corresponding partial cross section in the crucial energy range. This phenomenon is called a resonance. A resonance can be thought of as a long lived metastable state of the target molecule into which the scattering electron is temporarily trapped. The lifetime τ of this metastable state is longer than the usual collision time.

A resonance which occurs when many channels are open is described by its position, E^r_i, and its partial decay widths, Γ^r_i, into the open channels. The eigenphase sum is fitted to a Breit-Wigner profile (for example Atkins and Friedman (1997)) and the resonance parameters are obtained

$$\eta(E) = \sum_i \tan^{-1}\left[\frac{\Gamma^r_i}{E - E^r_i}\right] + \sum_j a_j(E)E^j \tag{3.28}$$

where $a_j(E)$ is the background eigenphase and $\eta(E)$ is eigenphase sum. The resonances in C_2 electron scattering are found and fitted by a computer program RESON (Tennyson and Noble, 1984). Some of the fits can prove difficult, for example if the resonance lies near a threshold. In these cases another computer program TIMEDEL (Stibbe and Tennyson, 1998) can be used. The relationship between the lifetime τ and the resonance width Γ can be express by Heisenberg uncertainty $\Delta t \Delta E \geq \hbar/2$. Therefore with $\Delta t \simeq \tau$ and $\Delta E \simeq \Gamma$ the lifetime can be written as

$$\tau \simeq \frac{\hbar}{\Gamma}. \tag{3.29}$$

Fitting a resonance to a simple analitic form in a multi-channel situation is difficult due to the possible presence of shadow poles in the S-matrix on other Riemann sheets (Eden and Taylor, 1964).

Another method for fitting the resonances is the time-delay method (Stibbe and Tennyson, 1996). The time-delay matrix (Smith, 1960) is used to find the extra time of flight of the projectile due to its interaction with the target. A resonance appears

in a characteristic Lorentzian form in the longest time-delay, which can be fitted to find the relevant parameters. The resonances dominate the longest time-delay so much that the background can be treated as constant. This is important in case of collisions with molecules which have many degenerate channels. All of these contribute to the eigenphase sum. The time-delay is calculated by TIMEDEL as a function of energy from K-matrices and then the resultant time-delay is fitted to a Lorentzian profile to find the resonance.

Resonances can be categorised into three types: shape, core-excited and nuclear-excited resonances. The first two species can be found in atoms and molecules. The nuclear-excited resonances occur only in molecules.

Shape resonances are defined as a one-electron event and happen when the scattering electron is captured by the effective potential, created by the target molecule, before tunnelling out. This potential is a combination of the attractive polarisation potential and centrifugal repulsive potential $(l(l+1)/r^2)$. This type of resonance is are usually linked with the ground state of the target molecule and lies a few eV above the ground state. They are normally broad and have short lifetimes as they can easily decay back into the ground state. They cannot be found in s-waves, $l = 0$. Low lying shape resonances can become a bound state when the molecular bond lengths are increased; this happens in dissociative attachment: $AB + e^- \longrightarrow A + B^-$ or $A^- + B$.

Core-excited resonances appear when the scattering electron excites the target molecule and is captured or forms a quasi bound state. This type of resonance is linked with excited states where the captured electron is in an orbital of the field generated by the excited target state. The core-excited resonances can be classified either as Feshbach or core-excited shape resonances.

Closed-channel resonances are known as *Feshbach resonances* (Feshbach, 1958, 1962) and are associated with parent single excited states which have a positive electron affinity. This type of resonance lies below the parent and the resonance energy curve follows the parent potential energy curve. This way energy restrictions do not allow the resonance to decay into its parent and it must decay into a lower state. Feshbach resonances are usually long lived and narrow. They are possible for all partial waves but cannot be obtained from models with a frozen target molecule.

Core-excited shape resonances are associated with parents of negative electron affinity. This type of resonances lies above its parent state. These resonances are similar to the

ground state shape resonances because they decay into all lower target states but usually preferably into their parent excited state.

Nuclear-excited resonances can be found at low energy, when the $(N+1)$-electron system has a weakly bound state. In this case the nuclear excitation is vibrational excitation or nuclear motion rather then excitation of a nucleus. This type of resonance is usually very narrow and low in energy. They always appear when a target molecule is an ion and can only be examined by going beyond the Born-Oppenheimer approximation. They will not be considered in this work.

3.3.2 Bound states

The total wave function of the bound $(N+1)$-electron system Ψ_i in the internal region can be expanded in term of the complete set of functions ψ_k^{N+1} of equation 3.5

$$\Psi_J = \sum_k \psi_k^{N+1} C_{kJ} \tag{3.30}$$

where C_{kJ} are the bound state coefficients. To obtain the bound states the external region functions must lead to zero as the distance of the scattered electron tend to infinity and must match the internal region functions at the R-matrix boundary. These external region functions are obtained by first using the Gailitis expansion method (Noble and Nesbet, 1984) and then propagated inwards to the R-matrix boundary using the Runge-Kutta-Nystrom method to solve numerically the asymptotic equations (NAG library routine D02LAF).

The matching conditions at the R-matrix boundary for bound state can be written as (Seaton, 1985)

$$F_i = \sum_j P_{ij} X_j \tag{3.31}$$

and

$$\frac{dF_i}{dr} = \sum_j \frac{dP_{ij}}{dr} X_j \tag{3.32}$$

where the F_i are the reduced radial functions specified in section 3.2, the P_{ij} are the outer region functions and X_j is a column vector necessary to produce the bound state coefficients C_{kJ} defined by the equation

$$C_{kJ} = \sum_i \frac{f_{ik}}{2(e_k - E)} \sum_j \left(\frac{dP_{ij}}{dr} - \beta P_{ij} \right) X_j. \tag{3.33}$$

The standard form of matching condition can be obtained by combining equations 3.14, 3.31 and 3.32

$$\sum_j B_{ij} X_j = \sum_j \left(P_{ij} - \left[\sum_k R_{ik}(E) Q_{kj} \right] \right) X_j = 0 \tag{3.34}$$

where

$$Q_{kj} = \frac{dP_{kj}}{dr} - \beta P_{kj}. \tag{3.35}$$

The equation 3.34 only has solutions at discrete values of energy E, the bound state energies, where the determinant of the B_{ij} matrix is zero. At the energies near to the R-matrix pole energies e_k the R-matrix in the equation 3.15 is not clearly defined and consequently neither is B_{ij}. These poles are eliminated using the method described by Burke and Seaton (1984). The B_{ij} matrix can be represented in a form where only for $i = I$ has energy dependent terms. This last row can be multiplied by $(e_K - E)$. K is the index of the R-matrix pole which lies closest to the total energy of the system in order to eliminate any computational errors caused by the closeness of the R-matrix pole. The K is determined by looking through the R-matrix poles to identify the pole closest to E. The equation for R-matrix (3.15) can be rewritten in a form

$$R_{ij} = \frac{S_{ij}}{2a(e_K - E)} + T_{ij} \tag{3.36}$$

where

$$S_{ij} = f_{iK}(a) f_{jK}(a) \tag{3.37}$$

and

$$T_{ij}(E) = \frac{1}{2a} \sum_{k \neq K} f_{ik} (e_k - E)^{-1} f_{jk}. \tag{3.38}$$

The next step is to find the solution of the eigenvalue problem

$$\sum_j S_{ij} U_{ik} = \sum_k U_{ik} s_k \tag{3.39}$$

Burke and Seaton (1984) showed that this equation is satisfied when U_{ij} is defined as

$$U_{ij} = \begin{cases} f_{iK} f_{(j+1)K} / \Gamma_j \Gamma_{j+1} & i = 1, \ldots, j \\ -\Gamma_j / \Gamma_{j+1} & i = j+1 \quad j = 1, \ldots, (I-1) \\ 0 & i > (j+1) \end{cases} \tag{3.40}$$

and

$$U_{iI} = \frac{f_{iK}}{\Gamma_I} \quad i = 1, \ldots, I \quad j = I \tag{3.41}$$

where I is the total number of channels and

$$\Gamma_j = \left(\sum_{i=1}^{j} f_{iK}^2 \right)^{\frac{1}{2}}. \tag{3.42}$$

Then the U_{ij} matrix is normalised to the form

$$\sum_l U_{il}^T U_{lj} = \delta_{ij} \tag{3.43}$$

where the U_{ij}^T is the transpose of U_{ij}. The solution for s_k can be written as

$$s_k = \delta_{kI} \Gamma_I^2. \tag{3.44}$$

The matching condition can be obtained by compounding equations 3.34 and 3.36 and by multiplying by the U_{ij}^T matrix

$$\sum_{i'=1}^{I} L_{ii'} X_{i'} = 0 \quad i = 1, \ldots, (I-1) \tag{3.45}$$

and

$$\sum_{i'=1}^{I} \left[L_{Ii'} - \frac{1}{2a(e_K - E)} \Gamma^2 M_{Ii'} \right] X_{i'} = 0 \tag{3.46}$$

where

$$L_{ij} = \sum_l U_{il}^T \left[P_{lj} - \left(\sum_l T_{lm} Q_{mj} \right) \right] \tag{3.47}$$

and

$$M_{ij} = \sum_l U_{il}^T Q_{lj}. \tag{3.48}$$

Now the quantity $(e_K - E)$ occurs only in the equation 3.38. To exclude any singularities the B_{ij} matrix can be redefined by multiplying this equation by this quantity

$$B_{ii'} = L_{ii'} \quad i = 1, \ldots, (I-1) \tag{3.49}$$

and

$$B_{Ii'} = (e_K - E) L_{Ii'} - \Gamma^2 M_{Ii'}. \tag{3.50}$$

In the atomic case there is only a small number of bound states associated with each value of a principal quantum number n for a given total symmetry. In general, this is not true in molecular cases. Hence a method of searching for arbitrary numbers of bound state poles for a given principal quantum number was introduced (Sarpal et al., 1991). The search for zeros in the determinant B_{ij} can be finalised by using a quantum defect grid. The effective quantum number ν can be written as (Seaton, 1985)

$$\nu = n - \delta_n \tag{3.51}$$

where n is the principal quantum number and δ_n is the quantum defect. An equally spaced grid of effective quantum number is determined around the lowest value of the principal quantum number considered. The determinant B_{ij} is calculated at energies which correspond to the effective quantum number grid points. Zeros of the determinant are detected by a change in sign of the determinant from one grid point to the next. If no change of sign is found, a search for two poles between grid points is initiated by fitting the determinant B_{ij} to a quadratic function. Once the energy region of a bound state is found, a Newton-Raphson search is carried out to gain an initial estimate of the bound state energy. This energy E_1 is considered to be very close to the true value E_0 and the first two terms of a Taylor series expansion are taken to establish the standard eigenvalue equation

$$\sum_j B_{ij}(E)X_j = \sum_j \left(B_{ij}(E_1) + (E_0 - E_1)\frac{dB_{ij}(E_1)}{dE} \right) X_j = 0. \tag{3.52}$$

This relation is applied recursively until the required accuracy in E_0 is achieved (appendix 3 of Seaton (1985)). This generates the bound state energy and eigenvector required to construct the bound state wave function.

3.4 Molecular R-matrix with pseudostates method

The standard close-coupling expansions used in the standard R-matrix method are incomplete since they cannot include all excited target states and they do not account for the continuum of the target. Intermediate energy processes, where the collision energy lies near to or above the ionisation threshold (IT), cannot be treated by the standard R-matrix approach. Bartschat et al. (1996) developed the atomic R-matrix with pseudostates (RMPS) method. This method was later adapted and implemented as a part of the UK R-matrix polyatomic code (Morgan et al., 1998) by Gorfinkiel and Tennyson (2004) and it is called molecular RMPS (MRMPS).

The basic idea of the RMPS method is to include in the close-coupling expansion a number of wave functions ϕ_i which correspond to pseudostates. These are not true eigenstates of the target molecule but they can describe the electronic continuum if selected correctly. The pseudostates are usually acquired by diagonalising the target Hamiltonian matrix described in a suitable basis of configurations. If the pseudostates are suppose to represent the continuum, some of the configurations used in the CI expansion correspond to the electronic density of an ionised state. This can be achieved

by the suitable selection of the target orbitals and particular configurations in the CI expansion must be involved.

Gorfinkiel and Tennyson (2004) introduced a new set of orbitals called pseudo-continuum orbitals (PCOs) to be able to obtain configurations which describe an ionised target. So in the CI expansion two sets of configurations are enclosed: the typical one where all the electrons occupy molecular orbitals and the new one in which one of the electrons occupies a PCO. For example in the calculations of Gorfinkiel and Tennyson (2004) for H_3^+ using the notation for irreducible representations of C_{2v} the configurations can be written as

$(1\text{ - }5a_1\ 1\text{ - }3b_1\ 1\text{ - }3b_2\ 1a_2)^2$

$1a_1^1(6\text{ - }35a_1\ 4\text{ - }17b_1\ 4\text{ - }18b_2\ 2\text{ - }8a_2)^1$

where the orbital in the first line are MOs and orbitals $(6\text{ - }35a_1\ 4\text{ - }17b_1\ 4\text{ - }18b_2\ 2\text{ - }8a_2)$ in the second line represent PCOs. Only excitations from the main ground state configuration are permitted. Selected this way, the configurations do not allow for excitation-ionisation but make the computation of the pure ionisation cross section easier. Gorfinkiel and Tennyson (2004) represented the PCOs using an even-tempered basis set (Schmidt and Ruedenberg, 1979) of GTOs centred at the centre of mass of the system. The exponents of the GTOs in this type of basis sets are

$$\alpha_i = \alpha_0 \beta^{(i-1)} \quad i = 1, \ldots, L. \tag{3.53}$$

Different basis sets can be produced by changing the parameters α_0 and β. This generation of different basis sets is very useful when an averaging process is used to omit emerging pseaudoresonances (see below). In any case, the parameters α_0 and β must be chosen sensibly so that the electronic density of all the target states involved in the close-coupling expansion (3.5) is included inside the R-matrix box. In other words, the amplitudes of the basis functions used to expand the MOs must be vanishingly small at the boundary. This must also be valid for the GTOs expanding the PCOs hence imposing a lower limit on the values of α_0 that can be applied. Smaller values of β produce a more complete set of pseudostate but make it difficult to avoid linear dependence, so the β must be selected very carefully. It is essential to confirm that

$$\alpha_i^{PCOs} \geq \alpha_j^{continuum} \quad \forall i, j \tag{3.54}$$

in order to avoid unnecessary complications in the orthogonalisation.

Gorfinkiel and Tennyson (2004) included an extra orthogonalisation step in order to

include PCOs. The PCOs are first Schmidt orthogonalised to the target MOs and then symmetric orthogonalised among themselves. The final set of MOs and PCOs is then handled as the target MOs set in the standard calculation.

The $(N + 1)$ wave functions must be constructed inside the R-matrix sphere. In the $(N + 1)$ expansion Gorfinkiel and Tennyson (2004) took into account the following configurations

$(1\text{ - }5a_1\ 1\text{ - }3b_1\ 1\text{ - }3b_2\ 1a_2)^2\ (COs)^1$

$1a_1^1\ (6\text{ - }35a_1\ 4\text{ - }17b_1\ 4\text{ - }18b_2\ 2\text{ - }8a_2)^1\ (COs)^1$

where COs are continuum orbitals and the L^2 functions can be written as

$(1\text{ - }5a_1\ 1\text{ - }3b_1\ 1\text{ - }3b_2\ 1a_2)^3$

$(1\text{ - }5a_1\ 1\text{ - }3b_1\ 1\text{ - }3b_2\ 1a_2)^2\ (6\text{ - }35a_1\ 4\text{ - }17b_1\ 4\text{ - }18b_2\ 2\text{ - }8a_2)^1$

$1a_1^1\ (6\text{ - }35a_1\ 4\text{ - }17b_1\ 4\text{ - }18b_2\ 2\text{ - }8a_2)^2$

so the N and $(N + 1)$ calculations are consistent. In this work it was necessary to generalise these to a problem involving a multiple electron target, see chapter 6.

In the standard R-matrix calculation, computationally the most challenging step is the diagonalisation of the $(N + 1)$ Hamiltonian matrix in order to define the wave functions of equation 3.5. In the MRMPS method, the number of channels increases and the propagation step takes longer. As the pseudostates are included in the calculation, unphysical resonances may appear above IT. To deal with the pseudoresonances above the IT, Gorfinkiel and Tennyson (2004) suggested a convolution process followed by an averaging of the convoluted results. The final cross section can be then written in a form

$$\sigma^{ION}(E) = \frac{1}{\sqrt[4]{\frac{\pi}{\sqrt{E}}}} \sum_i^4 \int_{E_m}^{E_M} e^{-\sqrt{E}(E'-E)^2} \sigma_i^{ion}(E'; \alpha_{0i}) dE' \tag{3.55}$$

where E_m is a given value 0.5 $E_\hbar$ smaller than IT and E_M is at least 0.5 $E_\hbar$ greater than the maximum energy for which the cross section is introduced. This technique smooths all resonances but will lead to errors. An correct procedure is to average the T-matrix (Burke et al., 1987; Slim and Stelbovics, 1987, 1988) although this has yet to be tried for MRMPS calculations.

3.5 Partitioned R-matrix

In the standard R-matrix theory all the solutions (eigenvalues and eigenvectors) of the Hamiltonian matrix (3.7) must be calculated explicitly. Problems arise when large configuration interaction expansions are required for the target molecule. In this case the

Hamiltonian matrix is usually too large to be diagonalised. Berrington and Ballance (2002) suggested a partitioned R-matrix theory in which only a proportion, P, of the solutions of the Hamiltonian matrix of dimension M are explicitly required. To save a significant amount of the computational time, P must be considerably smaller then M. Two quantities need to be defined in partitioned R-matrix theory (Berrington and Ballance, 2002). The first one is an effective energy E_0 for the poles excluded when only the lowest P solutions are explicitly acknowledge. This energy was determined as

$$E_0 = \frac{(\sum_{l=1}^{M} H_{I,I} - \sum_{k=1}^{P} E_k)}{M - P} \tag{3.56}$$

where the first sum runs over all the diagonal elements of the Hamiltonian matrix. The second quantity necessary in this method is the total probability distribution of a given channel on the R-matrix boundary

$$s_i = \sum_{l=1}^{n_i} (u_{il}(a))^2 \tag{3.57}$$

where u_{ilj} is a continuum orbital which explicitly depends on partial wave expansion. Berrington and Ballance (2002) then derived the equation for the partition R-matrix

$$R_{il,i'l_{i'}}(a,E) = \sum_{k=1}^{P} f_{ilk}(a) f_{i'lk}(a) \left(\frac{1}{e_k - E} - \frac{1}{E_0 - E} \right) + \delta_{ii'}\delta_{ll'} \left(\frac{s_{il}}{E_0 - E} + R_{il}^B + R_{il}^C \right) \tag{3.58}$$

where E is the electron collision energy, R_{il}^B is the Buttle correction (Buttle, 1967) and R_{il}^C is the error correction define be Berrington and Ballance (2002) as

$$R_{il}^C = \sum_{j=J_i}^{n_{il}} (u_{ilj}(a))^2 \left(\frac{1}{E_{ilj} - E} - \frac{1}{E_0 - E} \right) \tag{3.59}$$

where E_{ilj} is the energy of the continuum basis function u_{ilj}. The sum in the error correction term starts from J_i. This point is chosen such that $E_{ilj} > E_P$, where E_P is the highest R-matrix pole explicitly enclosed in the summation in equation (3.58).

Three problems were detected by Tennyson (2004) when the theory described above was applied to the molecular case. The first problem was related to the definition of the energy of individual continuum orbitals E_{ilj}. The numerical process for the generation of Gaussian type orbitals to describe the continuum for scattering from polyatomic molecules (Faure et al., 2002) provides a well defined energy for the continuum orbitals. Nevertheless, after the continuum orbitals and the molecular orbitals are orthonormalised (Morgan et al., 1998), the energy of the resultant continuum molecular orbital is not

well determined. The error correction term can be redefined by using the appropriate diagonal element of the Hamiltonian matrix $H_{I,I}$

$$R_{il}^{C} = \sum_{j=J_i}^{n_{il}} (u_{ilj}(a))^2 \left(\frac{1}{H_{ilj,ilj} - E} - \frac{1}{E_0 - E} \right). \tag{3.60}$$

The second problem which appears, is linked with the definition of the effective energy E_0, equation 3.56. This characterisation averages over all diagonal elements of the Hamiltonian matrix without considering whether the configuration involved makes any contribution to the boundary amplitude. In this sense, many high-lying L^2 configurations add to the value E_0 but do not contribute to the boundary amplitude. The number of the L^2 configurations increases with the systematic improvement of the CI representation of the target molecule. Due to this, E_0 will continuously rise even if all the other parameters in the calculation do not change. So E_0 must be defined in such way that only those configurations which contribute directly to the boundary amplitudes and consequently to the R-matrix are considered. Generally, the Hamiltonian matrix is diagonally dominant so the lowest P diagonal elements can be identified with the lowest P R-matrix poles. So E_0 can be obtained by averaging those diagonal elements of the Hamiltonian matrix, $H_{ilj,ilj}$, which are not among the lowest P diagonal elements. This process is suitable even when the values of higher lying R-matrix poles are not dominated by the diagonal elements. This is possible for the large CI expansion.

The last problem is linked to the error correction term in equation 3.59. The appliance of the whole boundary amplitude of the higher lying continuum orbitals $(u_{ilj}(a))^2$, will cause an over correction in the case when this orbital contributes to the lowest P states provided in the first summation in equation 3.58. The contribution of the continuum orbital to the states which are not explicitly included in this summation can be estimated (Tennyson, 2004) as

$$X_{ilj} = 1 - \sum_{k=1}^{P} a_{iljk}^2. \tag{3.61}$$

Then the final error correction term can be written as

$$R_{il}^{C} = \sum_{j=J_i}^{n_{il}} (u_{ilj}(a))^2 X_{ilj} \left(\frac{1}{H_{ilj,ilj} - E} - \frac{1}{E_0 - E} \right). \tag{3.62}$$

Implementing the partitioned R-matrix method requires significant changes to the outer region program code. These changes were performed as part of this thesis combined with testing the method for problems significantly larger than those previously considered.

3.6 Computational implementation

The UK Molecular R-matrix scattering package has been developed over many years by many people. R-matrix calculations can be divided into a few basic computational stages. These are the generation of integrals, the generation of a set of molecular orbitals, the construction and diagonalisation of the inner region Hamiltonian matrix, the calculation of the target properties and the solution of the outer region scattering.

The inner region polyatomic suite is built on the quantum chemistry 'Molecule-Sweden' codes generated by Almlof and Taylor (1984). In the initial quantum chemistry program the range of integration is over an infinite region, while in the inner $(N + 1)$ R-matrix calculations the range of spatial integration must be restricted to the finite sphere. To minimise the computational efforts, the contribution from the region outside the sphere was subtracted from the integrals over an infinite range. This was carried out in the program GAUSTAIL developed by Morgan et al. (1997, 1998). The figures 3.2 and 3.3 display respectively flow diagrams for the inner region N and $(N + 1)$-electron calculations.

SWMOL3 generates one and two electron atomic integrals. It provides the necessary integrals to be used by the module SWORD. SWMOL3 was developed from a Cray version of the integral generator 'MOL3'.

GAUSTAIL analyses the contribution to each integral from outside the R-matrix sphere. This has to be subtracted from the integrals over an infinite range. This program also modifies the Hamiltonian matrix by adding matrix elements of a Bloch operator, to make it Hermitian. These matrix elements are surface terms which contribute in the 'tail' integrals.

SWORD first subtracts the 'tail' integrals from the atomic integrals output from SWMOL3 and then carries out reordering of the integrals.

SWFJK builds up combinations of Coulomb and exchange integrals for the Fock matrix to be used in an SCF calculation.

SWSCF carries out a self consistent field calculation to produce target orbitals from linear combinations of atomic orbitals. This module is virtually unchanged version of the equivalent in the Molecule-Sweden package.

SWEDMOS forms orthogonal molecular orbitals. First, it uses the Schmidt method to orthogonalise each of the continuum orbital to all the target orbitals. Then it applies the symmetric method to orthogonalise the continuum orbitals among themselves and

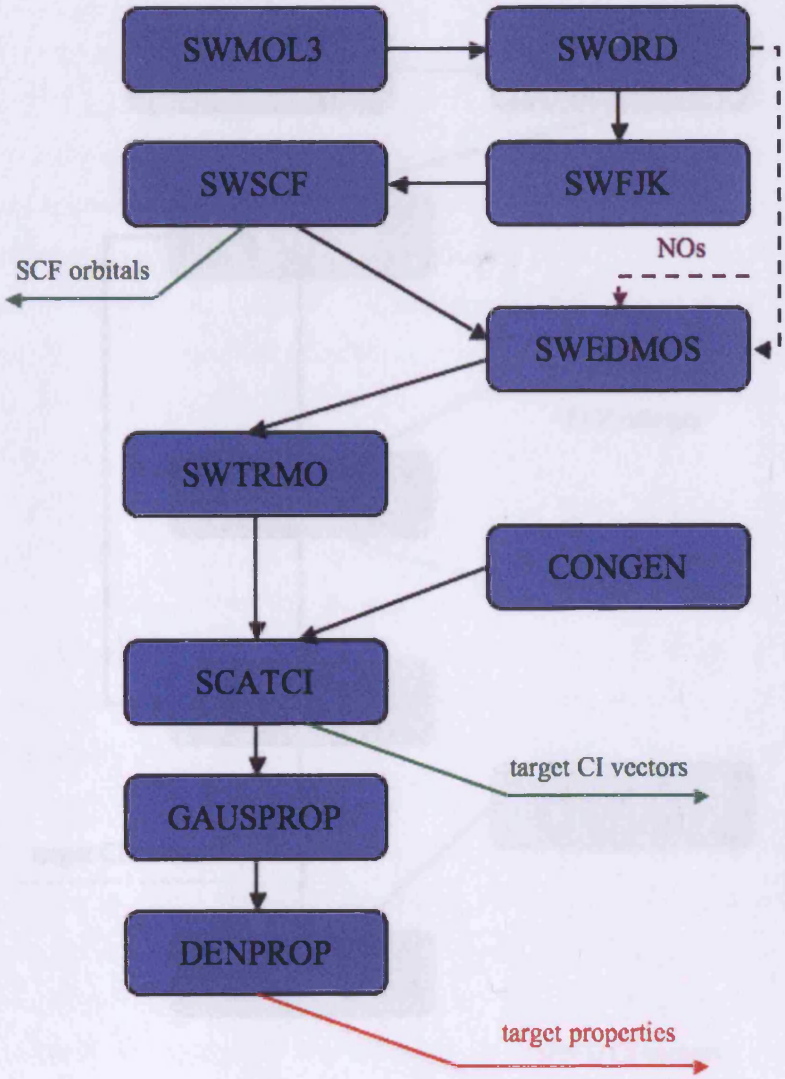

Figure 3.2: Flow diagram for the inner region target state calculation. Red arrows indicate an input required by the outer region programs. If NOs are used then the modules SWFJK and SWSCF are skipped.

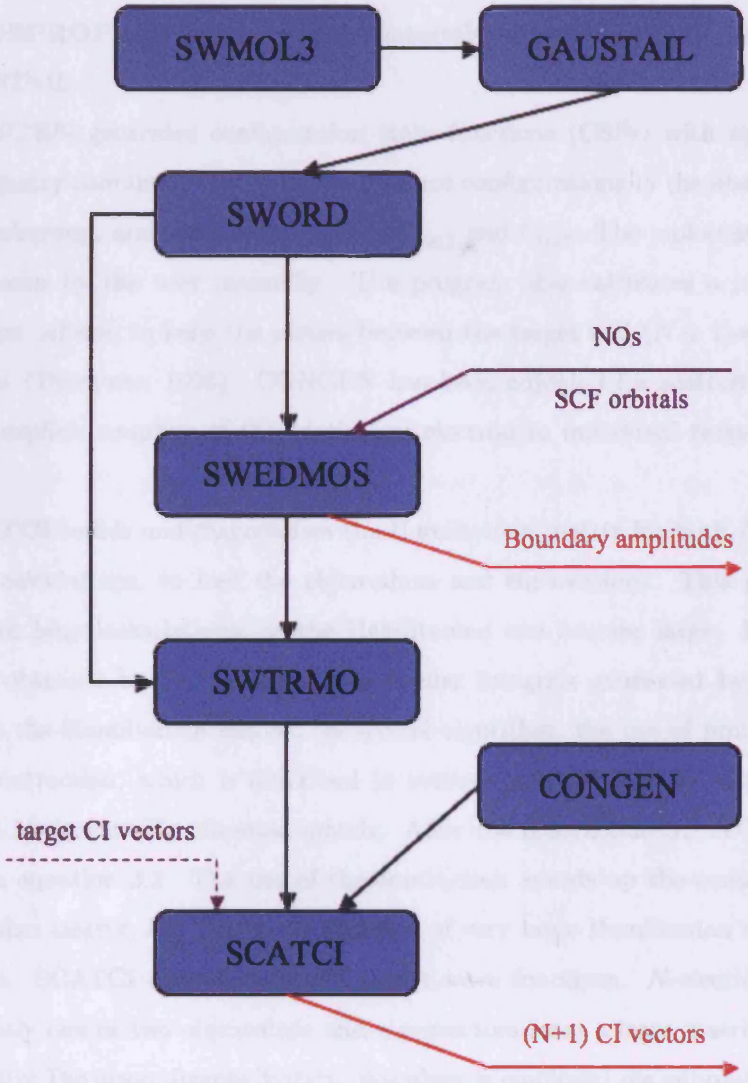

Figure 3.3: Flow diagram for the inner region scattering calculation. Red arrows indicate an input required by the outer region programs.

throws out those orbitals which correspond to very small eigenvalues of the overlap matrices. It is run twice for MRMPS calculations. Once to orthogonalise the PCOs and again to orthogonalise the COs.

SWTRMO implements the four-index transformation of ordered integrals generated by SWMOL3.

GAUSPROP analyses the property integrals demanded by DENPROP. It is based on GAUSTAIL.

CONGEN generates configuration state functions (CSFs) with appropriate spin and symmetry coupling. The code can produce configurations in the abelian group D_{2h} and its subgroup, and non-abelian groups $D_{\infty h}$ and $C_{\infty v}$. The molecular orbitals have to be chosen by the user manually. The program also calculates a phase factor for each target orbital, to keep the phases between the target and $(N+1)$-electron system consistent (Tennyson, 1996). CONGEN has been adjusted for scattering calculations to allow explicit coupling of the continuum electron to individual target state (Noble, 1982).

SCATCI builds and diagonalises the Hamiltonian matrix for both N and $(N+1)$-electron calculations, to find the eigenvalues and eigenvectors. This program is the slowest for large calculations, as the Hamiltonian can become large. It takes configurations obtained by CONGEN and molecular integrals generated by SWTRMO to construct the Hamiltonian matrix. A special algorithm, the use of prototype CSFs to do the contraction, which is described in section (3.2), is used to reduce the size of the $(N+1)$-electron Hamiltonian matrix. After the contraction SCATCI multiplies $\bar{\xi}_j$ by ψ_I^N in equation 3.5. The use of the contraction speeds up the construction of the Hamiltonian matrix, but the diagonalisation of very large Hamiltonian matrices is still expensive. SCATCI also produces CI target wave functions. N-electron calculations require only one or two eigenvalues and eigenvectors from a large matrix. In this case the iterative Davidson diagonalisation procedure is employed *via* subroutine DVDSON, written by Stathopoulos and Fisher (1982). For $(N+1)$-electron calculations all eigenvalues and eigenvectors are required and in-core Givens-Householder diagonalisation is applied *via* LAPACK subroutine *dsyev*. In case of the partitioned implementation, the diagonalisation is handled by the ARPACK diagonaliser (Lehoucq et al., 1996).

DENPROP computes properties such as permanent dipoles, transition moments and polarizabilities from input target wave functions obtained by SCATCI and the prop-

erty integrals generated by SWMOL3. The target properties are then used in the outer region scattering calculation.

PSN produces pseudo-natural orbitals by diagonalising the density matrices supplied by DENPROP. These are averaged by giving different weights to target states and hence the PSN can generate state-averaged NOs. This module is added to the end of the N-electron target calculation. Then a second target calculation is carried out (as shown in figure 3.2 indicated by the dashed arrows). This time there is no need to include in the calculation modules SWSCF and SWFJK. Hence the module SWEDMOS uses as input the newly obtained NOs.

The outer region programs for the electron scattering have been developed by Morgan unless specified otherwise. The figure 3.4 gives a flow diagram for the outer region calculations reported in these thesis. Other modules also exist.

SWINTERF supplies the interface between the inner and outer regions. This program uses three input files obtained in the inner region calculations: boundary amplitudes (SWEDMOS), eigenvalues and eigenvectors of the $(N+1)$-electron Hamiltonian (SCATCI), target data (DENPROP). Two output files from SWINTERF are required for other outer region calculations. The first file holds target properties, channel data and overall symmetry of the system. The second one contains data for the construction of the R-matrix and the coefficients of a multipole expansion of the long range scattering potentials. Saving these files allows calculations to be ported between computers and archived.

RSOLVE uses the outputs files from SWINTERF and builds up the R-matrix, solves the outer region scattering equation (3.18) and constructs K-matrices for specified energies. Within the subroutine RPROP (Baluja et al., 1982; Morgan, 1984) propagates the original R-matrix out to the asymptotic region and the subroutine CFASYM (Noble and Nesbet, 1984) calculates the K-matrices.

EIGENP diagonalises the K-matrices from RSOLVE in order to obtain eigenphase sums in equation 3.23.

RESON looks for resonances in eigenphase sums (Tennyson and Noble, 1984). It reads energy points and corresponding eigenphases. Then it numerically builds up the second derivative $d^2E/d\eta^2$ and looks for changes of its sign from positive to negative. Then a grid of points on which to calculate eigenphases is constructed and the eigenphase sums are fitted to Breit-Wigner profile.

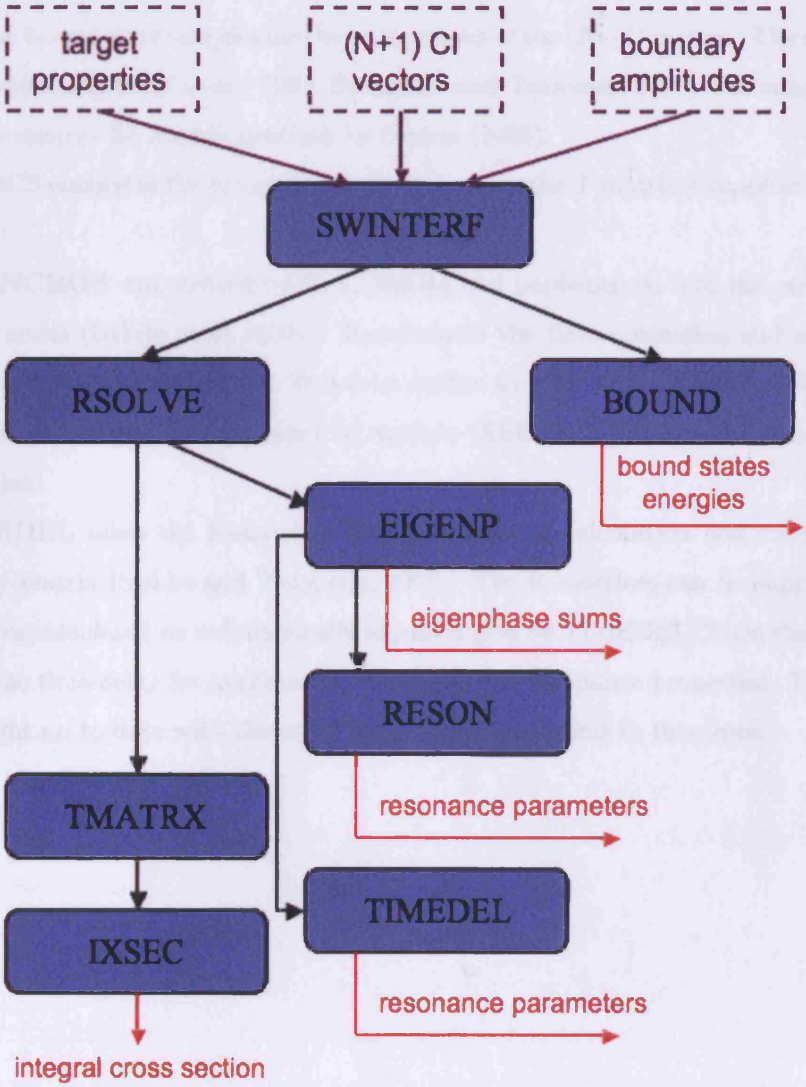

Figure 3.4: Flow diagram for the outer region scattering calculation.

Modules SWINTERF, RSOLVE and RESON have to be modified as part of this thesis to implement the R-matrix method.

TMATRX computes the T-matrices from the K-matrix and these can be passed on the IXSECS.

BOUND solves the scattering problem with bound state boundary conditions to obtain true bound state energies and wave functions of the $(N+1)$ system. The algorithm for this program (Sarpal et al., 1991; Branchett and Tennyson, 1992) was adapted from the one developed for atomic problem by Seaton (1985).

IXSECS computes the integral cross sections from the T-matrices supplied by TMATRX

BORNCROS was written by K. L. Baluja and implemented into the outer region R-matrix codes (Baluja et al., 2001). It calculates the Born correction and adds them to the total integral cross section. It has an option to sum the integral cross sections of different total symmetries calculated by module IXSECS to produce the total integral cross section.

TIMEDEL takes the K-matrices from a scattering calculation and computes the time-delay matrix (Stibbe and Tennyson, 1998). The K-matrices can be supplied from RSOLVE or calculated on a dynamically adjusted grid by TIMEDEL. Then the program searches the time-delay for maxima and computes the resonance properties. TIMEDEL was brought up to date with the other outer region programs in this work.

Chapter 4

Collisions of the C_2 molecule with electrons

4.1 Introduction

In this chapter electron collisions with C_2 molecule are studied as a function of internuclear distance, R. These calculations focus on obtaining the low-lying resonances (below 10 eV) and electronic excitation cross sections of two lowest states. The lowest 26 singlet and triplet target states were coupled, all of which lie less than 10 eV above the ground state at the C_2 equilibrium geometry. This is significantly more physical states than have been needed to obtain stable results for electron-molecule collisions studied previously using a standard close-coupled expansion.

The spectrum of the dicarbon molecule is well known from the comets, the interstellar clouds and the atmospheres of the Sun and cool carbon stars. C_2 is observed in most comets. The emission bands of the C_2 known as the Swan system ($d\ ^3\Pi_g \leftarrow a\ ^3\Pi_u$) result from C_2 molecules fluorescing in sunlight. Between their creation from a large or parent molecule and their destruction by solar ultraviolet photons, the C_2 molecules fluoresce in the sunlight for about 10^5 s and attain statistical equilibrium. Interstellar C_2 was first detected by Souza and Lutz (1977). The C_2 molecule is especially important in the study of conditions in the clouds which produce the interstellar absorption lines because the relative population of its long-lived ground-state rotational levels are measurable.

C_2 is present in flames and electric discharges through carbon-containing materials.

Recently the study of C_2 has become of particular interest because of the (possible) use of graphite walls in fusion devices (Stark et al., 2005; Fantz et al., 2005). An ability to understand electron collision cross sections is important for this and other applications. However there appears to be no previous published studies of electron collisions with neutral C_2.

The study of electron collisions with C_2 is challenging due to the unusually large number of low-lying electronic states of the system which are themselves difficult to represent using standard *ab initio* methods (Abrams and Sherrill, 2004).

4.2 Target calculation

The ground state electronic configuration of C_2 ($X\ ^1\Sigma_g^+$) is well known to be $1\sigma_g^2\ 1\sigma_u^2\ 2\sigma_g^2\ 2\sigma_u^2\ 1\pi_u^4$. Alternating depopulations of $1\pi_u$ and excitation of $3\sigma_g$ lead to configurations $1\sigma_g^2\ 1\sigma_u^2\ 2\sigma_g^2\ 2\sigma_u^2\ 1\pi_u^3\ 3\sigma_g$, producing the terms $a\ ^3\Pi_u$ and $A\ ^1\Pi_u$, and $1\sigma_g^2\ 1\sigma_u^2\ 2\sigma_g^2\ 2\sigma_u^2\ 1\pi_u^2\ 3\sigma_g^2$ with the states $b\ ^3\Sigma_g^-$, $B\ ^1\Delta_g$ and $B'\ ^1\Sigma_g^+$.

To obtain the potential curves, calculations were performed at a series of C_2 fixed internuclear separations. Within the Born-Oppenheimer approximation these fixed calculations can be used as the input for solving nuclear problems on the underlying curves.

In this work the UK polyatomic R-matrix codes (Morgan et al., 1997) were used. This is because the main aim of this work is to study electron collisions with C_2^- using the MRMPS method (see section 3.4). So far this method is implemented only as part of the polyatomic code as it is based on the use of GTOs. The highest symmetry available in the polyatomic code is D_{2h} which is a subgroup of the true $D_{\infty h}$ symmetry of C_2. All the calculation in this work were performed in D_{2h} symmetries. The table 4.1 shows the transformation of irreducible representations from $D_{\infty h}$ point group to D_{2h} point group. Therefore in order to identify resonances in $D_{\infty h}$ point group one has to examined all adequate symmetries in D_{2h} point group. For example, if there is a resonance for ^2A_g symmetry one has to look for corresponding resonance for $^2B_{1g}$ symmetry. If there is one the resonance is $^2\Delta_g$ resonance and if there is none the resonance is $^2\Sigma_g^+$ resonance.

Fixed-nuclei calculations were performed for 20 C_2 internuclear distances in the range from 1.648 a_0 to 3.548 a_0 (with a 0.1 a_0 step). The measured equilibrium geometry for the ground state is 2.348 a_0 (Huber and Herzberg, 1979). In the target calculation, 26 states (in $D_{\infty h}$ symmetry or 39 in D_{2h} symmetry) were used. Their potential energy curves are shown in figure 4.1.

Table 4.1: Character table for transformation of irreducible representations from $D_{\infty h}$ point group to D_{2h} point group.

$D_{\infty h}$	D_{2h}
Σ_g^+	A_g
Σ_u^+	B_{1u}
Σ_g^-	B_{1g}
Σ_u^-	A_u
Π_g	$B_{2g}+B_{3g}$
Π_u	$B_{2u}+B_{3u}$
Δ_g	A_g+B_{1g}
Δ_u	A_u+B_{1u}

In order to determine the target electronic wave functions and energies, a Hartree-Fock self-consistent-field (HF-SCF) calculation was performed first using the double-zeta plus polarisation (DZP) Gaussian basis set of Dunning (1970) for C. The molecular orbitals generated this way were used to obtain pseudo-natural orbitals (NOs). These were gained by diagonalising the first order density matrix for all target states included in the calculation. To retrieve a set of NOs that gives a good representation of the 26 target states included in the close-coupling expansion, a weighted averaging of the density matrices was carried out. Large singles and doubles configuration interaction (CAS-CISD) calculations (using around 70000 and 110000 configurations for the singlet and triplet states respectively) were performed to obtain the matrices. After a number of tests the best results (ie. the best threshold energies) were obtained when 13 states; ^1A_g (2 states), $^3B_{2u}$, $^3B_{3u}$, $^3B_{1g}$ (2 states), $^1B_{2u}$, $^1B_{3u}$, $^3B_{1u}$ (2 states), $^1B_{1g}$, ^3A_u, ^3A_g were averaged with weights 20, 5, 20, 20, 15, 5, 10, 10, 5, 20, 5, 20, 5 respectively. The same state-averaging procedure was used for all molecular geometries.

Finally, a complete active space configuration interaction (CASCI) calculation, which builds all the possible configurations by distributing the electrons among the orbitals in the active space, was performed. In this model the four $1s$ electrons were frozen in the $1\sigma_g$ and $1\sigma_u$ orbitals, and the remaining eight electrons were freely distributed among the $2\sigma_g$, $3\sigma_g$, $2\sigma_u$, $3\sigma_u$, $1\pi_u$ and $1\pi_g$ orbitals giving configurations which can be written $(1\sigma_g\ 1\sigma_u)^4\ (2\sigma_g\ 3\sigma_g\ 2\sigma_u\ 3\sigma_u\ 1\pi_u\ 1\pi_g)^8$.

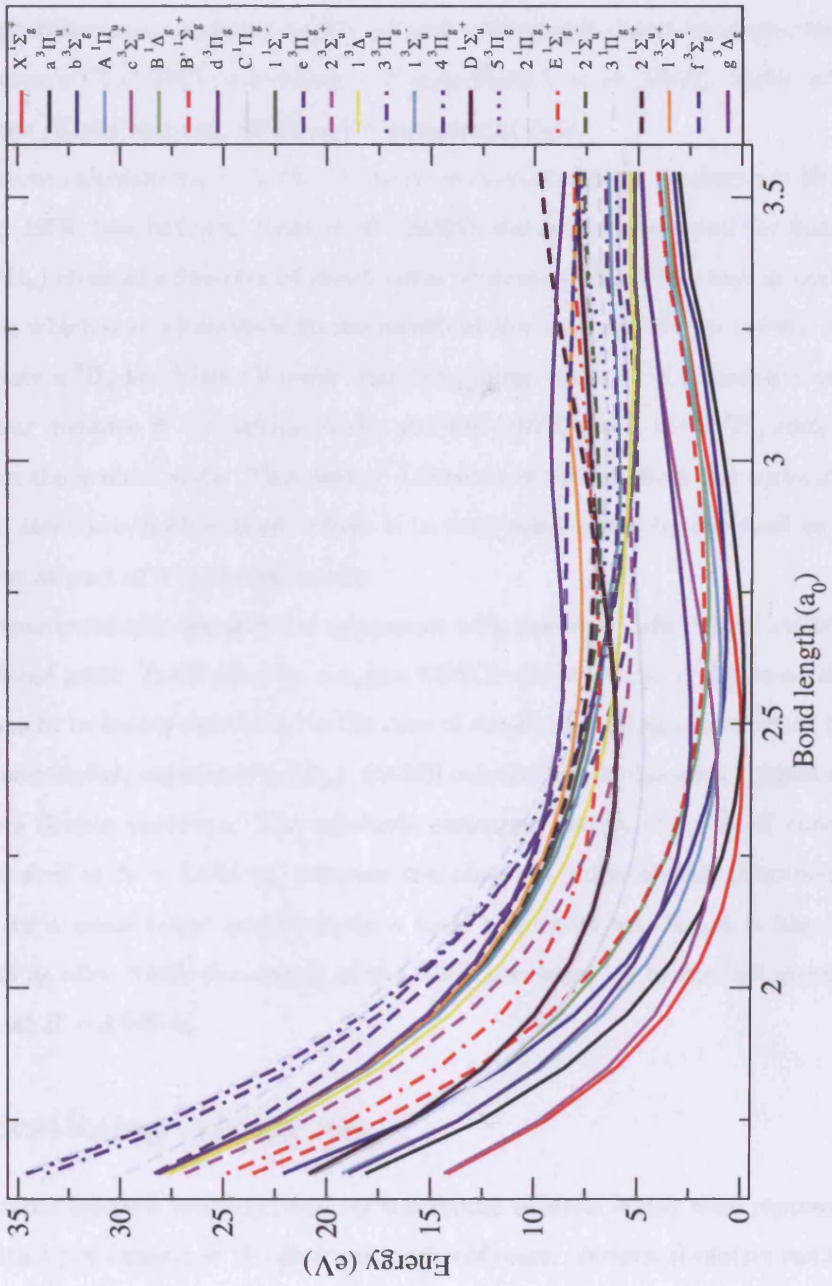

Figure 4.1: Potential energy curves for the 26 states of C_2 used in the calculations.

The ground state ($X\ ^1\Sigma_g^+$) energy obtained for our equilibrium geometry R_e = 2.448 a_0 is −75.55448 $E_\hbar$ in comparison with the value from full CI calculation of Christiansen et al. (1996), −75.730209 $E_\hbar$ for their R_e = 2.348 a_0. Table 4.2 shows the energy differences between the ground and excited states and compares them with multi-reference CI (MRCI) calculations (Boggio-Pasqua et al., 2000), Slater orbital CI calculations (Kirby and Liu, 1979) and experimental data.

In present calculations, as in the C_2 curves constructed from constants in Huber and Herzberg (1979) (see figure in Jones et al. (1980)), the ground state and the first excited state ($a\ ^3\Pi_u$) cross as a function of internuclear separation, R. This crossing occurs near $R = 2.5$ a_0 which is comparable with the results of Rosmus and Werner (1984). The first excited state a $^3\Pi_u$ lies 0.066 eV lower than the ground state $X\ ^1\Sigma_g^+$ (negative value) for internuclear distance $R = 2.548$ a_0. Kirby and Liu (1979) found the a $^3\Pi_u$ state 0.03 eV lower than the ground state. This energy difference is smaller than the accuracy of the electronic structure method used, which is in turn constrained by the need to use this calculation as part of a scattering study.

For other excitation energies the agreement with previous data, where available, can be considered good. Table 4.2 does not give CASCI values for the $f\ ^3\Sigma_g^-$ state since this state seems to be purely repulsive. In the case of the highest-lying excited state included in the close-coupling expansion ($g\ ^3\Delta_g$), CASCI calculations in this work suggest that this state has a double minimum. The adiabatic excitation energy of 8.678 eV corresponds to a minimum at R = 2.648 a_0, whereas the observed value quoted (Herzberg et al., 1969) is for a much larger bond length; a local maximum was found in the curve at $R = 3.048$ a_0 after which the energy of the curve decreases up to the last geometry we consider, at $R = 3.548$ a_0.

4.3 Scattering calculation

The scattered electron was described by continuum orbitals which were represented by GTOs with $l \leq 4$ centred at the dicarbon centre of mass. Various R-matrix radii, a, and continuum basis sets were tested. Computations were performed for an R-matrix radius of a=10 a_0 and a=13 a_0 and variety of continuum basis sets (Sarpal et al., 1996; Faure et al., 2002). The continuum basis of Sarpal et al. (1996) contains orbital with $l \leq 3$ and $l \leq 4$ partial waves, and orbitals of Faure et al. (2002) up to $l \leq 4$ partial waves. For testing purposes, 15 lowest electronic states were used in close-coupling expansion.

Table 4.2: C_2 adiabatic excitation energies obtained from CASCI target calculations compared with those from an MRCI calculation, a CI calculation and experiments. Excitation energies, T_e, are given in eV. R_e are the internuclear separations for equilibrium geometry in a_0.

Models	CASCI		MRCI[a]		CI[c]		Obs.[a,b]	
	T_e/eV	R_e/a_0	T_e/eV	R_e/a_0	T_e/eV	R_e/a_0	T_e/eV	R_e/a_0
$a\ ^3\Pi_u$	-0.066	2.548	0.099	2.477	-0.03	2.53	0.089[a]	2.479[a]
$b\ ^3\Sigma_g^-$	0.809	2.648	0.804	2.595	0.80	2.65	0.798[a]	2.587[a]
$A\ ^1\Pi_u$	1.052	2.548	1.076	2.500	1.14	2.53	1.040[a]	2.491[a]
$c\ ^3\Sigma_u^+$	1.206	2.348	1.178	2.285	1.09	2.32	1.131[a]	2.283[a]
$B\ ^1\Delta_g$	1.662	2.748	1.521	2.627	1.59	2.66	1.498[a]	2.617[a]
$B'\ ^1\Sigma_g^+$	1.879	2.648	1.922	2.612	1.81	2.66	1.910[a]	2.602[a]
$d\ ^3\Pi_g$	2.507	2.448	2.531	2.400	2.47	2.44	2.483[a]	2.392[a]
$C\ ^1\Pi_g$	4.789	2.448	4.388	2.379	4.81	2.40	4.248[a]	2.372[a]
$1\ ^1\Sigma_u^-$	5.067	2.948	4.961	3.258				
$e\ ^3\Pi_g$	5.135	2.948			5.51	3.17	5.058[b]	2.901[b]
$2\ ^3\Sigma_u^+$	5.182	3.248						
$1\ ^3\Delta_u$	5.291	3.248	5.098	3.262				
$3\ ^3\Pi_g$	5.693	3.048			6.47	3.00		
$1\ ^3\Sigma_u^-$	5.953	2.948						
$4\ ^3\Pi_g$	6.079	2.948						
$D\ ^1\Sigma_u^+$	6.092	2.448			6.23	2.38	5.361[b]	2.339[b]
$5\ ^3\Pi_g$	6.472	2.948						
$2\ ^1\Pi_g$	6.581	3.048						
$E\ ^1\Sigma_g^+$	6.928	2.548			7.18	2.46	6.823[b]	2.368[b]
$2\ ^1\Sigma_u^-$	6.930	2.848			7.92	3.00		
$3\ ^1\Pi_g$	7.128	2.748						
$2\ ^1\Sigma_u^+$	7.225	2.848						
$1\ ^3\Sigma_g^+$	7.788	2.648						
$f\ ^3\Sigma_g^-$	-	-					8.809[b]	2.632[b]
$g\ ^3\Delta_g$	8.678	2.648					9.074[b]	2.566[b]

[a] Boggio-Pasqua et al. (2000)

[b] Huber and Herzberg (1979)

[c] Kirby and Liu (1979)

Figure 4.2 gives a comparison of eigenphases obtained for ^2A_g symmetry for different continuum basis sets and R-matrix radius. The eigenphase sums shows good agreement between the various models. The final calculations used R-matrix radius of a=10 a_0 and the basis of Faure et al. (2002) because these gave the highest and smoothest eigenphase sums.

Three different models for the scattering calculation were tested. The first included, in the close-coupling expansion, the 15 lowest electronic states of C_2 (15,15), the second included the 26 lowest states (26,26) and third included 26 states in inner region and 15 in outer (26,15). All tests were performed for C_2 at its equilibrium bond length. Eigenphase sums were obtained by propagating the R-matrix to 100 a_0 (Baluja et al., 1982; Morgan, 1984). These are used to search for resonances. Resonance positions and widths were determined by fitting the eigenphase sum to a Breit-Wigner profile (Tennyson and Noble, 1984). For the lower energy resonances the differences between (15,15), (26,26) and (26,15) models is slight (see table 4.3). Results reported below are for the (26,26) model.

Table 4.3: C_2^- resonance energies for different doublet spin symmetries at the equilibrium bond length for (15,15) and (26,26) models.

Symmetry	$E_{(15,15)}$/eV	$E_{(26,26)}$/eV	$E_{(15,15)}$-$E_{(26,26)}$/eV
^2A_g	6.176	6.119	0.057
$^2B_{1g}$	7.634	7.577	0.057
$^2B_{1u}$	3.577	3.650	0.073
$^2B_{3g}$	4.319	4.261	0.058
^2A_u	3.671	3.726	0.055

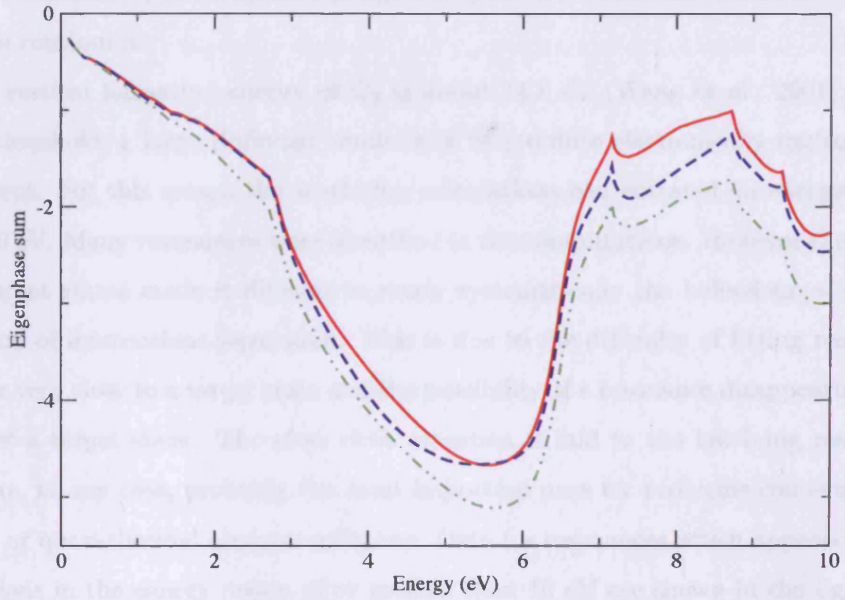

Figure 4.2: The eigenphase sums (in radians) for ^2A_g ($^2\Sigma_g^+ + {}^2\Delta_g$) symmetry of the low-energy electron collisions with C_2 . The solid red line represents the eigenphase sum calculated for R-matrix radius of a=10 a_0 and continuum basis of Faure et al. (2002); the dashed blue line represents the eigenphase sum calculated for R-matrix radius of a=13 a_0 and continuum basis of Faure et al. (2002) and the dot-dashed green line represents the eigenphase sum calculated for R-matrix radius of a=10 a_0 and continuum basis of Sarpal et al. (1996).

4.4 Results

4.4.1 Resonances

Autodetaching resonance states of C_2^- have been observed experimentally (Jones et al., 1980; Hefter et al., 1983). However these resonances are all associated with vibrational excited states of the bound C_2^- electronic states discussed below, which have sufficient energy to autodetach. The interest of this work does not lie with such nuclear excited Feshbach resonances, but resonance states associated with electronic states of C_2^- which lie in the continuum.

The vertical ionisation energy of C_2 is about 14.8 eV (Wang et al., 2001). Closer to this threshold, a large (infinite) numbers of very diffuse electronically excited states are present. For this reason the scattering calculations concentrated on energies below about 10 eV. Many resonances were identified in the computations. However the density of C_2 target states made it difficult to study systematically the behaviour of these as a function of internuclear separation. This is due to the difficulty of fitting resonances which lie very close to a target state and the possibility of a resonance disappearing when it crosses a target state. Therefore close attention is laid to the low-lying resonances which are, in any case, probably the most important ones for problems concerned with thermal or quasi-thermal electron collisions. Data for resonances which appeared in the calculations in the energy region of or greater than 10 eV are shown in the figures 4.3 - 4.5 as red triangles without a line connection (such as those with $^2\Pi_u$ symmetry). Nevertheless they cannot be considered reliable.

All resonance energies are relative to the target energies of the ground state of C_2 at the same R. For this reason the second column of the table 5.1 shows these as a function of R. The resonance energies for ^2A_g ($^2\Sigma_g^+ + {}^2\Delta_g$), $^2B_{1u}$ ($^2\Sigma_u^+ + {}^2\Delta_u$) and $^2B_{3g}$ ($^2\Pi_g$) symmetries are shown in figure 4.3 and in tables 4.4 and 4.5. The resonance energies for $^2B_{3u}$ ($^2\Pi_u$), $^2B_{1g}$ ($^2\Sigma_g^- + {}^2\Delta_g$) and ^2A_u ($^2\Sigma_u^- + {}^2\Delta_u$) symmetries are shown in figure 4.4 and in table 4.6 (except for $^2B_{3u}$ symmetry). The corresponding resonance widths are given in the figure 4.7 and tables 4.4 - 4.6. No systematic attempt was made to track resonances above 10 eV. Many of the resonances stopped at small internuclear distances. This is due to high density of C_2 target states. The resonance widths go to zero when the resonance becomes a bound state. The low-lying resonances for doublet spin symmetry, ^2A_u ($^2\Sigma_u^- + {}^2\Delta_u$) and $^2B_{1g}$ ($^2\Sigma_g^- + {}^2\Delta_g$) are the same as in the case of $^2B_{1u}$ ($^2\Sigma_u^+ + {}^2\Delta_u$) and ^2A_g ($^2\Sigma_g^+ + {}^2\Delta_g$) symmetries (respectively) so we can identify this resonance as $^2\Delta_u$

and $^2\Delta_g$. The quartet spin symmetry resonances and the corresponding resonance widths are given in the figures 4.5 - 4.8 and tables 4.7 - 4.12. Again the widths decrease to zero as the resonances become bound. Data on the high-lying resonance must be considered less reliable. On three occasions the low-lying resonances become bound states for larger internuclear distances. This can be seen for doublet spin symmetry resonance $^2B_{3g}$ ($^2\Pi_g$) shown in figure 4.3. The quartet spin symmetry resonances $^4B_{1u}$ ($^4\Sigma_u^+$) and $^4B_{3g}$ ($^4\Pi_g$) demonstrate the same behaviour (see figure 4.6).

The widths of the resonances do not vary as smoothly with geometry as the positions. There are a number of reasons for this. Firstly the resonances are characterised by fitting with experience showing that the resonance width is much more sensitive to details of the fit, and has a larger fitting error, than the position. Secondly there are many cases where the resonances cross target curves and, under these circumstances the resonance width can and does change significantly. Finally there are several symmetries which have nearby resonances which interact and this is well known to considerably effect the resonance width (Collins et al., 1986).

4.4.2 Cross sections

Given the closeness of the $X\ ^1\Sigma_g^+$ and the $a\ ^3\Pi_u$ states, and the fact that the latter is metastable, electron impact electronic excitation cross sections from both of these states were calculated. Figure 4.9 gives electron impact cross sections for both of these states at the C_2 equilibrium geometry of $R = 2.448$ a_0. These cross sections are only given for electron impact energies up to 10 eV since the close-coupling expansion is not complete above this value. Neglect of states can lead to spurious effects such as pseudo-resonances at higher energies.

The top row of graphs (figure 4.9) presents the fixed-nuclei total cross sections, which are very similar to the elastic cross sections. The total cross sections, and indeed the electronic excitation cross sections also shown, display a pronounced peak at about 3.5 eV; this corresponds to the low-lying $^2\Pi_g$ ($^2B_{2g}$ + $^2B_{3g}$) and $^2\Delta_u$ ($^2B_{1u}$ + ^2A_u) resonances.

The middle row displays cross sections for the excitation to $d\ ^3\Pi_g$ state. This excited state was selected because the system ($a\ ^3\Pi_u \leftarrow d\ ^3\Pi_g$) is well known as Swan bands, whose emission is used to monitor C_2 in plasmas (Stark et al., 2005; Fantz et al., 2005). This is smaller then the others because of forbidden dipole moment. The peak at 6 eV in

Table 4.4: C_2^- resonance energies and widths for ^2A_g and $^2B_{1u}$ symmetries as a function of the bond length.

^2A_g			$^2B_{1u}$		
R_e/a_0	E_0/eV	Γ/eV	R_e/a_0	E_0/eV	Γ/eV
1.748	18.594	0.068	2.348	4.532	1.107
1.848	15.244	1.616	2.448	3.945	1.062
1.948	12.446	1.373	2.548	3.507	0.929
2.048	10.179	1.098	2.648	3.271	0.797
2.148	8.549	0.836	2.748	3.199	0.603
2.248	7.391	0.631	2.848	3.292	0.536
2.448	6.119	0.380	2.948	3.650	0.403
2.548	5.864	0.307	3.048	3.978	0.386
2.648	5.746	0.256	3.148	4.167	0.377
2.748	5.728	0.239	3.248	4.392	0.243
2.848	5.724	0.294	3.348	4.522	0.152
2.948	5.695	0.386	3.448	4.630	0.116
3.048	5.586	0.469	3.548	4.740	0.096
3.248	5.465	0.306			

the ($X\ ^1\Sigma_g^+ \leftarrow d\ ^3\Pi_g$) cross section is caused by the $^2\Delta_g$ (^2A_g and $^2B_{1g}$) resonance which is not visible in the other cross sections reported and which are significantly larger due to allowance for dipole moment. The ($a^3\Pi_u \leftarrow d\ ^3\Pi_g$) cross section where the optical transitions are allowed, could be corrected for higher partial waves. This would make the cross section somewhat larger.

The bottom row gives the cross sections for the electron impact excitation to the five electronic states of C_2 lying between the two initial states and d $^3\Pi_g$ state. The correction for higher partial waves would make the cross section for the electron impact excitation to the five electronic states of C_2 lying between the $a^3\Pi_u$ and $d\ ^3\Pi_g$ states larger.

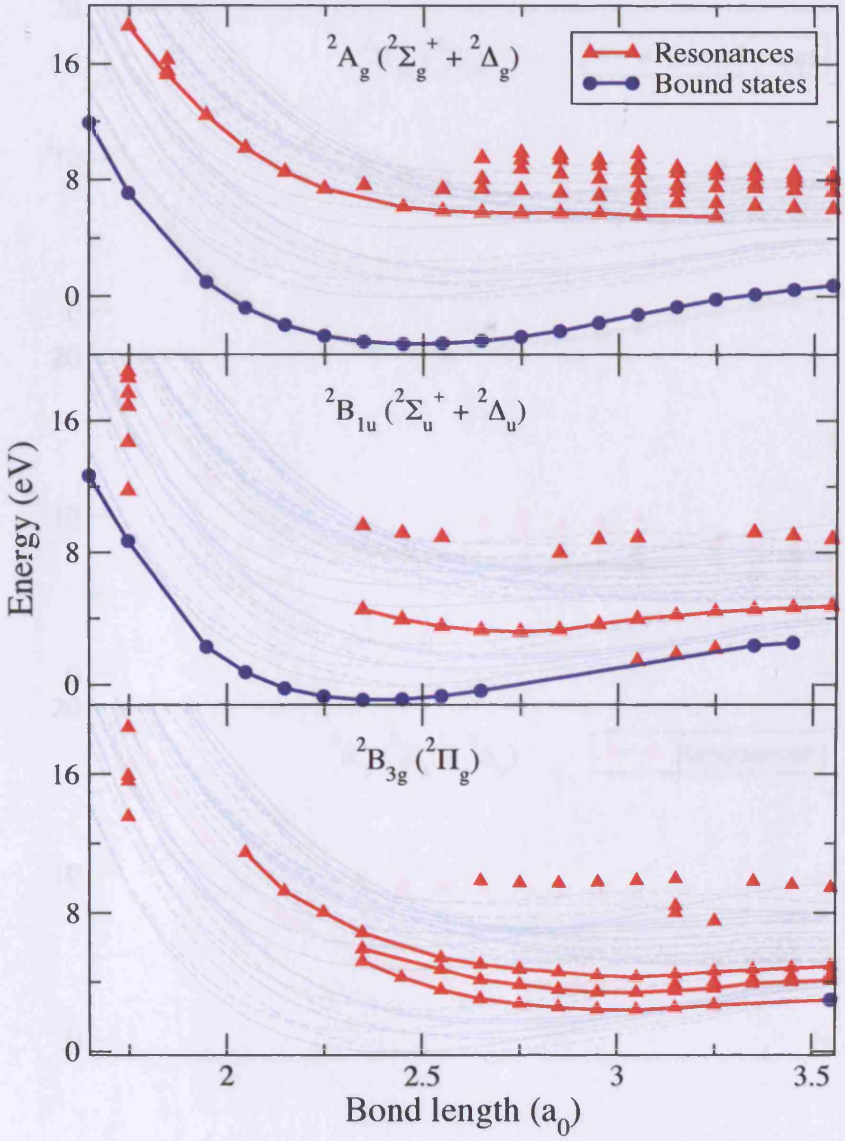

Figure 4.3: C_2^- bound state and resonance energies for ^2A_g ($^2\Sigma_g^+ + {}^2\Delta_g$), $^2B_{1u}$ ($^2\Sigma_u^+ + {}^2\Delta_u$) and $^2B_{3g}$ ($^2\Pi_g$) symmetries as a function of the bond length. The energies of the C_2 electronic states used in our calculations are shown in the background.

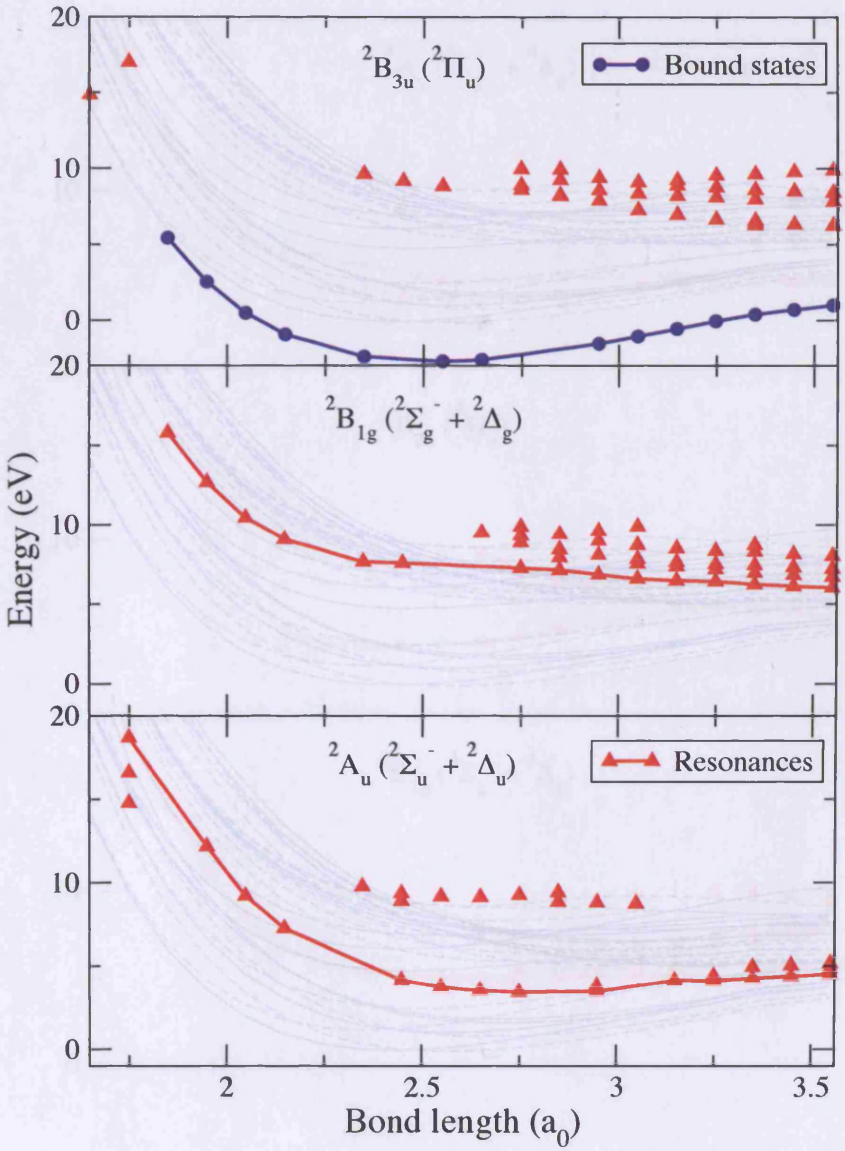

Figure 4.4: C_2^- bound state and resonance energies for $^2B_{3u}$ ($^2\Pi_u$), $^2B_{1g}$ ($^2\Sigma_g^- + {}^2\Delta_g$) and ^2A_u ($^2\Sigma_u^- + {}^2\Delta_u$) symmetries as a function of the bond length. The energies of the C_2 electronic states used in our calculations are shown in the background.

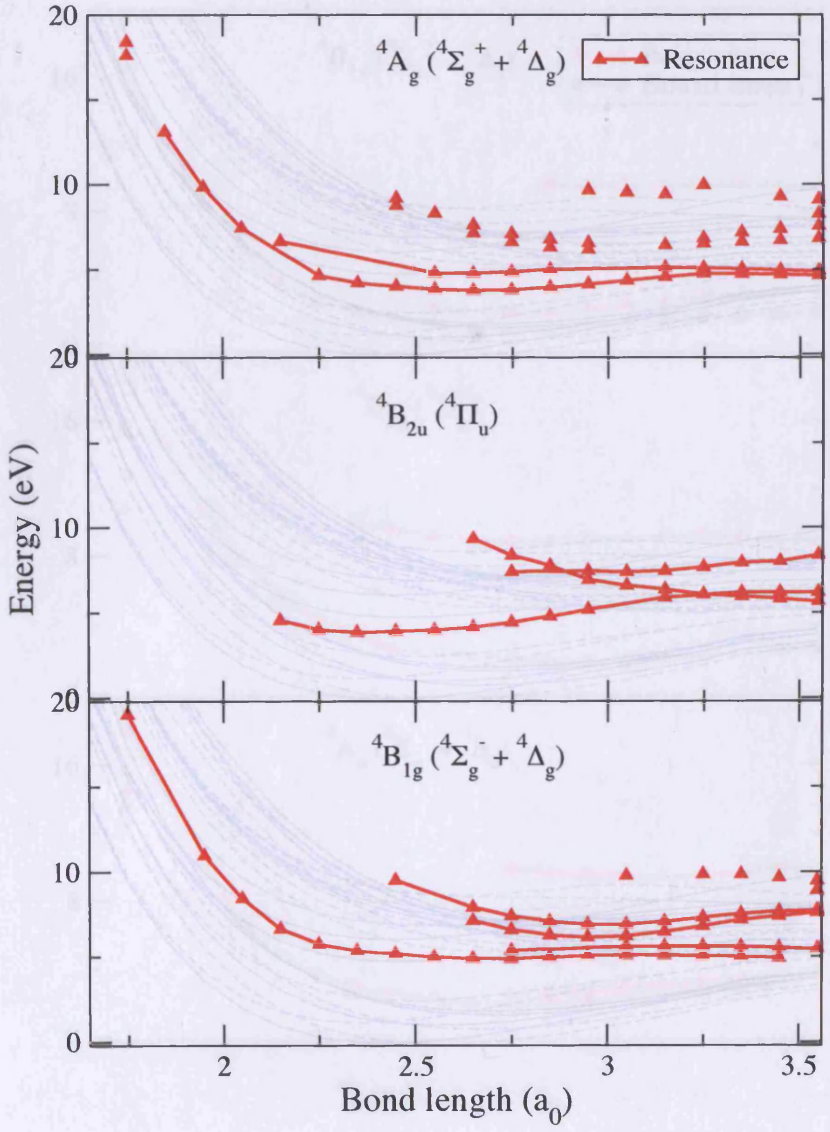

Figure 4.5: C_2^- resonance energies for ^4A_g ($^4\Sigma_g^+ + {}^4\Delta_g$), $^4B_{2u}$ ($^4\Pi_u$) and $^4B_{1g}$ ($^4\Sigma_g^- + {}^4\Delta_g$) symmetries as a function of the bond length. The energies of the C_2 electronic states used in our calculations are shown in the background.

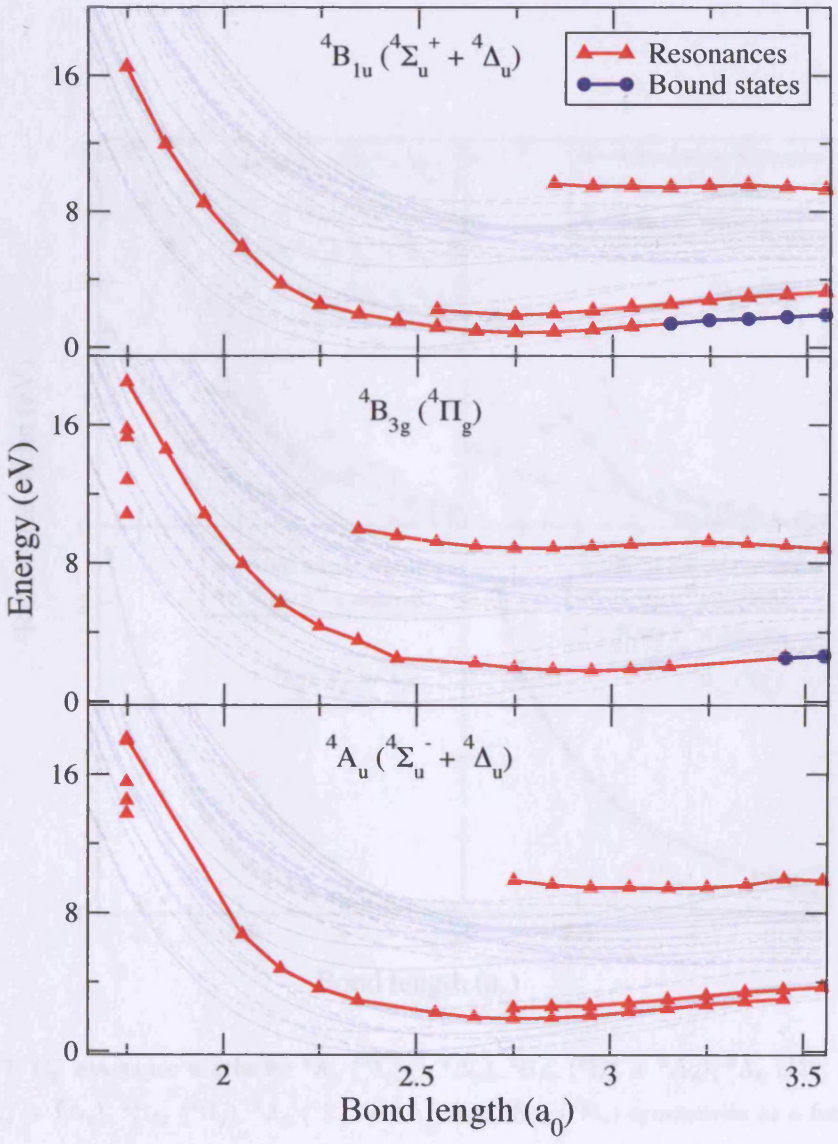

Figure 4.6: C_2^- bound state and resonance energies for $^4B_{1u}$ ($^4\Sigma_u^+ + {}^4\Delta_u$), $^4B_{3g}$ ($^4\Pi_g$) and ^4A_u ($^4\Sigma_u^- + {}^4\Delta_u$) symmetries as a function of the bond length. The energies of the C_2 electronic states used in our calculations are shown in the background.

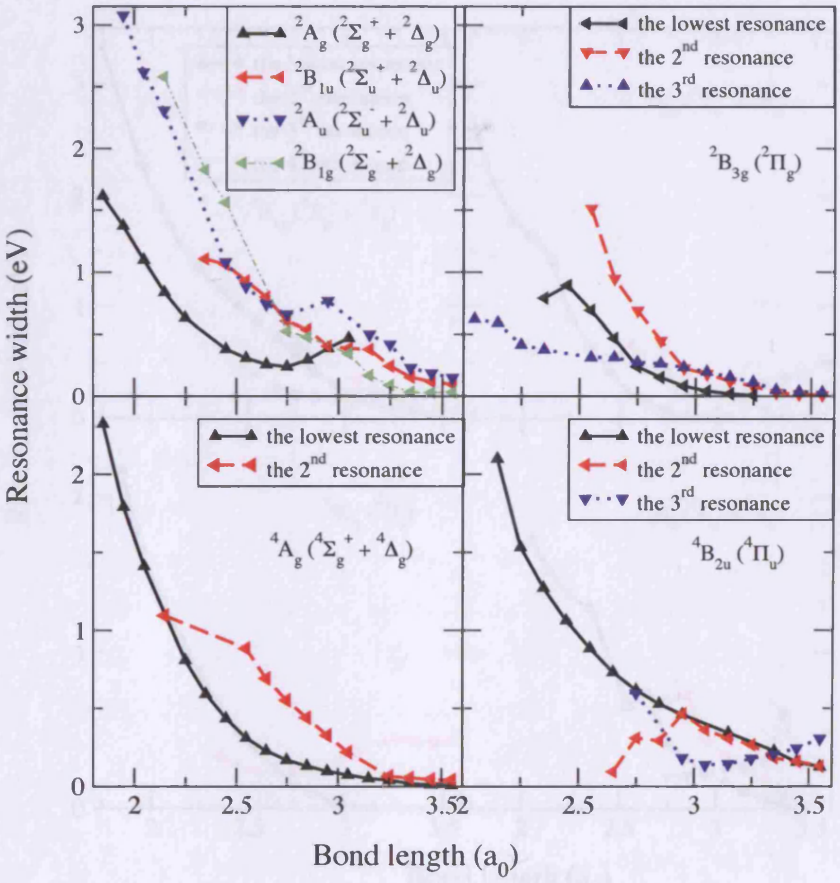

Figure 4.7: C_2^- resonance widths for ^2A_g ($^2\Sigma_g^+ + {}^2\Delta_g$), $^2B_{1u}$ ($^2\Sigma_u^+ + {}^2\Delta_u$), ^2A_u ($^2\Sigma_u^- + {}^2\Delta_u$), $^2B_{1g}$ ($^2\Sigma_g^- + {}^2\Delta_g$), $^2B_{3g}$ ($^2\Pi_g$), ^4A_g ($^4\Sigma_g^+ + {}^4\Delta_g$) and $^4B_{2u}$ ($^4\Pi_u$) symmetries as a function of the bond length.

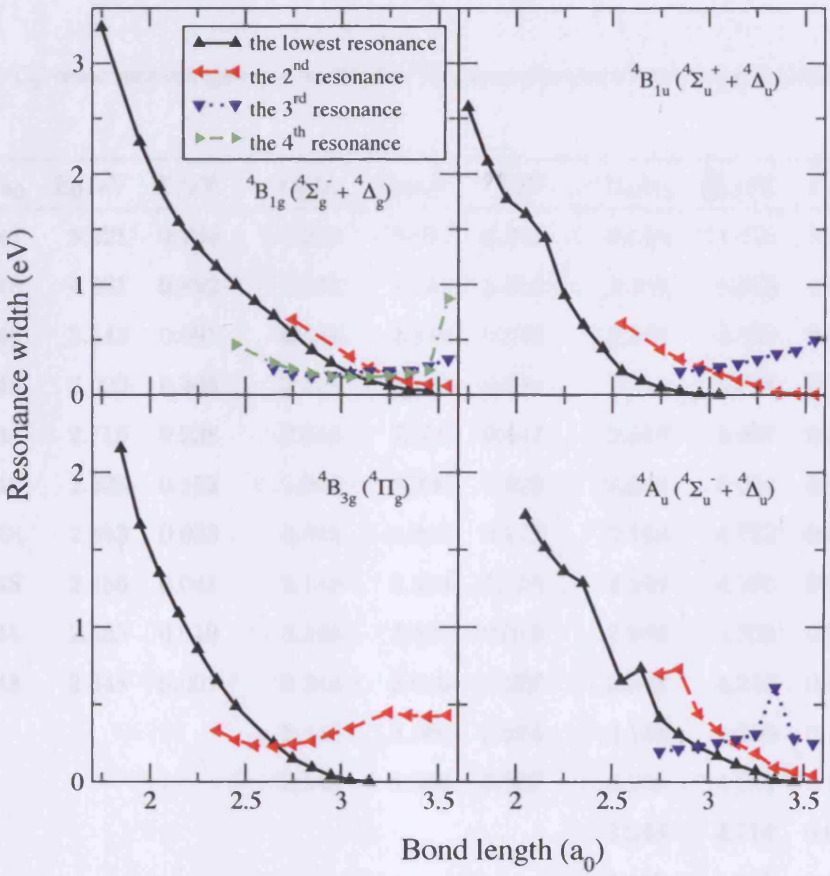

Figure 4.8: C_2^- resonance widths for $^4B_{1g}$ ($^4\Sigma_g^-$ + $^4\Delta_g$), $^4B_{1u}$ ($^4\Sigma_u^+$ + $^4\Delta_u$), $^4B_{3g}$ ($^4\Pi_g$) and ^4A_u ($^4\Sigma_u^-$ + $^4\Delta_u$) symmetries as a function of the bond length.

Table 4.5: C_2^- resonance energies and widths for $^2B_{3g}$ symmetry as a function of the bond length.

R_e/a_0	E_0/eV	Γ/eV	R_e/a_0	E_0/eV	Γ/eV	R_e/a_0	E_0/eV	Γ/eV
2.348	5.221	0.790	2.348	5.931	0.793	2.048	11.475	0.621
2.448	4.261	0.892	2.548	4.746	1.513	2.148	9.255	0.591
2.548	3.543	0.691	2.648	4.119	0.946	2.248	8.032	0.415
2.648	3.020	0.469	2.748	3.840	0.686	2.348	6.857	0.377
2.748	2.716	0.238	2.848	3.556	0.447	2.548	5.407	0.314
2.848	2.525	0.152	2.948	3.396	0.226	2.648	5.024	0.314
2.948	2.393	0.083	3.048	3.393	0.177	2.748	4.752	0.274
3.048	2.386	0.041	3.148	3.484	0.119	2.848	4.585	0.263
3.148	2.485	0.019	3.248	3.637	0.079	2.948	4.359	0.235
3.248	2.648	0.007	3.348	3.916	0.027	3.048	4.282	0.196
			3.448	3.999	0.015	3.148	4.410	0.156
			3.548	4.084	0.007	3.248	4.598	0.114
						3.348	4.714	0.050
						3.448	4.811	0.037
						3.548	4.917	0.030

Table 4.6: C_2^- resonance energies and widths for $^2B_{1g}$ and ^2A_u symmetries as a function of the bond length.

$^2B_{1g}$			^2A_u		
R_e/a_0	E_0/eV	Γ/eV	R_e/a_0	E_0/eV	Γ/eV
1.848	15.782	2.289	1.748	18.676	0.103
1.948	12.674	2.150	1.948	12.169	3.079
2.048	10.445	1.916	2.048	9.208	2.620
2.148	9.083	2.581	2.148	7.272	2.309
2.348	7.646	1.828	2.448	4.150	1.080
2.448	7.577	1.565	2.548	3.726	0.883
2.748	7.261	0.523	2.648	3.517	0.741
2.848	7.130	0.480	2.748	3.424	0.658
2.948	6.844	0.681	2.948	3.463	0.766
3.048	6.582	0.345	3.148	4.129	0.500
3.148	6.472	0.169	3.248	4.111	0.420
3.248	6.412	0.090	3.348	4.256	0.230
3.348	6.232	0.034	3.448	4.382	0.186
3.448	6.114	0.031	3.548	4.514	0.149
3.548	6.018	0.033			

Table 4.7: C_2^- resonance energies and widths for ^4A_g symmetry as a function of the bond length.

R_e/a_0	E_0/eV	Γ/eV	R_e/a_0	E_0/eV	Γ/eV
1.848	13.087	2.174	2.148	6.645	1.025
1.948	9.835	1.680	2.548	4.777	0.836
2.048	7.430	1.342	2.648	4.757	0.663
2.248	4.634	0.756	2.748	4.846	0.528
2.348	4.189	0.552	2.848	4.973	0.419
2.448	4.000	0.408	3.148	5.090	0.127
2.548	3.815	0.290	3.248	5.064	0.083
2.648	3.745	0.212	3.348	5.021	0.049
2.748	3.785	0.150	3.448	4.940	0.041
2.848	3.924	0.115	3.548	4.879	0.038
2.948	4.105	0.084			
3.048	4.339	0.062			
3.148	4.546	0.046			
3.248	4.734	0.031			
3.348	4.722	0.015			
3.448	4.680	0.009			
3.548	4.638	0.005			

Table 4.8: C_2^- resonance energies and widths for $^4B_{2u}$ symmetry as a function of the bond length.

R_e/a_0	E_0/eV	Γ/eV	R_e/a_0	E_0/eV	Γ/eV	R_e/a_0	E_0/eV	Γ/eV
2.148	4.549	2.099	2.648	9.326	0.093	2.748	7.395	0.597
2.248	4.001	1.533	2.748	8.360	0.308	2.948	7.431	0.183
2.348	3.832	1.272	2.848	7.751	0.292	3.048	7.381	0.138
2.448	3.911	1.062	2.948	6.922	0.466	3.148	7.444	0.144
2.548	3.974	0.885	3.048	6.586	0.361	3.248	7.662	0.178
2.648	4.136	0.732	3.148	6.350	0.307	3.348	7.931	0.208
2.748	4.431	0.617	3.348	5.949	0.181	3.448	8.008	0.244
2.848	4.773	0.528	3.448	5.798	0.160	3.548	8.365	0.305
2.948	5.173	0.460	3.548	5.6448	0.129			
3.148	5.878	0.343						
3.248	6.061	0.266						
3.348	6.178	0.227						
3.448	6.177	0.156						
3.548	6.180	0.126						

Table 4.9: C_2^- resonance energies and widths for $^4B_{1g}$ symmetry as a function of the bond length.

R_e/a_0	E_0/eV	Γ/eV	E_0/eV	Γ/eV	E_0/eV	Γ/eV	E_0/eV	Γ/eV
1.748	19.233	3.327						
1.948	10.955	2.288						
2.048	8.439	1.882						
2.148	6.657	1.565						
2.248	5.769	1.341						
2.348	5.359	1.160						
2.448	5.175	0.990					9.508	0.455
2.548	4.986	0.847						
2.648	4.903	0.715			7.134	0.240	7.919	0.290
2.748	4.886	0.559	5.387	0.678	6.606	0.189	7.417	0.232
2.848	4.967	0.402			6.285	0.170	7.089	0.192
2.948	5.053	0.288			6.151	0.173	6.912	0.166
3.048	5.087	0.193	5.613	0.346	6.233	0.199	6.911	0.161
3.148	5.066	0.124	5.620	0.239	6.477	0.214	7.065	0.163
3.248	5.041	0.080	5.621	0.174	6.811	0.219	7.315	0.172
3.348	4.996	0.046	5.610	0.116	7.184	0.221	7.538	0.198
3.448	4.919	0.039	5.530	0.093	7.392	0.259	7.668	0.225
3.548			5.469	0.078	7.604	0.322	7.725	0.874

Table 4.10: C_2^- resonance energies and widths for $^4B_{1u}$ symmetry as a function of the bond length.

R_e/a_0	E_0/eV	Γ/eV	R_e/a_0	E_0/eV	Γ/eV	R_e/a_0	E_0/eV	Γ/eV
1.748	16.502	2.601	2.548	1.175	0.214	2.848	9.603	0.212
1.848	11.951	2.114	2.748	1.887	0.409	2.948	9.456	0.229
1.948	8.502	1.775	2.848	1.978	0.324	3.048	9.458	0.255
2.048	5.888	1.637	2.948	2.152	0.255	3.148	9.843	1.013
2.148	3.713	1.420	3.048	2.364	0.195	3.248	9.485	0.322
2.248	2.522	0.904	3.148	2.564	0.133	3.348	9.558	0.373
2.348	1.953	0.631	3.248	2.794	0.085	3.448	9.428	0.401
2.448	1.543	0.418	3.348	2.986	0.024	3.548	9.290	0.497
2.548	1.175	0.214	3.448	3.129	0.010			
2.648	0.946	0.130	3.548	3.267	0.003			
2.748	0.864	0.067						
2.848	0.896	0.029						
2.948	1.032	0.009						
3.048	1.230	0.001						

Table 4.11: C_2^- resonance energies and widths for $^4B_{3g}$ symmetry as a function of the bond length.

R_e/a_0	E_0/eV	Γ/eV	R_e/a_0	E_0/eV	Γ/eV
1.748	18.480	0.182	2.348	9.962	0.331
1.848	14.580	2.154	2.448	9.575	0.268
1.948	10.830	1.659	2.548	9.200	0.235
2.048	7.954	1.348	2.648	8.958	0.228
2.148	5.698	1.088	2.748	8.864	0.242
2.248	4.341	0.858	2.848	8.858	0.262
2.348	3.529	0.656	2.948	8.934	0.308
2.448	2.497	0.488	3.048	9.061	0.344
2.648	2.188	0.249	3.248	9.249	0.449
2.748	1.935	0.149	3.348	9.121	0.430
2.848	1.837	0.091	3.448	8.986	0.421
2.948	1.781	0.039	3.548	8.837	0.431
3.048	1.844	0.013			
3.148	2.004	0.003			

Table 4.12: C_2^- resonance energies and widths for ^4A_u symmetry as a function of the bond length.

R_e/a_0	E_0/eV	Γ/eV	R_e/a_0	E_0/eV	Γ/eV	R_e/a_0	E_0/eV	Γ/eV
1.748	15.563	0.226	2.748	2.506	0.698	2.748	9.860	0.195
2.048	6.752	1.722	2.848	2.579	0.727	2.848	9.606	0.212
2.148	4.765	1.515	2.948	2.630	0.439	2.948	9.457	0.229
2.248	3.637	1.362	3.048	2.801	0.335	3.048	9.453	0.252
2.348	2.945	1.286	3.148	2.995	0.248	3.148	9.415	0.273
2.548	2.223	0.655	3.248	3.220	0.183	3.248	9.460	0.308
2.648	1.955	0.731	3.348	3.425	0.092	3.348	9.604	0.609
2.748	1.887	0.411	3.448	3.566	0.062	3.448	9.956	0.280
2.848	1.921	0.307	3.548	3.704	0.041	3.548	9.852	0.248
2.948	2.044	0.226						
3.048	2.255	0.169						
3.148	2.462	0.112						
3.248	2.700	0.069						
3.348	2.878	0.014						
3.448	3.026	0.005						

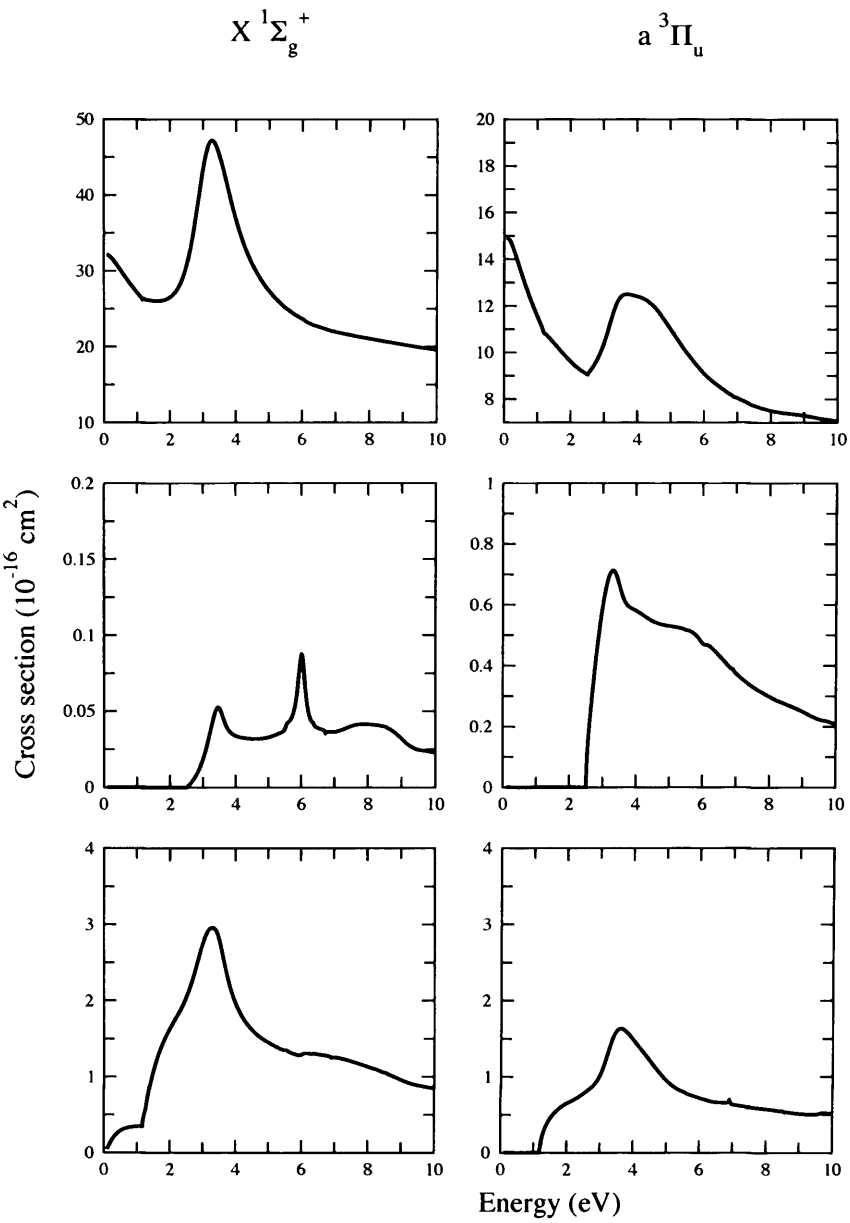

Figure 4.9: Electronic excitation cross sections from ground state ($X\ ^1\Sigma_g^+$) and first excited state ($a\ ^3\Pi_u$) of C_2 at its equilibrium geometry. The first row represents the fixed-nuclei total cross sections. The second row represents cross sections for the excitation to $d\ ^3\Pi_g$ state. The third row represents the cross sections for the electron impact excitation to the five electronic states of C_2 lying between the two initial states and $d\ ^3\Pi_g$ state.

Chapter 5

Bound states of C_2^-

5.1 Introduction

In this chapter the results for bound states of the C_2^- system are presented. As noted in the previous chapter, the calculations were performed for 20 C_2 internuclear distances and 16 symmetries.

C_2^- is isoelectronic to the group of species with 13 electrons CN, N_2^+ and CO^+. The optical spectra of this species have been studied extensively (Huber and Herzberg, 1979). Herzberg and Lagerqvist (1968) tried to observe the absorption spectra of carbon-ions CH_4^+, CH_3^+, CH_2^+ and CH^+ in a flash discharge of methane. They observed new very simple $\Sigma - \Sigma$ bands. After extensive studied these bands were assigned to the $^2\Sigma_u^+$ - $^2\Sigma_g^+$ transition of C_2^-. Milligan and Jacox (1969) concluded that this band system of carbon vapour trapped in inert gas matrices, which had previously been assigned to C_2 by McCarty and Robinson (1959), were $\Sigma - \Sigma$ transition of C_2^-. More matrix isolation studies were carried out (Frosch, 1971; Bondybey and Nibler, 1972) and they supported the new interpretation of these bands. Two-photon photodetachment spectroscopy of C_2^- was conducted by Lineberger and Patterson (1972) which showed definitely that the spectrum was of C_2^-. Later further photodetachment studies were conducted (Jones et al., 1980; Hefter et al., 1983).

5.2 Calculation

Bound states energies were obtained using the method described by Sarpal et al. (1991). In this method, the eigenvalue problem is reduced to finding the roots of a determinant, which depend on the energy of the system. A Gailitis expansion was applied at radius of 30 a_0 and 50 a_0. The model with radius of 50 a_0 did not yield good results therefore the radius of 30 a_0 was used through out the calculations. Then the wave functions were propagated inwards to the R-matrix boundary. The (15,15) and (26,15) models showed better results for $^2\Sigma_g^+$ symmetry than the (26,26) model. The results in table 5.1 are for the (15,15) model which did not differ from the (26,15) model. These bound state studies, unlike the scattering ones, require calculation of the wave function in the outer region. This makes the calculations numerically sensitive to the inclusion of very strongly closed channels in the outer region. As a test the bound state energies were computed simply by diagonalising a Hamiltonian based on inner region wave function. This test was performed for the equilibrium geometry $R_e = 2.448$ a_0 and gave energies very similar, but slightly (less than 0.01 eV) higher. For $^2\Sigma_g^+$ symmetry the value is -75.67194 E_h compared with -75.67213 E_h. For $^2\Sigma_u^+$ symmetry it is -75.58443 E_h in comparison with -75.58459 E_h.

5.3 Results

Three bound states of C_2^- were detected. They are $X\ ^2\Sigma_g^+$, $A\ ^2\Pi_u$ and $B\ ^2\Sigma_u^+$. Their energies are shown in table 5.1 as a function of internuclear distance. These energies are all relative to the energy of the ground state of C_2. The comparison between calculations and experiments are presented in table 5.2. The agreement can be considered good. The bound state potential energy curves are shown in figure 5.1 along with the ground state potential energy curve of C_2 and in figures 4.3 and 4.4 along with the energies of resonances of the same symmetry. The calculations found, somewhat unusually, that the $B\ ^2\Sigma_u^+$ bound state becomes a resonance in the region between 2.648 and 3.348 a_0.

All the bound states of C_2^- discussed above are of doublet spin symmetry. However Bondybey and Brus (1975) also reported the observation of $a\ ^4\Sigma_u^+$ bound state. As shown in figure 4.6, at short internuclear distance R this state is a low-lying resonance which only becomes a bound state for $R > 3.1$ a_0. Since the Bondybey and Brus' spectra were recorded in a Noble gas matrix, it is possible that matrix effects could have

led to this state becoming bound. The similar behaviour is also formed for the lowest resonance of $^4\Pi_g$ symmetry. This resonance becomes a bound state for $R > 3.4$ a_0.

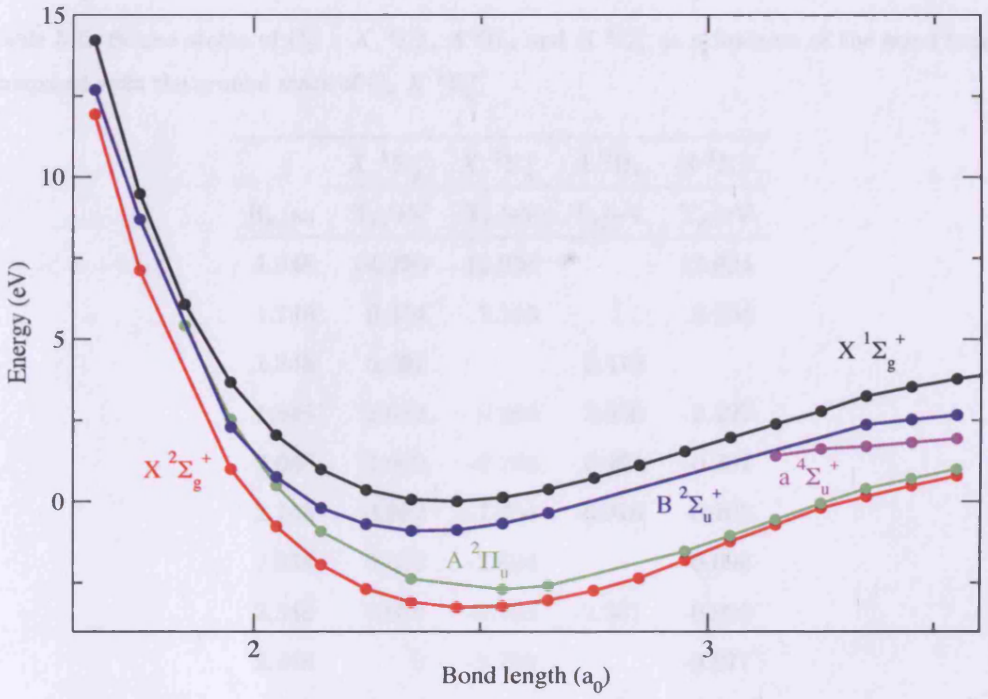

Figure 5.1: Bound states of C_2^- : $X\ ^2\Sigma_g^+$, $A\ ^2\Pi_u$ and $B\ ^2\Sigma_u^+$ as a function of the bond length compared with the ground state of C_2 $X\ ^1\Sigma_g^+$.

Table 5.1: Bound states of C_2^- : $X\ ^2\Sigma_g^+$, $A\ ^2\Pi_u$ and $B\ ^2\Sigma_u^+$ as a function of the bond length compared with the ground state of C_2 $X\ ^1\Sigma_g^+$.

	$X\ ^1\Sigma_g^+$	$X\ ^2\Sigma_g^+$	$A\ ^2\Pi_u$	$B\ ^2\Sigma_u^+$
R_e/a_0	T_e/eV	T_e/eV	T_e/eV	T_e/eV
1.648	14.220	11.936		12.694
1.748	9.474	7.115		8.694
1.848	6.067		5.419	
1.948	3.672	0.996	2.536	2.297
2.048	2.040	-0.769	0.491	0.757
2.148	0.982	-1.954	-0.916	-0.203
2.248	0.357	-2.694		-0.696
2.348	0.058	-3.103	-2.381	-0.906
2.448	0	-3.259		-0.877
2.548	0.121	-3.225	-2.702	-0.676
2.648	0.370	-3.046	-2.587	-0.355
2.748	0.720	-2.745		
2.848	1.116	-2.364		
2.948	1.540	-1.809	-1.526	
3.048	1.970	-1.230	-1.048	
3.148	2.386	-0.723	-0.556	
3.248	2.781	-0.203	-0.054	
3.348	3.247	0.149	0.399	2.369
3.448	3.529	0.478	0.708	2.525
3.548	3.779	0.784	0.997	2.660

Table 5.2: Bound states of C_2^- from various methods and observation compared with the calculations from this thesis. IP is ionisation potential for the ground state and T_e is the adiabatic excitation threshold for the excited states.

	$X\ ^2\Sigma_g^+$		$A\ ^2\Pi_u$		$B\ ^2\Sigma_u^+$	
	R_e/a_0	IP/eV	R_e/a_0	T_e/eV	R_e/a_0	T_e/eV
MRD-CI [a]	2.415	~ 3.4	2.491	0.403	2.309	2.335
MCSCF [b]	2.411	~ 3.3	2.491	0.435	2.326	2.348
QCISD [c]	2.414	2.74				
CCSD [d]	2.394	3.09	2.470	0.553	2.309	2.453
Obs. [e]	2.397	~ 3.4[g]	2.471[f]	0.494[f]	2.312	2.280
This work	2.448	3.26	2.548	0.557	2.348	2.355

[a] Zeitz et al. (1979)

[b] Rosmus and Werner (1984)

[c] Wang et al. (2001)

[d] Watts and Bartlett (1992)

[e] Huber and Herzberg (1979)

[f] Rehfuss et al. (1988)

[g] Jones et al. (1980)

Chapter 6

Electron collisions with C_2^- anions

6.1 Introduction

In this chapter, the R-matrix method with pseudostates is used to study electron collisions with the C_2^- anion at its equilibrium geometry. These calculations concentrate on obtaining the low-lying resonances (from the ionisation threshold to 15 eV) and ionisation cross sections. Electronic excitation cross sections are also obtained.

The negative molecular ion C_2^- is one of few molecular anions which has bound electronic excited states. This special feature of C_2^- is due to the high electronic affinity of C_2 and the low electronic excited states of C_2^-. The unusual stability of C_2^- was first noted by Honig (1954) when he observed the emission of neutral and charged carbon molecules from pure graphite filaments. He determined the electron affinity of C_2 to be 3.1 or 4 eV depending on the method of determination. The latest values published by Jones et al. (1980) are in the range 3.374 and 3.408 eV.

A number of studies of electron-impact detachment cross sections of C_2^- was performed by Andersen et al. (1996)and Pedersen et al. (1998, 1999). Andersen et al. (1996) discovered a structure in the electron-impact detachment cross section of C_2^- and suggested the possibility of the existence of temporary C_2^{2-} dianion. They constructed a potential curve of C_2^{2-} as the sum of the isoelectronic N_2 potential curve and Coulomb repulsion e^2/R. They concluded that the position of the observed resonance structure (about 10 eV) agreed with a prediction based on the constructed potential curve of C_2^{2-}. Later Sommerfeld et al. (1997) calculated the metastable ground state of C_2^{2-} at about

3 eV above the negative ion ground state therefore it could not be the origin of the 10 eV resonance. The new measurement of Pedersen et al. (1998) where they bombarded singly charged negative ions of B_2^- and C_2^- with electrons reproduced the resonance structure of Andersen et al. (1996) for C_2^- in the detachment cross section and discovered a significant peak in the dissociation cross section at about the same energy where the structure appeared in the detachment channel. They performed *ab initio* L^2 electronic structure calculations which suggested that excited states of C_2^{2-} of $^1\Pi_g$ and $^3\Pi_g$ symmetries lie about 8 eV above the ground state of C_2^-. They concluded that the calculated excited states have energies of the right order and magnitude to explain the observed resonances. In the latest experiment (Pedersen et al., 1999) the electron collisions with negative ions of B_2^-, C_2^-, O_2^-, BN^- and OH^- were performed. Two resonance features of the same positions but with different widths were identified. The resonance from the detachment cross section had a width of 2.1 eV and the one from the dissociation cross section with a width of 3-4 eV. They calculated that the $^1\Sigma_g^+$ ground state of C_2^{2-} is around 3.8 eV above the ground state of C_2^- and excited states of C_2^{2-} of Σ_u symmetry at $\sim$ 6.3 eV and of Π_g symmetry at $\sim$ 7.6 eV. Sommerfeld et al. (2000) carried out an *ab initio* absorbing potential calculation of the energies and lifetimes of metastable C_2^{2-} resonance and found the C_2^{2-} $^1\Sigma_g^+$ resonance state at 3.5 eV.

The study of C_2^{2-} resonances is challenging since the resonances lie above the low ionisation threshold. The standard close-coupling techniques cannot be used to investigate the behaviour of these resonances. The calculations describe in the next sections were performed using R-matrix method with pseudostates (see chapter 3.4).

6.2 Target calculations

C_2^- is an open shell diatomic anion with 13 electrons. The ground state of the C_2^- is a $X\ ^2\Sigma_g^+$ state with the electronic configuration $1\sigma_g^2\ 1\sigma_u^2\ 2\sigma_g^2\ 2\sigma_u^2\ 1\pi_u^4\ 3\sigma_g$. The next two lowest electron configurations of C_2^- should be $1\sigma_g^2\ 1\sigma_u^2\ 2\sigma_g^2\ 2\sigma_u^2\ 1\pi_u^3\ 3\sigma_g^2$ and $1\sigma_g^2\ 1\sigma_u^2\ 2\sigma_g^2\ 2\sigma_u\ 1\pi_u^4\ 3\sigma_g^2$ producing the states $A\ ^2\Pi_u$ and $B\ ^2\Sigma_u^+$.

All previous MRMPS calculations (Gorfinkiel and Tennyson, 2004) were performed for $2e^-$ targets. In the case of a system with 13 electrons, considerable experimentation was required to make the calculations both tractable and reliable. Target calculations were performed for C_2^- in its equilibrium geometry at 2.396 a_0 (Huber and Herzberg, 1979). First, a Hartree-Fock self-consistent field (HF SCF) calculation was carried out

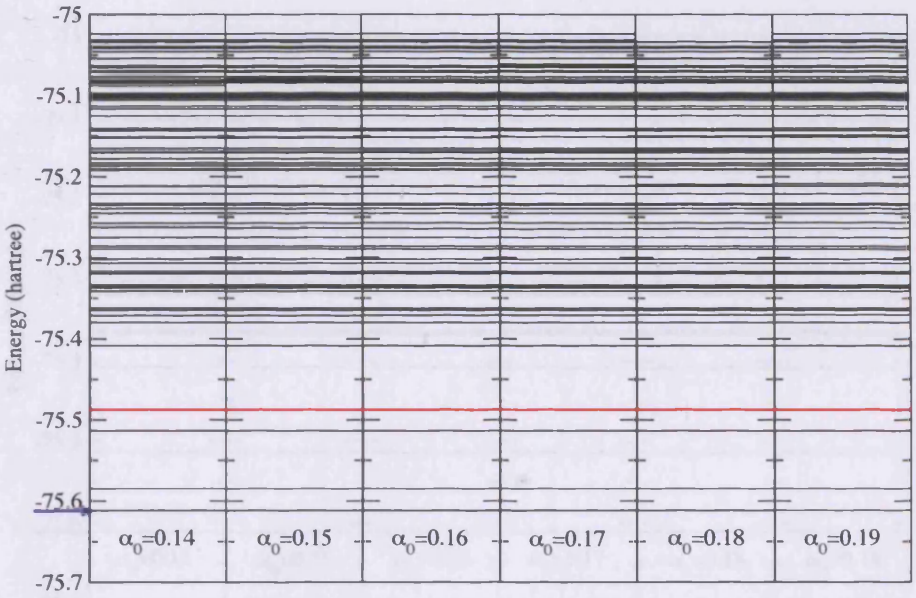

Figure 6.1: Target state distribution for C_2^- for β=1.3 and the α_0 values indicated in the figure. The red line represents the ionisation threshold and the blue arrow indicates the location of the ground state of C_2^-.

using the double zeta plus polarisation (DZP) Gaussian basis set of Dunning (1970) for C to obtain the SCF molecular orbitals (MOs). Second, to create the pseudo-continuum orbitals (PCOs) the CI calculation was performed with the deletion threshold $\delta = 4\times10^{-6}$. These orbitals are used to describe the ionised electron. Therefore, along with the usual configurations, one needs to add another set in which one of the electrons occupies a PCOs within the CI expansion. In the calculations a 10*s* 10*p* 6*d* PCOs set of basis functions were used. The PCOs are expanded in terms of an even-tempered basis set (Schmidt and Ruedenberg, 1979) of GTOs centred at the centre of mass of the system. The exponents of the GTOs in this type of basis sets (see equation 3.53) are calculated for different (α_0,β) values and so different basis sets can be systematically generated. In order to avoid linear dependence problems, several PCO bases were tested (with α_0 = 0.13, 0.14, 0.15, 0.16 0.17, 0.18, 0.19 and β = 1.3, 1.4, 1.5) for *model 1*. The energy distribution of bound states and pseudo states for different (α_0,β) values is shown in figures 6.1 - 6.3. The deviation in the state distributions for different (α_0,β) values is fairly small which suggests that the calculations are trustworthy. The (α_0,β) values were chosen from the middle of the tested scale (α_0 = 0.17 and β = 1.4). Due to the computational limitations the PCO basis sets were restricted to $l \leq 2$.

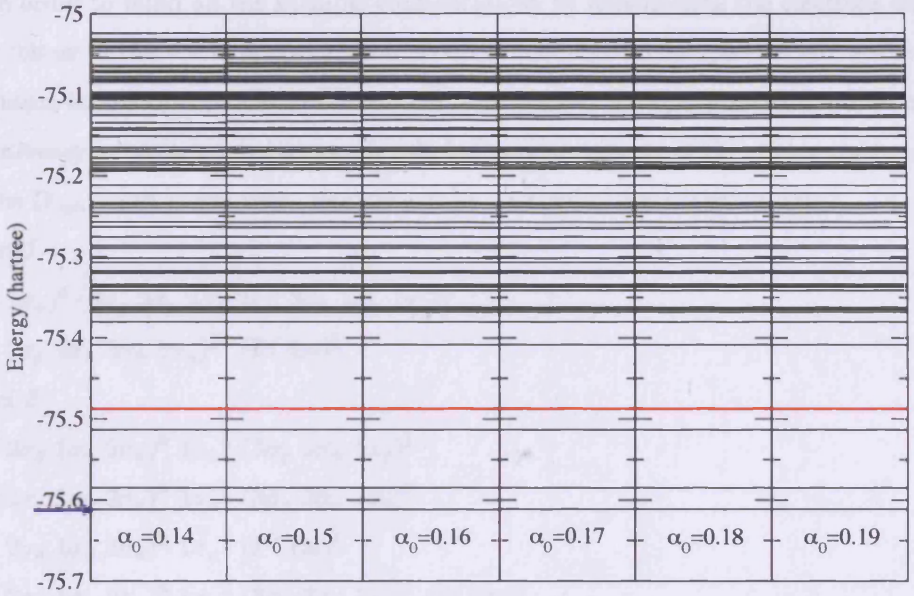

Figure 6.2: Target state distribution for C_2^- for β=1.4 and the α_0 values indicated in the figure. The red line represents the ionisation threshold and the blue arrow indicates the location of the ground state of C_2^-.

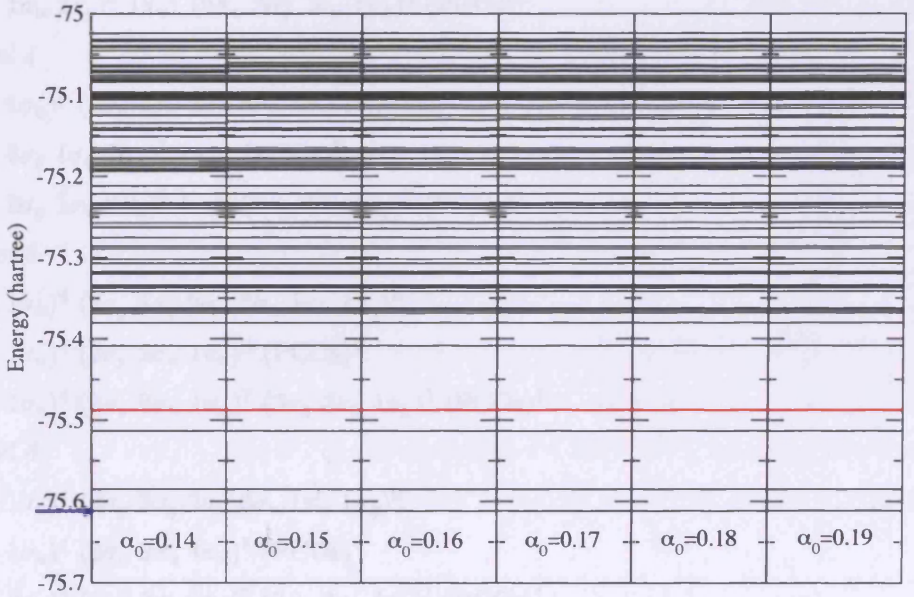

Figure 6.3: Target state distribution for C_2^- for β=1.5 and the α_0 values indicated in the figure. The red line represents the ionisation threshold and the blue arrow indicates the location of the ground state of C_2^-.

In order to build all the possible configurations by distributing the electrons among the orbitals in the active space, several different models of a complete active space configuration interaction (CASCI) calculation were tested. The purpose of these tests was to achieve good agreement with previously found bound states of C_2^-. Using the notation for the $D_{\infty h}$ point group these models can be written in the following way:

model 1

$(1\sigma_g\ 1\sigma_u)^4\ (2\sigma_g\ 3\sigma_g\ 4\sigma_g\ 2\sigma_u\ 3\sigma_u\ 1\pi_u\ 1\pi_g)^9$

$(1\sigma_g\ 2\sigma_g\ 1\sigma_u\ 2\sigma_u\ 1\pi_u)^{12}\ (\mathrm{PCOs})^1$

model 2

$(1\sigma_g\ 2\sigma_g\ 1\sigma_u\ 2\sigma_u)^8\ 1\pi_u{}^4\ (3\sigma_g\ 3\sigma_u\ 1\pi_g)^1$

$(1\sigma_g\ 2\sigma_g\ 1\sigma_u\ 2\sigma_u)^8\ 1\pi_u{}^3\ (3\sigma_g\ 3\sigma_u\ 1\pi_g)^2$

$(1\sigma_g\ 2\sigma_g\ 1\sigma_u\ 2\sigma_u)^8\ 1\pi_u{}^4\ (\mathrm{PCOs})^1$

$(1\sigma_g\ 2\sigma_g\ 1\sigma_u\ 2\sigma_u)^8\ 1\pi_u{}^3\ (3\sigma_g\ 3\sigma_u\ 1\pi_g)^1\ (\mathrm{PCOs})^1$

model 3

$(1\sigma_g\ 1\sigma_u\ 2\sigma_g)^6\ 1\pi_u{}^4\ (2\sigma_u\ 3\sigma_g\ 3\sigma_u\ 1\pi_g)^3$

$(1\sigma_g\ 1\sigma_u\ 2\sigma_g)^6\ 1\pi_u{}^3\ (2\sigma_u\ 3\sigma_g\ 3\sigma_u\ 1\pi_g)^4$

$(1\sigma_g\ 1\sigma_u\ 2\sigma_g)^6\ 1\pi_u{}^4\ (2\sigma_u\ 3\sigma_g\ 3\sigma_u\ 1\pi_g)^2\ (\mathrm{PCOs})^1$

$(1\sigma_g\ 1\sigma_u\ 2\sigma_g)^6\ 1\pi_u{}^3\ (2\sigma_u\ 3\sigma_g\ 3\sigma_u\ 1\pi_g)^3\ (\mathrm{PCOs})^1$

model 4

$(1\sigma_g\ 1\sigma_u)^4\ (2\sigma_g\ 3\sigma_g\ 2\sigma_u\ 3\sigma_u\ 1\pi_u\ 1\pi_g)^9$

$(1\sigma_g\ 2\sigma_g\ 1\sigma_u\ 2\sigma_u)^8\ 1\pi_u{}^4\ (\mathrm{PCOs})^1$

$(1\sigma_g\ 2\sigma_g\ 1\sigma_u\ 2\sigma_u)^8\ 1\pi_u{}^3\ (3\sigma_g\ 3\sigma_u\ 1\pi_g)^1\ (\mathrm{PCOs})^1$

model 5

$(1\sigma_g\ 1\sigma_u)^4\ (2\sigma_g\ 3\sigma_g\ 2\sigma_u\ 3\sigma_u\ 1\pi_u\ 1\pi_g)^9$

$(1\sigma_g\ 1\sigma_u)^4\ (2\sigma_g\ 2\sigma_u\ 1\pi_u)^8\ (\mathrm{PCOs})^1$

$(1\sigma_g\ 1\sigma_u)^4\ (2\sigma_g\ 2\sigma_u\ 1\pi_u)^7\ (3\sigma_g\ 3\sigma_u\ 1\pi_g)^1\ (\mathrm{PCOs})^1$

model 6

$(1\sigma_g\ 1\sigma_u)^4\ (2\sigma_g\ 3\sigma_g\ 2\sigma_u\ 3\sigma_u\ 1\pi_u\ 1\pi_g)^9$

$(1\sigma_g\ 1\sigma_u)^4\ (2\sigma_g\ 2\sigma_u\ 1\pi_u)^8\ (\mathrm{PCOs})^1$

$(1\sigma_g\ 1\sigma_u)^4\ (2\sigma_g\ 2\sigma_u\ 1\pi_u)^7\ (3\sigma_g\ 3\sigma_u\ 1\pi_g)^1\ (\mathrm{PCOs})^1$

$(1\sigma_g\ 1\sigma_u)^4\ (2\sigma_g\ 2\sigma_u\ 1\pi_u)^6\ (3\sigma_g\ 3\sigma_u\ 1\pi_g)^2\ (\mathrm{PCOs})^1$

model 7

$(1\sigma_g\ 1\sigma_u\ 2\sigma_g)^6\ (2\sigma_u\ 3\sigma_g\ 3\sigma_u\ 1\pi_g\ 1\pi_u)^7$

$(1\sigma_g\ 1\sigma_u\ 2\sigma_g)^6\ (2\sigma_u\ 3\sigma_g\ 3\sigma_u\ 1\pi_g\ 1\pi_u)^6$ $(\text{PCOs})^1$

model 8

$(1\sigma_g\ 1\sigma_u)^4\ (2\sigma_g\ 3\sigma_g\ 4\sigma_g\ 2\sigma_u\ 3\sigma_u\ 1\pi_u\ 1\pi_g)^9$

$(1\sigma_g\ 1\sigma_u)^4\ (2\sigma_g\ 3\sigma_g\ 4\sigma_g\ 2\sigma_u\ 3\sigma_u\ 1\pi_u\ 1\pi_g)^8$ $(\text{PCOs})^1$

Table 6.1: The dimension of final Hamiltonian for N and $(N+1)$-electron calculations for different models for ^1A_g and ^2A_g symmetry (respectively).

	N	(N+1)
Model 1	1100	21705
Model 2	140	6447
Model 3	1600	52270
Model 4	425	6575
Model 5	597	12283
Model 6	3111	12283
Model 7	20454	823823
Model 8	97500	too big

In these models, the first set of configuration represent CAS CSFs constructed from target MOs and the second part represent configurations involving PCOs. Two different sets of PCOs were tested:

4-14a_g 2-7b_{2u} 2-7b_{3u} 1-4b_{1g} 4-8b_{1u} 2-5b_{3g} 2-5b_{2g} 1a_u

4-24a_g 2-10b_{2u} 2-10b_{3u} 1-7b_{1g} 4-12b_{1u} 2-8b_{3g} 2-8b_{2g} 1a_u

using the notation for the irreducible representations of D_{2h} point group. The eigenphase sum calculated with the larger PCO set was slightly higher then the ones which used fewer PCOs, therefore the final calculations used the larger PCO set. This set spans an energy range from ~6 eV to 16 eV for all models except the *model 4*, 5 and 6 where this range runs from ~5.2 eV to 19 eV.

The first criteria for choosing amongst the models was the size of Hamiltonian matrix due to the computational limitations. The table 6.1 shows the dimensions of the final Hamiltonian matrix for all models. The second criteria was to gain a good agreement with the previous calculations of electron collisions with C_2. The values of the bound states $X\ ^2\Sigma_g^+$, $A\ ^2\Pi_u$ and $B\ ^2\Sigma_u^+$ obtained from these calculations were -75.672128 E_h,

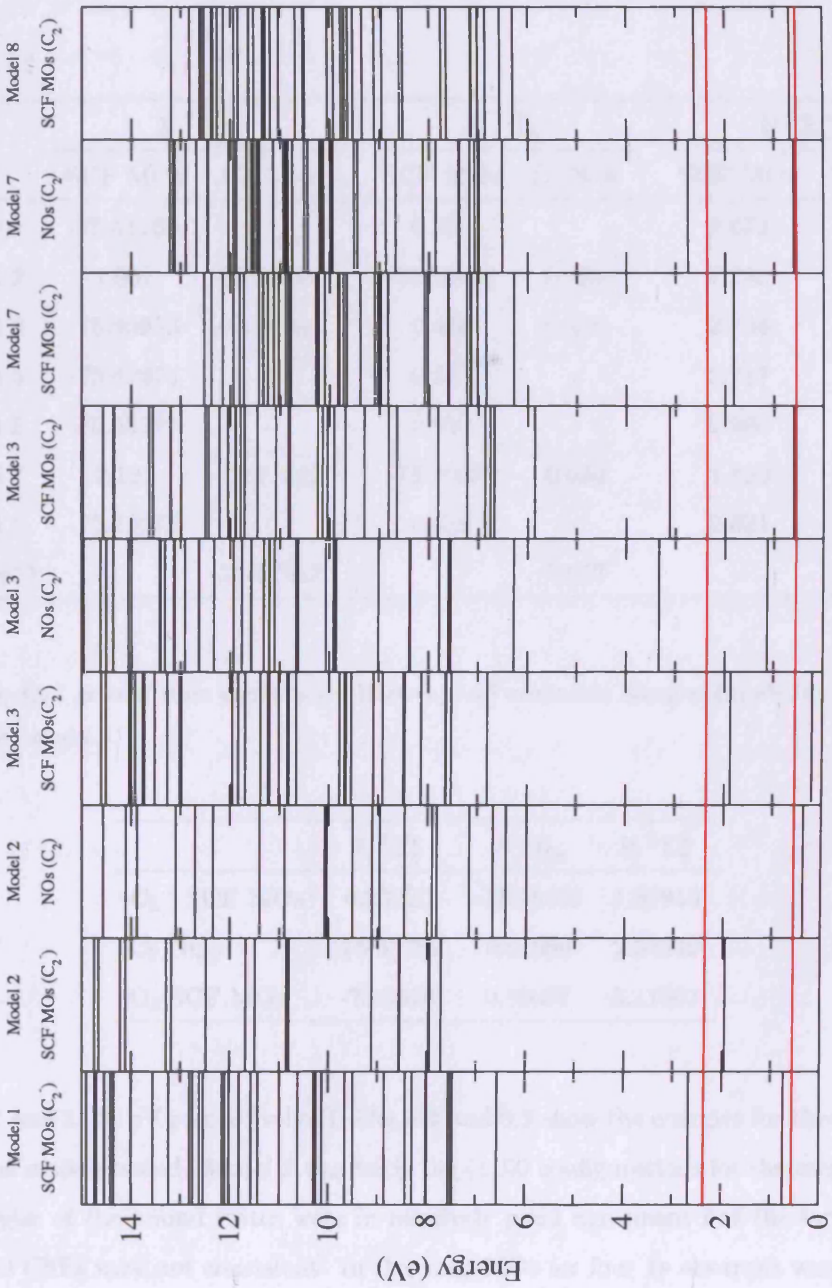

Figure 6.4: Target state distribution for C_2^- for various models and orbitals as indicated in the figure. Two red lines represent the two lowest excited states obtained from $(C_2 + e^-)$ calculation.

Table 6.2: C_2^- ground state energies (in Hartree) and excitation energies (in eV) for different models and orbitals.

	$X\ ^2\Sigma_g^+$		$A\ ^2\Pi_u$		$B\ ^2\Sigma_u^+$	
	SCF MOs	C_2 NOs	SCF MOs	C_2 NOs	SCF MOs	C_2 NOs
Model 1	-75.61166	-	0.729	-	2.673	-
Model 2	1.951	-75.53709	-75.56659	0.850	7.955	5.813
Model 4	-75.60956	-75.60944	0.468	0.419	2.734	2.506
Model 5	-75.62675	-	0.883	-	2.717	-
Model 6	-75.65777	-	0.912	-	2.908	-
Model 7	0.123	-75.71419	-75.66055	0.686	1.823	2.621
Model 8	-75.72075	-	0.689	-	2.621	-
($C_2 + e^-$)	-	-75.67213	-	0.557	-	2.355

Table 6.3: C_2^- ground state energies (in Hartree) and excitation energies (in eV) for different orbitals for *model 3*.

	$X\ ^2\Sigma_g^+$	$A\ ^2\Pi_u$	$B\ ^2\Sigma_u^+$
C_2^- SCF MOs	0.23220	-75.58408	1.87910
C_2 NOs	-75.58782	0.61069	2.54949
C_2 SCF MOs	-75.5948	0.59687	3.11503

0.557 eV and 2.355 eV respectively. Tables 6.2 and 6.3 show the energies for these states for all the models tested. *Model 1* was fairly big (1100 configurations for the target) and the energies of the bound states were in relatively good agreement but the target MO and PCO CSFs were not consistent. In this case MOs for four $1s$ electrons were frozen in the $1\sigma_g$ and $1\sigma_u$ orbitals, and remaining nine electrons were freely distributed among $2\sigma_g$ $3\sigma_g$ $4\sigma_g$ $2\sigma_u$ $3\sigma_u$ $1\pi_u$ $1\pi_g$ orbitals. In the second configuration twelve electrons were frozen in $1\sigma_g$ $2\sigma_g$ $1\sigma_u$ $2\sigma_u$ $1\pi_u$ orbitals and the remaining electron was put into the PCOs. Hence the more consistent *model 2* was designed. In this model, eight electrons were frozen in the core and therefore the size of the Hamiltonian matrix decreased (140).

However the ground state changed to $A\ ^2\Pi_u$ and the energies of two lowest excited states did not agree with the values calculated above. In order to improve these and to increase the size of the Hamiltonian matrix two electrons were freed from the core. This led to 1600 configurations in *model 3*. This slightly improved the energies but unfortunately $A\ ^2\Pi_u$ still remained the ground state. *model 4* was conceived by using MO CSFs from *model 1* and PCO CSFs from *model 2*. With a size of 425 for the Hamiltonian matrix, the model was suitable for testing purposes. The ground state for this model was $X\ ^2\Sigma_g^+$ and better values of energies were obtained. The next step was to design bigger models for testing the partitioned R-matrix method. Therefore *model 5* used MO CSFs from *model 4* and two configurations for PCO CSFs were obtained from these MO CSFs making the model consistent. The size of Hamiltonian matrix increased (4464) but still did not required the use of the partitioned R-matrix method. Nevertheless the energies of the ground state and first excited state are better then in *model 4*. So *model 6* was constructed from *model 5* by adding one more configuration for MO CSFs which increased the Hamiltonian matrix to 23152. *Model 7* and 8 were designed to use the partitioned R-matrix method in the target calculations, so the Hamiltonian matrices are already reduced.

Three different sets of molecular orbitals were tested with the various models: SCF MOs of C_2^-, natural orbitals (NOs) of C_2 and SCF MOs of C_2. Table 6.2 shows the energies of the ground state $X\ ^2\Sigma_g^+$ and two lowest excited states $A\ ^2\Pi_u$ and $B\ ^2\Sigma_u^+$ of C_2^- for the *model 1*, 2, 4, 5, 6, 7 and 8. Two sets of molecular orbitals have been used: SCF MOs and NOs of C_2. Table 6.3 shows the energies for the same states as table 6.2 but just for *model 3*. In this model, three sets of molecular orbitals have been used: SCF MOs, NOs of C_2 and SCF MOs of C_2. Figure 6.4 shows the target state distributions for different models using various orbitals. The best agreement with the previous calculations was found for the *model 4* and 5.

6.3 Scattering calculations

The final calculations used 114 states in the close-coupling expansion of which 66 are doublets and only the 3 lowest state are real physical states ($X\ ^2\Sigma_g^+$, $A\ ^2\Pi_u$ and $B\ ^2\Sigma_u^+$), the rest being pseudo states. The range of scattering energies was restricted to energies below 19 eV. The deletion threshold δ for COs was 2×10^{-6}. The (N+1)-electron calculations used the models which balance the ones for the C_2^- target. The L^2 functions χ_m in

equation 3.5 are constructed from the target orbitals. Using the notation for irreducible representations of $D_{\infty h}$, the CI models can be expressed following way:

model 1

$(1\sigma_g\ 1\sigma_u)^4\ (2\sigma_g\ 3\sigma_g\ 4\sigma_g\ 2\sigma_u\ 3\sigma_u\ 1\pi_u\ 1\pi_g)^9\ (\mathrm{COs})^1$

$(1\sigma_g\ 2\sigma_g\ 1\sigma_u\ 2\sigma_u\ 1\pi_u)^{12}\ (\mathrm{PCOs})^1\ (\mathrm{COs})^1$

$(1\sigma_g\ 1\sigma_u)^4\ (2\sigma_g\ 3\sigma_g\ 4\sigma_g\ 2\sigma_u\ 3\sigma_u\ 1\pi_u\ 1\pi_g)^{10}$

$(1\sigma_g\ 2\sigma_g\ 1\sigma_u\ 2\sigma_u\ 1\pi_u)^{12}\ (\mathrm{PCOs})^2$

$(1\sigma_g\ 2\sigma_g\ 1\sigma_u\ 2\sigma_u\ 1\pi_u)^{12}\ (3\sigma_g\ 4\sigma_g\ 3\sigma_u\ 1\pi_g)^1\ (\mathrm{PCOs})^1$

model 2

$(1\sigma_g\ 2\sigma_g\ 1\sigma_u\ 2\sigma_u)^8\ 1\pi_u{}^4\ (3\sigma_g\ 3\sigma_u\ 1\pi_g)^1\ (\mathrm{COs})^1$

$(1\sigma_g\ 2\sigma_g\ 1\sigma_u\ 2\sigma_u)^8\ 1\pi_u{}^3\ (3\sigma_g\ 3\sigma_u\ 1\pi_g)^2\ (\mathrm{COs})^1$

$(1\sigma_g\ 2\sigma_g\ 1\sigma_u\ 2\sigma_u)^8\ 1\pi_u{}^4\ (\mathrm{PCOs})^1\ (\mathrm{COs})^1$

$(1\sigma_g\ 2\sigma_g\ 1\sigma_u\ 2\sigma_u)^8\ 1\pi_u{}^3\ (3\sigma_g\ 3\sigma_u\ 1\pi_g)^1\ (\mathrm{PCOs})^1\ (\mathrm{COs})^1$

$(1\sigma_g\ 2\sigma_g\ 1\sigma_u\ 2\sigma_u)^8\ 1\pi_u{}^4\ (3\sigma_g\ 3\sigma_u\ 1\pi_g)^2$

$(1\sigma_g\ 2\sigma_g\ 1\sigma_u\ 2\sigma_u)^8\ 1\pi_u{}^4\ (3\sigma_g\ 3\sigma_u\ 1\pi_g)^1\ (\mathrm{PCOs})^1$

$(1\sigma_g\ 2\sigma_g\ 1\sigma_u\ 2\sigma_u{}^8\ 1\pi_u{}^4\ (\mathrm{PCOs})^2$

$(1\sigma_g\ 2\sigma_g\ 1\sigma_u\ 2\sigma_u)^8\ 1\pi_u{}^3\ (3\sigma_g\ 3\sigma_u\ 1\pi_g)^2\ (\mathrm{PCOs})^1$

$(1\sigma_g\ 2\sigma_g\ 1\sigma_u\ 2\sigma_u)^8\ 1\pi_u{}^3\ (3\sigma_g\ 3\sigma_u\ 1\pi_g)^1\ (\mathrm{PCOs})^2$

model 3

$(1\sigma_g\ 1\sigma_u\ 2\sigma_g)^6\ 1\pi_u{}^4\ (2\sigma_u\ 3\sigma_g\ 3\sigma_u\ 1\pi_g)^3\ (\mathrm{COs})^1$

$(1\sigma_g\ 1\sigma_u\ 2\sigma_g)^6\ 1\pi_u{}^3\ (2\sigma_u\ 3\sigma_g\ 3\sigma_u\ 1\pi_g)^4\ (\mathrm{COs})^1$

$(1\sigma_g\ 1\sigma_u\ 2\sigma_g)^6\ 1\pi_u{}^4\ (2\sigma_u\ 3\sigma_g\ 3\sigma_u\ 1\pi_g)^2\ (\mathrm{PCOs})^1\ (\mathrm{COs})^1$

$(1\sigma_g\ 1\sigma_u\ 2\sigma_g)^6\ 1\pi_u{}^3\ (2\sigma_u\ 3\sigma_g\ 3\sigma_u\ 1\pi_g)^3\ (\mathrm{PCOs})^1\ (\mathrm{COs})^1$

$(1\sigma_g\ 1\sigma_u\ 2\sigma_g)^6\ 1\pi_u{}^4\ (2\sigma_u\ 3\sigma_g\ 3\sigma_u\ 1\pi_g)^4$

$(1\sigma_g\ 1\sigma_u\ 2\sigma_g)^6\ 1\pi_u{}^4\ (2\sigma_u\ 3\sigma_g\ 3\sigma_u\ 1\pi_g)^3\ (\mathrm{PCOs})^1$

$(1\sigma_g\ 1\sigma_u\ 2\sigma_g)^6\ 1\pi_u{}^4\ (2\sigma_u\ 3\sigma_g\ 3\sigma_u\ 1\pi_g)^2\ (\mathrm{PCOs})^2$

$(1\sigma_g\ 1\sigma_u\ 2\sigma_g)^6\ 1\pi_u{}^3\ (2\sigma_u\ 3\sigma_g\ 3\sigma_u\ 1\pi_g)^4\ (\mathrm{PCOs})^1$

$(1\sigma_g\ 1\sigma_u\ 2\sigma_g)^6\ 1\pi_u{}^3\ (2\sigma_u\ 3\sigma_g\ 3\sigma_u\ 1\pi_g)^3\ (\mathrm{PCOs})^2$

model 4

$(1\sigma_g\ 1\sigma_u)^4\ (2\sigma_g\ 3\sigma_g\ 2\sigma_u\ 3\sigma_u\ 1\pi_u\ 1\pi_g)^9\ (\mathrm{COs})^1$

$(1\sigma_g\ 2\sigma_g\ 1\sigma_u\ 2\sigma_u)^8\ 1\pi_u{}^4\ (\mathrm{PCOs})^1\ (\mathrm{COs})^1$

$(1\sigma_g\ 2\sigma_g\ 1\sigma_u\ 2\sigma_u)^8\ 1\pi_u{}^3\ (3\sigma_g\ 3\sigma_u\ 1\pi_g)^1\ (\mathrm{PCOs})^1\ (\mathrm{COs})^1$

$(1\sigma_g\ 1\sigma_u)^4\ (2\sigma_g\ 3\sigma_g\ 2\sigma_u\ 3\sigma_u\ 1\pi_u\ 1\pi_g)^{10}$

$(1\sigma_g\ 2\sigma_g\ 1\sigma_u\ 2\sigma_u)^8\ 1\pi_u{}^4\ (\mathrm{PCOs})^2$

$(1\sigma_g\ 2\sigma_g\ 1\sigma_u\ 2\sigma_u)^8\ 1\pi_u{}^3\ (3\sigma_g\ 3\sigma_u\ 1\pi_g)^2\ (\mathrm{PCOs})^1$

$(1\sigma_g\ 2\sigma_g\ 1\sigma_u\ 2\sigma_u)^8\ 1\pi_u{}^3\ (3\sigma_g\ 3\sigma_u\ 1\pi_g)^1\ (\mathrm{PCOs})^2$

model 5

$(1\sigma_g\ 1\sigma_u)^4\ (2\sigma_g\ 3\sigma_g\ 2\sigma_u\ 3\sigma_u\ 1\pi_u\ 1\pi_g)^9\ (\mathrm{COs})^1$

$(1\sigma_g\ 1\sigma_u)^4\ (2\sigma_g\ 2\sigma_u\ 1\pi_u)^8\ (\mathrm{PCOs})^1\ (\mathrm{COs})^1$

$(1\sigma_g\ 1\sigma_u)^4\ (2\sigma_g\ 2\sigma_u\ 1\pi_u)^7\ (3\sigma_g\ 3\sigma_u\ 1\pi_g)^1\ (\mathrm{PCOs})^1\ (\mathrm{COs})^1$

$(1\sigma_g\ 1\sigma_u)^4\ (2\sigma_g\ 3\sigma_g\ 2\sigma_u\ 3\sigma_u\ 1\pi_u\ 1\pi_g)^{10}$

$(1\sigma_g\ 1\sigma_u)^4\ (2\sigma_g\ 2\sigma_u\ 1\pi_u)^8\ (\mathrm{PCOs})^2$

$(1\sigma_g\ 1\sigma_u)^4\ (2\sigma_g\ 2\sigma_u\ 1\pi_u)^7\ (3\sigma_g\ 3\sigma_u\ 1\pi_g)^2\ (\mathrm{PCOs})^1$

$(1\sigma_g\ 1\sigma_u)^4\ (2\sigma_g\ 2\sigma_u\ 1\pi_u)^7\ (3\sigma_g\ 3\sigma_u\ 1\pi_g)^1\ (\mathrm{PCOs})^2$

model 6

$(1\sigma_g\ 1\sigma_u)^4\ (2\sigma_g\ 3\sigma_g\ 2\sigma_u\ 3\sigma_u\ 1\pi_u\ 1\pi_g)^9\ (\mathrm{COs})^1$

$(1\sigma_g\ 1\sigma_u)^4\ (2\sigma_g\ 2\sigma_u\ 1\pi_u)^8\ (\mathrm{PCOs})^1\ (\mathrm{COs})^1$

$(1\sigma_g\ 1\sigma_u)^4\ (2\sigma_g\ 2\sigma_u\ 1\pi_u)^7\ (3\sigma_g\ 3\sigma_u\ 1\pi_g)^1\ (\mathrm{PCOs})^1\ (\mathrm{COs})^1$

$(1\sigma_g\ 1\sigma_u)^4\ (2\sigma_g\ 2\sigma_u\ 1\pi_u)^6\ (3\sigma_g\ 3\sigma_u\ 1\pi_g)^2\ (\mathrm{PCOs})^1\ (\mathrm{COs})^1$

$(1\sigma_g\ 1\sigma_u)^4\ (2\sigma_g\ 3\sigma_g\ 2\sigma_u\ 3\sigma_u\ 1\pi_u\ 1\pi_g)^{10}$

$(1\sigma_g\ 1\sigma_u)^4\ (2\sigma_g\ 2\sigma_u\ 1\pi_u)^8\ (\mathrm{PCOs})^2$

$(1\sigma_g\ 1\sigma_u)^4\ (2\sigma_g\ 2\sigma_u\ 1\pi_u)^7\ (3\sigma_g\ 3\sigma_u\ 1\pi_g)^2\ (\mathrm{PCOs})^1$

$(1\sigma_g\ 1\sigma_u)^4\ (2\sigma_g\ 2\sigma_u\ 1\pi_u)^7\ (3\sigma_g\ 3\sigma_u\ 1\pi_g)^1\ (\mathrm{PCOs})^2$

model 7

$(1\sigma_g\ 1\sigma_u\ 2\sigma_g)^6\ (2\sigma_u\ 3\sigma_g\ 3\sigma_u\ 1\pi_g\ 1\pi_u)^7\ (\mathrm{COs})^1$

$(1\sigma_g\ 1\sigma_u\ 2\sigma_g)^6\ (2\sigma_u\ 3\sigma_g\ 3\sigma_u\ 1\pi_g\ 1\pi_u)^6\ (\mathrm{PCOs})^1\ (\mathrm{COs})^1$

$(1\sigma_g\ 1\sigma_u\ 2\sigma_g)^6\ (2\sigma_u\ 3\sigma_g\ 3\sigma_u\ 1\pi_g\ 1\pi_u)^8$

$(1\sigma_g\ 1\sigma_u\ 2\sigma_g)^6\ (2\sigma_u\ 3\sigma_g\ 3\sigma_u\ 1\pi_g\ 1\pi_u)^7\ (\mathrm{PCOs})^1$

$(1\sigma_g\ 1\sigma_u\ 2\sigma_g)^6\ (2\sigma_u\ 3\sigma_g\ 3\sigma_u\ 1\pi_g\ 1\pi_u)^6\ (\mathrm{PCOs})^2$

$(1\sigma_g\ 1\sigma_u)^4\ (2\sigma_g\ 3\sigma_g\ 2\sigma_u\ 3\sigma_u\ 1\pi_u\ 1\pi_g)^{10}$

$(1\sigma_g\ 1\sigma_u)^4\ (2\sigma_g\ 2\sigma_u\ 1\pi_u)^8\ (\mathrm{PCOs})^2$

$(1\sigma_g\ 1\sigma_u)^4\ (2\sigma_g\ 2\sigma_u\ 1\pi_u)^7\ (3\sigma_g\ 3\sigma_u\ 1\pi_g)^2\ (\mathrm{PCOs})^1$

$(1\sigma_g\ 1\sigma_u)^4\ (2\sigma_g\ 2\sigma_u\ 1\pi_u)^7\ (3\sigma_g\ 3\sigma_u\ 1\pi_g)^1\ (\mathrm{PCOs})^2$

model 8

$(1\sigma_g\ 1\sigma_u)^4\ (2\sigma_g\ 3\sigma_g\ 4\sigma_g\ 2\sigma_u\ 3\sigma_u\ 1\pi_u\ 1\pi_g)^9\ (\mathrm{COs})^1$

$(1\sigma_g\ 1\sigma_u)^4\ (2\sigma_g\ 3\sigma_g\ 4\sigma_g\ 2\sigma_u\ 3\sigma_u\ 1\pi_u\ 1\pi_g)^8\ (\mathrm{PCOs})^1\ (\mathrm{COs})^1$

$(1\sigma_g\ 1\sigma_u)^4\ (2\sigma_g\ 3\sigma_g\ 4\sigma_g\ 2\sigma_u\ 3\sigma_u\ 1\pi_u\ 1\pi_g)^{10}$

$(1\sigma_g\ 1\sigma_u)^4\ (2\sigma_g\ 3\sigma_g\ 4\sigma_g\ 2\sigma_u\ 3\sigma_u\ 1\pi_u\ 1\pi_g)^9$ $(\mathrm{PCOs})^1$

$(1\sigma_g\ 1\sigma_u)^4\ (2\sigma_g\ 3\sigma_g\ 4\sigma_g\ 2\sigma_u\ 3\sigma_u\ 1\pi_u\ 1\pi_g)^8$ $(\mathrm{PCOs})^2$

Three different types of L^2 functions were used in these calculations. Firstly, all fourteen electrons were placed into a configuration which represent the MOs. Secondly, the configurations with the PCOs for target is taken and instead of one electron in PCOs two are put in. Thirdly, the second type of L^2 function is adopted but one electron from PCOs is taken out and distributed into orbitals,in order to maintain consistency with the configuration of MOs. The incident electron was described by continuum orbitals which were represented as described in chapter 4.3. The continuum basis set of Faure et al. (2002) was used in the calculations. Two different R-matrix radii were tested: a=10 a_0 and a=13 a_0. Figure 6.5 gives a comparison of the eigenphase sums obtained for the ^2A_g symmetry for *model 4* using different R-matrix radii. Due to the larger radius of the C_2^- target states compared with the C_2 target states, a larger integral region radius than used for e^- - C_2 collisions would be necessary. Using too small radius may explain the large differences between the eigenphase sums at low energies in figure 6.5 and the lack of pseudostates near threshold (shown in the target state distribution figure 6.7) leading to a negligible ionization cross section below 7 eV, seen in figures 6.8 and 6.9. The final calculations used the R-matrix radius of 10 a_0 because the eigenphase sums are smoother and lie higher. They were propagated to a radius 100 a_0. This model does not give any linear dependence.

In order to decrease the computational time the partitioned R-matrix method was introduced as described in chapter 3.5. Figure 6.6 shows the eigenphase sums for ^2A_g symmetry for *model 4* using different number of eigenvalues and eigenvectors in calculations. The eigenphase sums show good agreement between the full calculation and the partitioned once. These calculations indicate that use of only 10% of the R-matrix poles from the full calculation is sufficient to give good results.

6.4 Results

The target calculations described in section 6.2 provided the properties of C_2^- target such as energies and transition moments. These were used to obtain the polarizabilities for different models which are shown in the table 6.4. It can be noticed that the models with worst target energy distribution have very inconsistent polarizability. *Model 4*, which

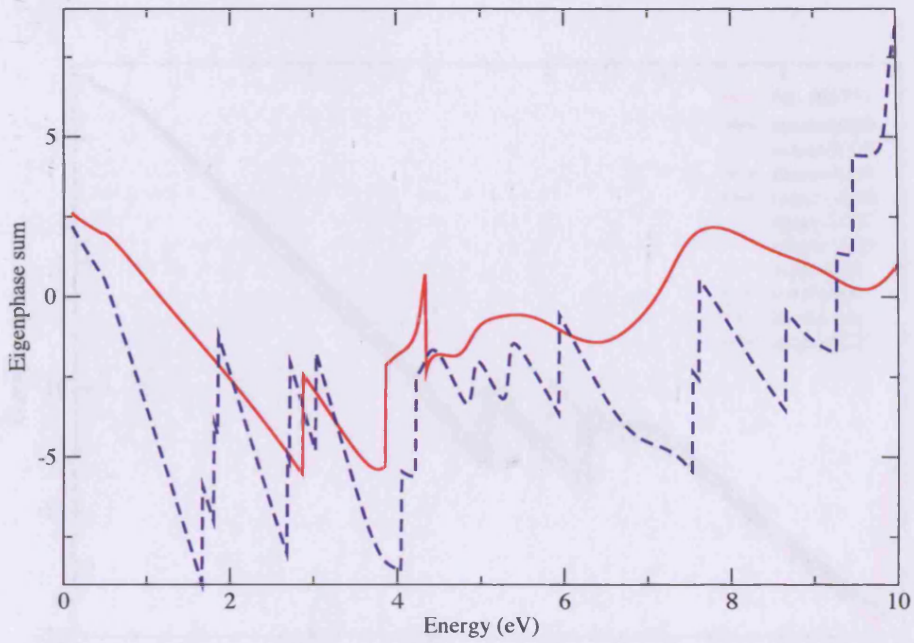

Figure 6.5: The eigenphase sums for ^2A_g symmetry of the (C_2^- + e^-) system at equilibrium geometry as a function of energy for *model 4*. The solid red line represents the eigenphase sum calculated for R-matrix radius a=10 a_0 and the dashed blueline represents the eigenphase sum calculated for a=13 a_0.

was considered good, shows consistency in polarizabilities tested for different (α_0,β) values. This model gives a large C_2^- isotropic polarizability of about 32 a_0^3 depending slightly on the (α_0,β) values. A large polarizability is to be expected for a system with weakly bound and relatively diffuse outer electrons. This value decreases about 0.02 a_0^3 when only states up to 16 eV are included. However the polarizability given by just considering the physical states is only 9.5 a_0^3. This indicate the importance of the pseudostates included in the calculations. Figure 6.7 shows the target state distribution for *model 4* with different (α_0,β) values and orbitals.

6.4.1 Cross sections

The electron collisions with the C_2^- were studied with the MRMPS method. Hence the problem of possible unphysical resonances arose as the pseudostates were included in the calculations. In order to eliminate these pseudo resonances and to identify the real ones, the cross sections have to be examined. As established above, the best model for testing was *model 4*, hence the tests were performed within this model for various values

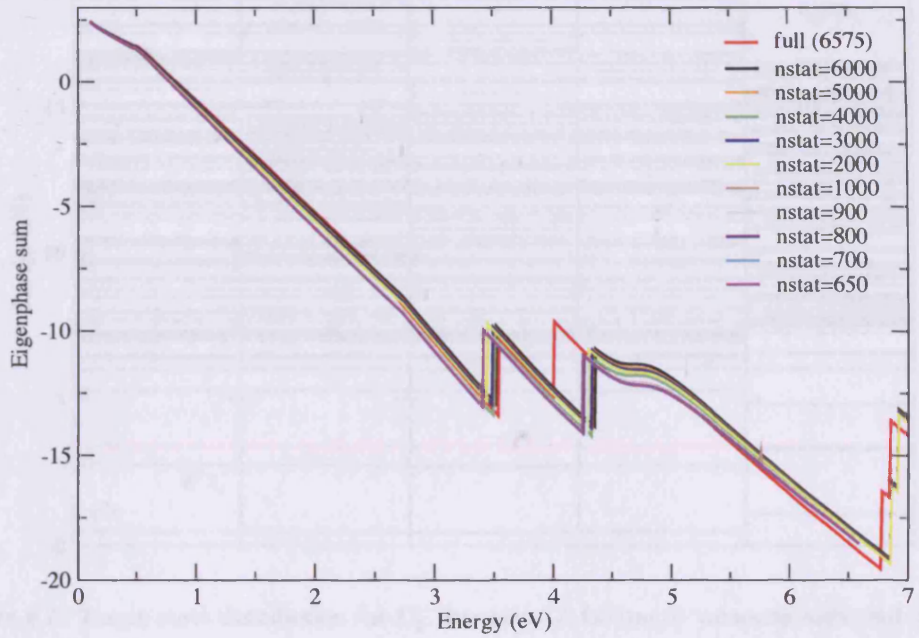

Figure 6.6: The eigenphase sums for ^2A_g symmetry of the (C_2^- + e^-) system at equilibrium geometry as a function of energy using the partitioned R-matrix method for *model 4*. The different dimensions of Hamiltonian were tested as indicated in the legend.

Table 6.4: Polarizabilities of C_2^- in a_0^3 for different models with various (α_0,β) values and orbitals.

	α_0=0.17 β=1.4		α_0=0.15 β=1.4	α_0=0.17 β=1.5	α_0=0.17 β=1.3	
	SCF MOs	C_2 NOs	SCF MOs	SCF MOs	SCF MOs	C_2 NOs
Model 1	26.4237					
Model 2	28.5816	109.5147				
Model 3	67.4873	12.2408				
Model 4	32.2385		32.4776	31.2402	31.9813	18.7999
Model 5	24.9989					
Model 6	24.5477					

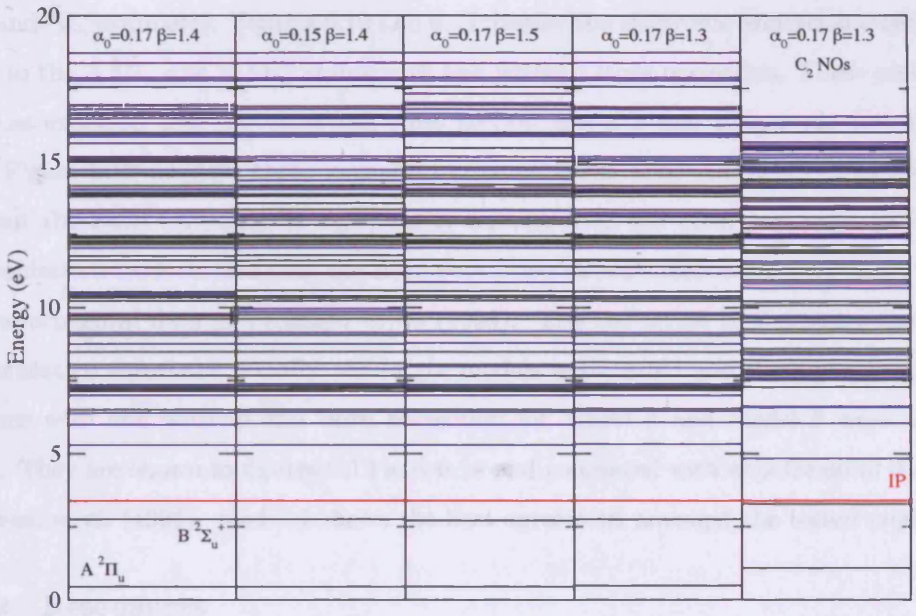

Figure 6.7: Target state distribution for C_2^- for *model 4* for (α_0,β) values as indicated in the figure. The SCF MOs of C_2^- were used in the calculations except where indicated otherwise.

of (α_0,β). The partial ionisation cross sections for all spin symmetries were studied and the consistency in the peaks in the partial ionisation cross sections were discovered in $^1\Pi_g$ and $^3\Pi_g$ symmetries as shown in figure 6.8. From this figure it is apparent that the calculation with α_0=0.17 and β=1.3 can be considered as best because the cross sections do not show as many pseudo resonances in comparison with α_0=0.17 and β=1.5.

Figure 6.9 shows the ionisation cross sections for different (α_0,β) values. Two calculations proved not reliable, one already mentioned above with α_0=0.17 and β=1.5 and the calculations which uses NOs of C_2. The rest of the calculations show a good agreement as to peaks (about 10 and 11 eV). This is why all the other cross sections shown will be taken from the calculation with α_0=0.17 and β=1.3. These electron impact electron detachment cross sections are much smaller than those observed by Pedersen et al. (1999). This can be expected since the dominant, non-resonant, detachment process will be through long range collisions which are favoured by dominant Coulomb interaction. Therefore it is necessary to include such collisions which are almost entirely associated with higher partial waves ($l > 4$) not allowed for in the CO basis set used in this work. Higher partial waves were established by applying a Born correction to all the cross sections arising from dipole allowed electronic excitation channels associated with states of

$^2\Sigma_u^+$ and $^2\Pi_u$ symmetry. Figures 6.10 and 6.11 display the electronic excitation cross sections to the $A\ ^2\Pi_u$ and $B\ ^2\Sigma_u^+$ states with and without Born correction. These pictures show as expected that the corrected cross section are of bigger magnitude (by factor 20). Figure 6.12 displays three ionisation cross sections. The ionisation cross section without the Born correction is significantly smaller then the other two cross sections. The ionisation cross section with the Born correction shows a reasonable agreement with the experimental data of Pedersen et al. (1999). The red arrow in the figure indicate the ionisation threshold. Finally, the larger models were tested and the ionisation cross sections with and without the Born correction fot *model 5* and *model 6* were calculated. They are shown in figures 6.13 and 6.14 and compared with experimental data of Pedersen et al. (1999). *model 5* shows the best agreement amongst the tested models.

6.4.2 Resonances

The scattering calculations for *model 4* identified three low-lying resonances. The reliability of the resonances were tested within the *model 4* by changing (α_0,β) values. This way any pseudo resonances arising from use of the MRMPS method would be eliminated. Table 6.5 compares the resonance positions for different (α_0,β) values. The worst agreement is for the lowest lying resonance $^1\Sigma_g^+$. The difference between the values is 0.16 eV which is within the accuracy of the method. The resonances shown in table 6.6 are from previous works and compared with values obtained from this work for the *model 4* with α_0=0.17 β=1.3. The lowest C_2^{2-} resonance was identified as $^1\Sigma_g^+$ resonance which is in agreement with all the previous work. In comparison with value of Sommerfeld et al. (2000), the value from the presented calculations lies higher and is broader. This maybe due to the fact that it lies very near the ionisation threshold.

Two higher lying resonances are the ones which were observed by Andersen et al. (1996) and Pedersen et al. (1998, 1999). The first one was determined in the detachment cross section and the authors fitted the peak with Lorentzian profile at 10 eV and width of 2.1 eV. The second resonance peak was observed in the dissociation cross section around the same position but with width of 3 - 4 eV. The symmetry of these resonances were not identified. However Andersen et al. (1996) and Pedersen et al. (1998, 1999) have performed *ab initio* calculation which showed that state of C_2^{2-} are of $^1\Pi_g$ and $^3\Pi_g$ symmetry and lie about 8 eV above the $^2\Sigma_g^+$ ground state of C_2^-. Scattering calculations from this thesis show that these two resonances are of $^1\Pi_g$ and $^3\Pi_g$ symmetry and lie

Table 6.5: Resonances of C_2^{2-} for different (α_0,β) values used in *model 4*. The resonance parameters are in eV.

(α_0,β)	$^1\Sigma_g^+$		$^1\Pi_g$		$^3\Pi_g$	
	E_r/eV	Γ/eV	E_r/eV	Γ/eV	E_r/eV	Γ/eV
(0.17,1.4)	5.01	0.58	10.95	0.45	9.68	0.94
(0.15,1.4)	4.99	0.61	10.91	0.39	9.70	0.92
(0.17,1.5)	5.02	0.55	10.98	0.52	9.76	0.99
(0.17,1.3)	4.86	0.65	10.92	0.48	9.71	1.04

Table 6.6: Resonances of C_2^{2-} from previous work and observation compared with calculations from this thesis. The resonance parameters are in eV.

Previous work			This work		
Symmetry	Position	Width	Symmetry	Position	Width
$^1\Sigma_g^{+(a)}$	3.5	0.3	$^1\Sigma_g^+$	4.86	0.65
$^{(b)}$	10.0	2.1	$^1\Pi_g$	10.92	0.52
$^{(b)}$	10.0	3-4	$^3\Pi_g$	9.71	1.14

$^{(a)}$ Sommerfeld et al. (2000) - theory

$^{(b)}$ Andersen et al. (1996); Pedersen et al. (1998, 1999) - experiment

at 10.92 eV and 9.71 eV respectively. These resonances are visible in partial ionisation cross sections for $^1\Pi_g$ and $^3\Pi_g$ symmetries which are shown in figure 6.8. These cross sections were calculated for *model 4* and different (α_0,β) values. These resonances are consistent within the R-matrix box (for lower (α_0,β) values). They are also visible in the total ionisation cross sections shown in figure 6.9. Figures 6.12, 6.13 and 6.14 shows the comparison between the experimental values and the values obtained from calculations for this thesis for different models. The agreement can be considered as good once the theoretical data is augmented with Born correction. In later calculations Pedersen et al. (1999) identified another state of C_2^{2-} of the Σ_u symmetry. Calculations presented in this thesis show no evidence of this additional state.

Due to the fact that a range of diatomic anions appear to temporarily attach an extra electron, a major aim of this study is to establish the binding mechanism for this. As previously suggested by Collins et al. (2005), these calculations show that these resonances can be classified as shape resonances in the sense that the extra electron is temporarily bound by a potential given by the C_2 ground state. These quasibound shape resonances of the C_2^{2-} system are significantly different than the usual shape resonances as they also require a good representation of the long range polarisation potential in order to achieve the temporary binding of the extra electron. As demonstrated here, this can be done using pseudostates to give a discretised representation of the continuum in the geometric region close to the target.

The resonances of the C_2^{2-} system detected in this work do not conform to a standard pattern of shape resonances as the dominant repulsive term is not an angular momentum barrier but the Coulomb repulsion between the anion and the scattering electron. A local minimum which is deep enough to temporarily bind an electron, is caused by polarisation interactions between the C_2^- anion and the scattering electron. This dip in the potential does not depend on the partial wave of the scattering electron and can therefore bind an s-wave, hence the $^1\Sigma_g^+$ resonance.

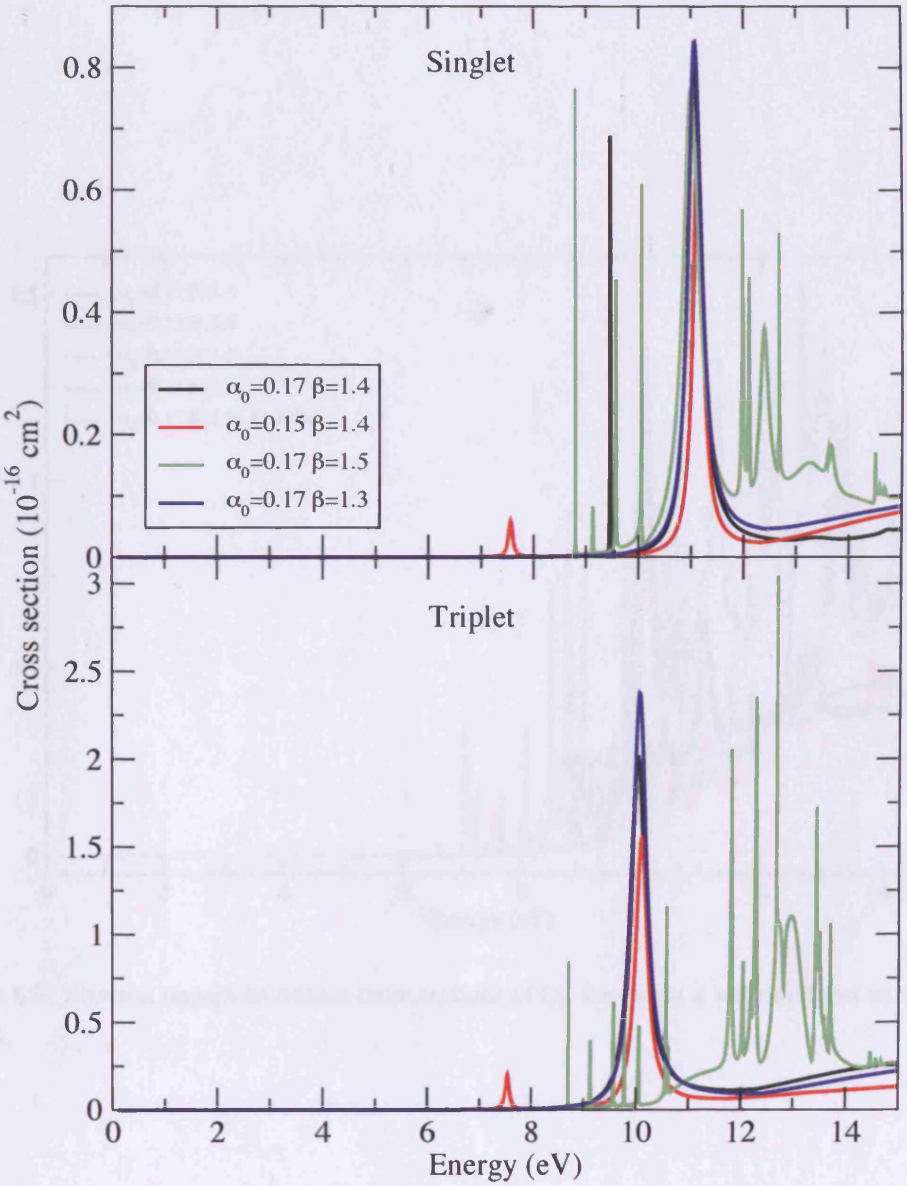

Figure 6.8: Partial ionisation cross sections of C_2^- for *model 4* for $^2B_{3g}$ symmetry for different values of (α_0,β).

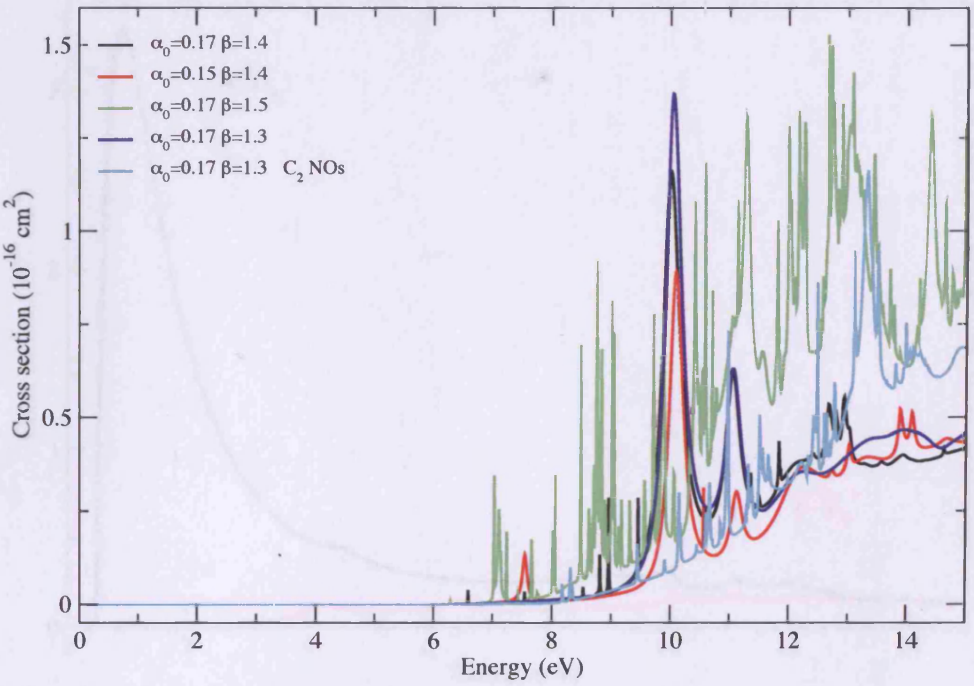

Figure 6.9: Electron impact ionisation cross sections of C_2^- for *model 4* with different values of (α_0,β).

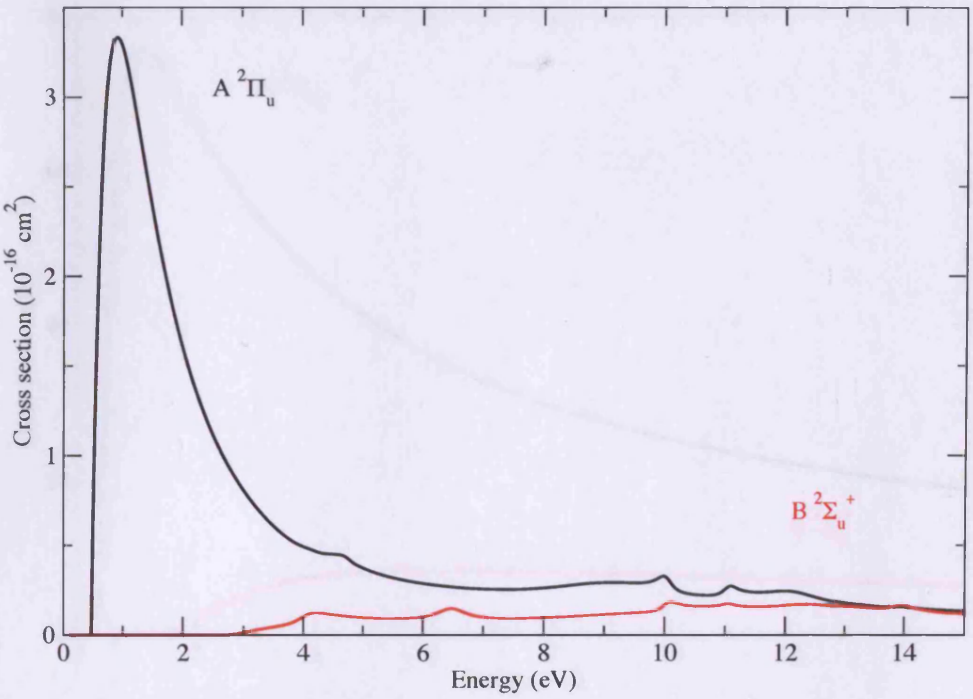

Figure 6.10: Electronic excitation cross sections to the $A\ ^2\Pi_u$ and $B\ ^2\Sigma_u^+$ states without any corrections for *model 4* with α_0=0.17 and β=1.3.

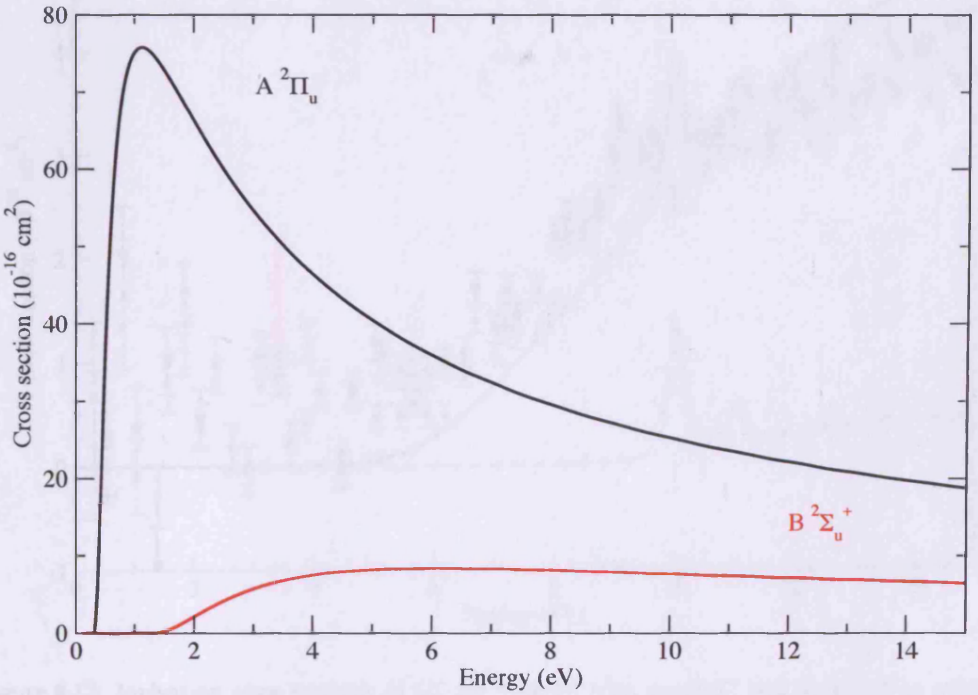

Figure 6.11: Electronic excitation cross sections to the $A\ ^2\Pi_u$ and $B\ ^2\Sigma_u^+$ states with Born correction for *model 4* with α_0=0.17 and β=1.3.

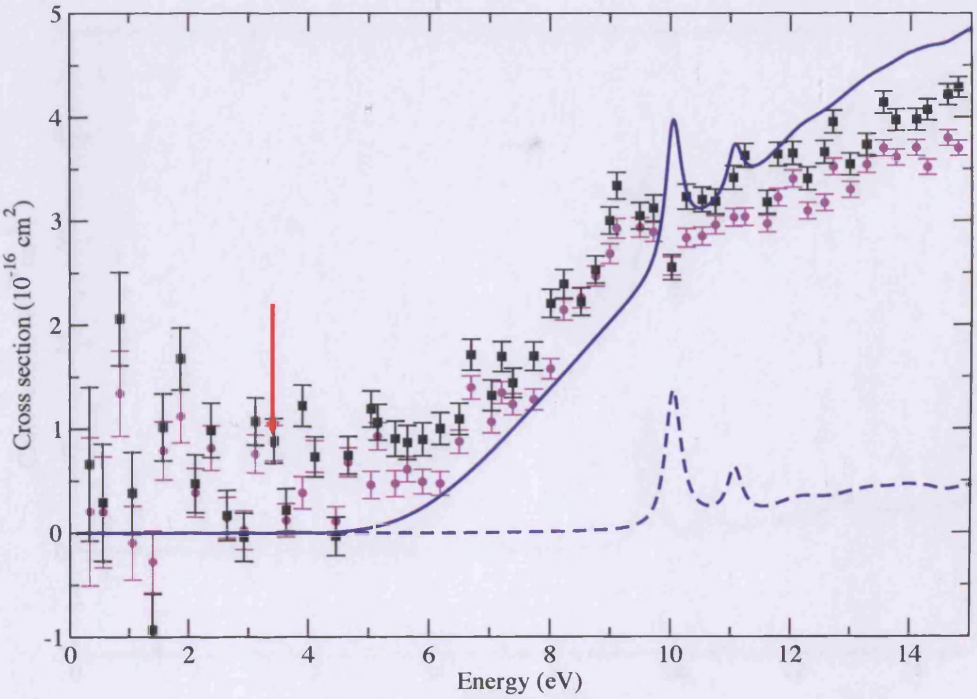

Figure 6.12: Ionisation cross sections of C_2^- for *model 4* with α_0=0.17 and β=1.3. The experimental data (Pedersen et al., 1999) is indicated with full magenta circles (without dissociative channels) and black squares (with dissociative channels); the dashed line represents cross section without Born correction; the solid line represents cross section with Born correction and the red arrow indicate the location of the ionisation threshold.

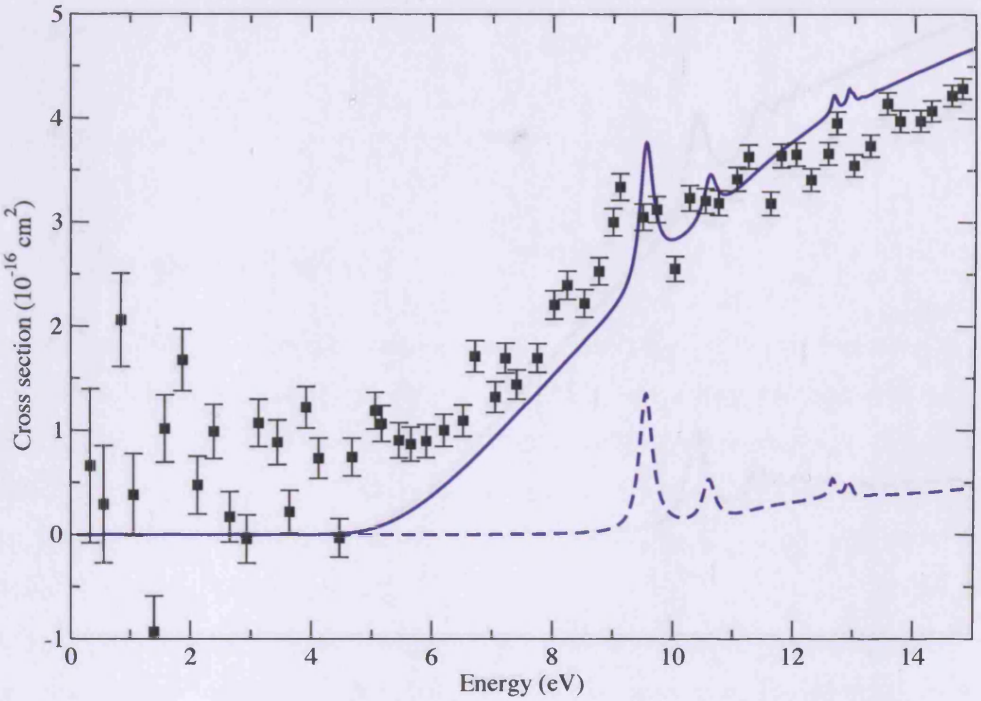

Figure 6.13: Ionisation cross sections of C_2^- for *model 5* with α_0=0.17 and β=1.3. The experimental data (Pedersen et al., 1999) is indicated with full black squares (with dissociative channels); the dashed line represents cross section without Born correction and the solid line represents cross section with Born correction.

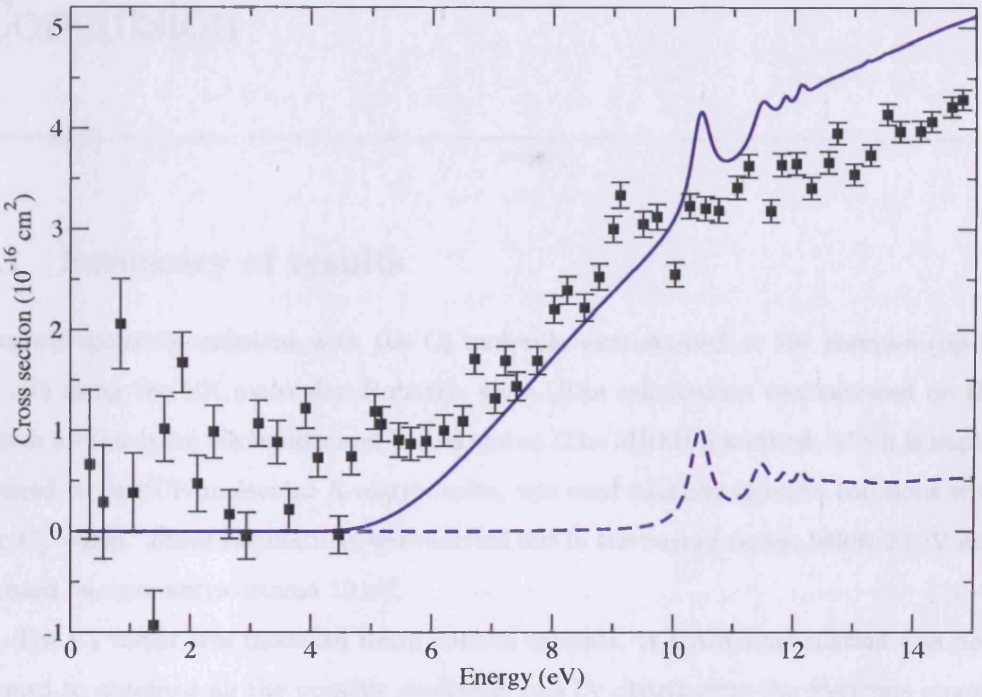

Figure 6.14: Ionisation cross sections of C_2^- for *model 6* with α_0=0.17 and β=1.3. The experimental data (Pedersen et al., 1999) is indicated with full black squares (with dissociative channels); the dashed line represents cross section without Born correction and the solid line represents cross section with Born correction.

Chapter 7

Conclusion

7.1 Summary of results

Electron molecule collisions with the C_2 molecule were studied at low energies (up to 10 eV) using the UK molecular R-matrix suite. The calculations concentrated on the search for low-lying resonances and bound states. The MRMPS method, which is implemented for the UK molecular R-matrix suite, was used to study electron collisions with the C_2^- anion. These calculations were carried out in the energy region below 20 eV and focused on resonances around 10 eV.

The C_2 target was modelled using natural orbitals. A CASCI calculation was performed to obtained all the possible configurations by distributing the electrons among the orbitals in the active space. The potential curves of C_2 were calculated as a function of internuclear distance in the region from 1.648 a_0 to 3.548 a_0. The energies for the equilibrium geometries of lowest states are in good agreement with the available experimental and theoretical values.

The scattering calculations identified many resonances lying in the energy region up to 10 eV. However the high density of the C_2 target states made it difficult to study the behaviour of many of these resonances. Therefore the emphasis was given to the low-lying resonances. Resonances were found with both doublet and quartet spin symmetries. The low-lying resonances of $^2\Pi_g$, $^4\Sigma_u^+$ and $^4\Pi_g$ symmetry became bound states for larger internuclear distances. The excitation cross sections from the ground state ($X\ ^1\Sigma_g^+$) and first excited state ($A\ ^3\Pi_u$) for C_2 were calculated at its equilibrium geometry. They showed evidence for the low-lying resonances at 3.5 and 6 eV. Resonances associated

with excited vibrational states of electronically bound states of C_2^- have been observed using high-resolution techniques (Jones et al., 1980; Hefter et al., 1983). However, there appears to have been no previous study of electronically excited resonance states. These resonances are important because they enhance the elastic and electronically inelastic cross sections. They also provide the route to dissociative electron attachment and are the dominant means for electron impact vibrational excitation.

Three truly bound states were detected: $X\ ^2\Sigma_g^+$, $A\ ^2\Pi_u$ and $B\ ^2\Sigma_u^+$, in good agreement with the different methods and observations. The bound $^4\Sigma_u^+$ state observed by Bondybey and Brus (1975) in a matrix isolation experiment is a low-lying resonance which becomes bound state for internuclear distance $R > 3.1$ a_0.

The C_2^- target was described using the pseudo-continuum orbitals. Because all the previous MRMPS calculations (Gorfinkiel and Tennyson, 2004) were performed for two electron targets, different CASCI calculations had to be performed. This way the consistence with (C_2 + e^-) calculation was guaranteed. The scattering calculations were balanced with the target once.

The target calculations produced the polarizability of C_2^- of about 32 a_0^3 which depends slightly on (α_0,β) values. There is no available value for this property in literature. However a large isotropic polarizability can be expected for C_2^- anion.

The scattering calculations for energies about 6 eV give a number of resonances which is usual for the MRMPS method. Most of these resonances are narrow and change significantly with different PCOs. Nevertheless two much broader resonances have been obtained which do not vary with changing PCOs. They are of $^1\Pi_g$ and $^3\Pi_g$ symmetry and sit at 10.92 and 9.71 eV respectively. These resonances are visible in the partial ionisation cross sections of corresponding symmetries as well as in the total electron impact ionisation cross sections. Pedersen et al. (1999) observed two resonance features both at around 10 eV. The structure visible in the electron impact detachment cross section was 2.1 eV wide and the one in dissociative channels was 3 to 4 eV wide. The resonances obtained in this work were considerably narrower but this may be due to the exclusion of nuclear motion. Another low-lying resonance of $^1\Sigma_g^+$ symmetry at 4.86 eV was obtained from the calculations. This resonance has been identified by Sommerfeld et al. (2000) at slightly lower energy 3.5 eV. Calculations by Pedersen et al. (1999) suggested existence of a resonance of "Σ_u" symmetry at 6.8 eV. However the present calculations showed no evidence of this.

7.2 Future outlook

In order to verify the results of presented calculations there is a need for more experimental and theoretical data. Further calculations using the partitioned R-matrix method should be carried out.

The calculation of the cross sections of the electron collisions with the C_2^- anion extended the range of opportunities for future calculations. The resonances in the experiment were observed in several channels. The presented calculations do not differentiate between the electron impact detachment cross section and dissociation cross section. The separation of these two processes would provide better comparison with the experimental values.

The resonance structures in the electron impact detachment cross section of other diatomic anions were observed B_2^-, O_2^-, BN^- and OH^- by Pedersen et al. (1998, 1999), CN^- and BO^- by Andersen et al. (2001) and Cl_2^- by Collins et al. (2005). These observations led to a number of theoretical calculations. However, the bound state electronic structure calculations performed by Pedersen et al. (1999) cannot be taken as the reliable way for describing resonances (Stibbe and Tennyson, 1999). More qualitative theoretical models were proposed by Andersen et al. (1996) and Collins et al. (2005). Nevertheless there is still need for more theoretical interpretation of these resonance structures. The latest observed electron collision were with the Cl_2^- anion by Collins et al. (2005). This open shell system with 35 electrons could be the next potential candidate for investigation with the partitioned MRMPS method. Due to the absence of value for the polarizability of C_2^- in the literature, another future work prospect could be independent electronic structure calculations on the polarizability of C_2^- and for the other anions studied as most current procedures are probably not really designed for anions.

Bibliography

Abrams M L and Sherrill C D 2004 *J. Chem. Phys.* **121**, 9211–9219.

Almlof J and Taylor P R, eds 1984 *Advances theories and computational approaches to the electronic structure of molecules, (ed. C.E. Dykstra)* Dordrecht: Reidel.

Andersen L H, Bak J, Boyé S, Clausen M, Hovgaard M, Jensen M J, Lapierre A and Seiersen K 2001 *J. Chem. Phys.* **115**, 3566.

Andersen L H, Hvelplund P, Kella D, Mokler P H, Pedersen B, Schmidt H T and Vejby-Christensen L 1996 *J. Phys. B: At. Mol. Opt. Phys.* **29**, L643–L649.

Atkins P W and Friedman R S, eds 1997 *Molecular quantum mechanics* Oxford University Press.

Baluja K L, Burke P G and Morgan L A 1982 *Comput. Phys. Commun* **27**, 299.

Baluja K L, Mason N J, Morgan L A and Tennyson J 2001 *J. Phys. B: At. Mol. Opt. Phys.* **34**, 2807–2821.

Bartschat K, Hudson E T, Scott M P, Burke P G and Burke V M 1996 *J. Phys. B: At. Mol. Opt. Phys.* **29**, 115.

Behringer K and Fantz U 2000 *New. J. Phys.* **2**, 23.1–23.19.

Berrington K A and Ballance C P 2002 *J. Phys. B: At. Mol. Opt. Phys.* **35**, 2275–2282.

Bloch C 1957 *Nucl. Phys.* **4**, 5039.

Boggio-Pasqua M, Voronin A I, Halvick P and Rayez J C 2000 *J. Mol. Struct.* **531**, 159.

Bondybey V E and Brus L E 1975 *J. Chem. Phys.* **63**, 2223.

BIBLIOGRAPHY

Bondybey V E and Nibler J W 1972 *J. Chem. Phys.* **56**, 4719.

Born M and Oppenheimer R 1927 *Ann. Phys. (Leipzig)* **84**, 457–484.

Boys S F 1950 *Proc. R. Soc. A* **200**, 542–554.

Branchett S E and Tennyson J 1992 *J. Phys. B: At. Mol. Opt. Phys.* **25**, 2017–2026.

Burke P G 1976 *Proc. 5th Int. Conf. on Atomic Physics ed. R.Marrus, M.Prior and H.Shugart (New York): Plenum* p. p.293.

Burke P G and Berrington K A, eds 1993 *Atomic and Molecular Processes: An R-matrix Approach* Institute of Physics Publishing, UK.

Burke P G, Berrington K A and Sukumar C V 1987 *J. Phys. B: At. Mol. Opt. Phys.* **14**, 289–305.

Burke P G, ed. 1982 *Physics of electronic and atomic collisions* S. Datz, Amsterdam: North-Holland.

Burke P G, Hibbert A and Robb W D 1971 *J. Phys. B: At. Mol. Opt. Phys.* **4**, 153–161.

Burke P G, Mackey I and Shimamura I 1977 *J. Phys. B: At. Mol. Opt. Phys.* **10**, 2497–2512.

Burke P G and Robb W D 1975 *Adv. At. Mol. Phys.* **11**, 143–214.

Burke P G and Seaton M J 1984 *J. Phys. B: At. Mol. Opt. Phys.* **58**, 199–202.

Buttle P 1967 *Phys. Rev.* **160**, 719.

Chang E S and Fano U 1972 *Phys. Rev. A* **6**, 173.

Christiansen O, Koch H, Jørgensen P and Olsen J 1996 *Chem. Phys. Lett.* **259**, 185.

Chu S I and Dalgarno A 1974 *Phys. Rev. A* **10**, 788.

Collins G F, Pegg D J, Fritioff K, Sandström J, Hanstorp D, Thomas R D, Hellberg F, Ehlerding A, Larson M, Österdahl F, Källberg A and Danared H 2005 *Phys. Rev. A* **72**, 042708.

Collins L A, Schneider B I, Noble C J, McCurdy C W and Yabushita S 1986 *Phys. Rev. Lett.* **57**, 980–983.

BIBLIOGRAPHY

Dalgarno A and McCray R A 1972 *Annu. Rev. Astron. Astrophys.* **10**, 375.

Demaria A J 1973 *Proc. IEEE* **61**, 731.

Dorset D L 1996 *Acta. Crystallogr. A* **52**, 480.

Dunning T H 1970 *J. Chem. Phys.* **53**, 2823.

Eden R J and Taylor J R 1964 *Phys. Rev.* **133**, B 1575.

Fantz U, Balden S and ASDEX Upgrade Team 2005 *J. Nucl. Materials* **337-339**, 1087–1091.

Fantz U, Behringer K, Gafert J and Coster D 1999 *J. Nucl. Materials* **266-269**, 490–494.

Fantz U, Reiter D, Heger B and Coster D 2001 *J. Nucl. Materials* **290-293**, 367–373.

Faure A, Gorfinkiel J D, Morgan L A and Tennyson J 2002 *Computer Phys. Comms.* **144**, 224–241.

Feshbach H 1958 *Ann. Phys. (N.Y.)* **5**, 357.

Feshbach H 1962 *Ann. Phys. (N.Y.)* **19**, 287.

Fliflet A W and McKoy V 1980 *Phys. Rev. A* **21**, 1863.

Fock V 1930 *Z. Phys.* **61**, 126–148.

Frosch R P 1971 *J. Chem. Phys.* **54**, 2660.

Gailitis M 1976 *J. Phys. B: At. Mol. Opt. Phys.* **9**, 843–854.

Gibson T L, Lima M, McKoy V and Huo W M 1987 *Phys. Rev. A* **35**, 2473.

Gillan C J, Tennyson J and Burke P G 1995 *in* W Huo and F. A Gianturco, eds, 'Computational methods for Electron-molecule collisions' pp. 239–254.

Gorfinkiel J D and Tennyson J 2004 *J. Phys. B: At. Mol. Opt. Phys.* **37**, L343–L350.

Gruber O, Arslanbekov R, Atanasiu C and et al. 2001 *Nucl. Fusion* **41**, 1369–1389.

Hartree D R 1928 *Proc. Camb. Phil. Soc.* **24**, 89–110.

Hefter U, Mead R D, Schulz P A and Lineberger W C 1983 *Phys. Rev. A* **28**, 1429–1439.

Heger B, Fantz U and Behringer K 2001 *J. Nucl. Materials* **290-293**, 413–417.

Herzberg G and Lagerqvist A 1968 *Can. J. Phys.* **46**, 2363.

Herzberg G, Lagerqvist A and Malmberg C 1969 *Can. J. Phys.* **47**, 2735.

Hey J D, Chu C C and Hintz E 2000 *Contrib. Plasma Phys.* **40**, 9–22.

Hines C O, Paghis I, Hartz T R and Fejer J A, eds 1965 *Physics of the Earth's Upper Atmosphere* Prentice-Hall, Englewood Cliffs, NJ, USA.

Honig R E 1954 *J. Chem. Phys.* **22**, 126.

Huber K P and Herzberg G, eds 1979 *Constants of Diatomic Molecules* Van Nostrand Reinhold.

Jones P L, Mead R D, Kohler B E, Rosner S D and Lineberger W C 1980 *J. Chem. Phys.* **73**, 4419.

Kirby K and Liu B 1979 *J. Chem. Phys.* **70**, 893.

Kokkin D L, Reilly N J, Morris C W, Nakajima M, Nauta K, Kable S H and Schmidt T W 2006 *J. Chem. Phys.* **125**, 231101–1–231101–3.

Kushner M J 1998 *Invited talks, Meeting on Electron Molecule Collision Data for Modelling and Simulation of Plasma Processing, France* .

Lane N F 1980 *Rev. Mod. Phys.* **52**, 29.

Lehoucq R, Maschhoff K, Sorensen D and Yang C 1996 *ARPACK http://www.caam.rice.edu/software/ARPACK/* .

Lineberger W C and Patterson T A 1972 *Chem. Phys. lett.* **13**, 40.

Löwdin P O 1955 *Phys. Rev.* **97**, 1474.

Martin M 1992 *J. Photochem. Photobiol. A* **66**, 263.

McCarty M and Robinson G W 1959 *J. Chem. Phys.* **56**, 723.

Milligan D E and Jacox M E 1969 *J. Chem. Phys.* **51**, 1952.

Morgan L A 1984 *Comput. Phys. Commun.* **31**, 419–422.

Morgan L A, Gillan C J, Tennyson J and Chen X 1997 *J. Phys. B: At. Mol. Opt. Phys.* **30**, 4087–4096.

Morgan L A, Tennyson J and Gillan C J 1998 *Computer Phys. Comms.* **114**, 120–128.

Nestmann B M and Peyerimfoff S D 1990 *J. Phys. B: At. Mol. Opt. Phys.* **23**, L773.

Nestmann B M, Pfingst K and Peyerimfoff S D 1994 *J. Phys. B: At. Mol. Opt. Phys.* **27**, 2297.

Noble C J 1982 *Daresbury Laboratory Technical Memorandum* **DL/SCI/TMT33T**.

Noble C J and Nesbet R K 1984 *Comput. Phys. Commun.* **33**, 399–411.

Pearton S J and Ren F 1994 *J. Mater. Sci. - Mater. El.* **27**, 61.

Pedersen B, Djurić N, Jensen M J, Kella D, Safvan C, Schmidt H T, Vejby-Christensen L and Andersen L H 1999 *Phys. Rev. A* **60**, 2882.

Pedersen H B, Djurić N, Jensen M J, Kella D, Safvan C, Vejby-Christensen L and Andersen L H 1998 *Phys. Rev. Lett.* **81**, 5302.

Rehfuss B D, Liu D J, Dinelli B M, Jagod M F, Ho W C, Crofton M W and Oka T 1988 *J. Chem. Phys.* **89**, 129–137.

Rosmus P and Werner H J 1984 *J. Chem. Phys.* **80**, 585.

Sarpal B K, Branchett S E, Tennyson J and Morgan L A 1991 *J. Phys. B: At. Mol. Opt. Phys.* **24**, 3685–3699.

Sarpal B K, Pfingst K, Nestmann B M and Peyerimhoff S D 1996 *J. Phys. B: At. Mol. Opt. Phys.* **29**, 857.

Schmidt M W and Ruedenberg K 1979 *J. Chem. Phys.* **71**, 3951.

Schneider B I 1975 *Chem. Phys. Lett.* **31**, 237.

Schneider B I and Hay P J 1976 *Phys. Rev. A* **13**, 2049.

Seaton M J 1985 *J. Phys. B: At. Mol. Opt. Phys.* **18**, 2111.

Shimamura I 1977 *J. Phys. B: At. Mol. Opt. Phys.* **10**, 2597–2618.

Shimamura I 1998 *Mol. Phys.* **93**, 3–17.

Slater J C, ed. 1960 *Quantum theory of atomic structure* McGraw-Hill.

Slim H A and Stelbovics A T 1987 *J. Phys. B: At. Mol. Opt. Phys.* **20**, L211–L215.

Slim H A and Stelbovics A T 1988 *J. Phys. B: At. Mol. Opt. Phys.* **21**, 1519–1536.

Smith F T 1960 *Phys Rev.* **114**, 349.

Sommerfeld T, Riss U V, Meyer H D and Cederbaum L S 1997 *Phys. Rev. Lett.* **79**, 1237.

Sommerfeld T, Tarantelli F, Meyer H D and Cederbaum L S 2000 *J. Chem. Phys.* **112**, 6635–6642.

Souza S P and Lutz B L 1977 *Astrophys. J. Lett.* **216**, L49–L51.

Spence F E and Phelps A V 1976 *in 'Proc. 15th Symposium on Engineering Aspects of MHD' University of Pennsylvania, Philadelphia* .

Springer E W, Cameron B J and Reeves G A 1997 *Fusion Technology* **31**, 449.

Stark P, Fantz U and Balden M 2005 *J. Nucl. Materials* **337-339**, 1005–1009.

Stathopoulos A and Fisher C F 1982 *Comput. Phys. Commun* **79**, 268.

Stibbe D T and Tennyson J 1996 *J. Phys. B: At. Mol. Opt. Phys.* **29**, 4267–4283.

Stibbe D T and Tennyson J 1998 *Computer Phys. Comms.* **114**, 236–242.

Stibbe D T and Tennyson J 1999 *Chem. Phys. Letts.* **308**, 532–536.

Szabo A and Ostlund N S, eds 1996 *Modern quantum chemistry* Dover Publication, Inc.

Tennyson J 1996 *J. Phys. B: At. Mol. Opt. Phys.* **29**, 1817–1828.

Tennyson J 2004 *J. Phys. B: At. Mol. Opt. Phys.* **37**, 1061–1071.

Tennyson J and Morgan L A 1999 *Phil. Trans. A* **357**, 1161–1173.

Tennyson J and Noble C J 1984 *Computer Phys. Comms.* **33**, 421–424.

Wang R, Zhu Z H and Yang C L 2001 *J. Mol. Struct.(Theochem)* **571**, 133–138.

Watson D K and McKoy V 1979 *Phys. Rev. A* **20**, 1474.

Watts D J and Bartlett R J 1992 *J. Chem. Phys.* **96**, 6073.

Wigner E P 1946 *Phys. Rev.* **70**, 606.

Wigner E P and Eisenbud L 1947 *Phys. Rev.* **72**, 29.

Zeitz M, Peyerimhoff S D and Buenker R J 1979 *Chem. Phys. Lett.* **64**, 243.